

Correlation between physical properties and flowability indicators for fine powders

A Thesis Submitted to the College of Graduate Studies and Research
in partial fulfilment of the requirements for the degree of
Master of Science
in the Department of Chemical Engineering
University of Saskatchewan
Saskatoon, Saskatchewan

By

Abhaykumar Bodhmage

Copyright Abhaykumar Bodhmage July 2006

All Rights Reserved

PERMISSION FOR USE

The author has agreed that the Libraries of the University of Saskatchewan may make this thesis freely available for inspection. Moreover, the author has agreed that permission for extensive copying of this thesis for scholarly purposes may be granted by the professor(s) who supervised this thesis work recorded herein or, in their absence, by the Head of the Department of Chemical Engineering or the Dean of the College of Graduate Studies. Copying or publication or any other use of the thesis or parts thereof for financial gain without written approval by the University of Saskatchewan is prohibited. It is also understood that due recognition will be given to the author of this thesis and to the University of Saskatchewan in any use of the material of the thesis.

Request for permission to copy or to make other use of material in this thesis in whole or parts should be addressed to:

Head
Department of Chemical Engineering
University of Saskatchewan
57 Campus Drive
Saskatoon, Saskatchewan
S7N 5A9
Canada

ABSTRACT

Approximately 80% of pharmaceutical products and the ingredients required for their manufacture are in powder form. The solid dosage form (tablets and capsules) is manufactured by either dry-blending of fine powder ingredients or combining the ingredients in a wet granulation step, followed by drying. Arching, ratholing, caking, segregation and flooding are some of the commonly encountered flow problems in the handling of fine powders. These problems lead to losses worth thousands of dollars at production scale. Poor powder flowability is a consequence of the combined effects of many variables, including improper equipment design, particle size, size distribution, shape, moisture content and surface texture. In the present work, a systematic study has been performed to determine the relationship between the flowability of fine powders and their physical properties of mean size and size distribution, density and shape.

Flowability studies were done on six different powders: the NutraSweet® Brand sweetener (aspartame), Respitose ML001, Alpha-D-Lactose monohydrate, the pharmaceutical binder Methocel (R) F50 Premium Hydroxypropyl methylcellulose-HPMC, a placebo pharmaceutical granulate, and common pastry flour. Scanning electron microscopy (SEM) and stereomicroscopy were used for particle shape and size analysis. Particle size distribution was determined using the laser light scattering technique. Powder flowability was measured using shear strength, angle of repose, and tapped-to-bulk density measurements. A novel method of measuring the dynamic angle of repose using electrical capacitance tomography (ECT) was developed.

Analysis of the images from microscopy revealed that the particles of aspartame and HPMC powders were elongated, the particles of ML001, pastry flour and lactose

monohydrate powders were irregular, and the particles of placebo granulate were nearly spherical. Particle size was found to be the most reliable indicator of powder flowability, with decreasing particle size corresponding to lower flowability; however other parameters such as particle elongation and irregularity, were also found to have an influence on powder flowability. Although HPMC and pastry flour had similar particle sizes, they exhibited differences in flowability. This can be explained by the greater irregularity of the flour particles. Particle irregularity may cause mechanical interlocking between the particles, thus reducing powder flowability. ECT was found to be a promising non-intrusive tool for the measurement of the dynamic angle of repose. Unlike other methods for the measurement of dynamic angle of repose, the results obtained from ECT were not influenced by the effect of end caps. The present technique could be used by pharmaceutical industries in process analytical technology (PAT) for the detection and elimination of potential flow problems early in the manufacturing process.

ACKNOWLEDGMENT

I wish to express my gratitude to Dr. Todd S. Pugsley for his thoughtful guidance and his insistence on excellence. His guidance throughout my graduate program has contributed immensely to the success of this work. I am also indebted to other members of the advisory committee, Dr. J. Sharma and Dr. H. Wang for their helpful discussions and suggestions.

I thank Mr. T. Wallentiny and Mr. R. Blondin of the Chemical Engineering Department and Mr. A. Kozlow of the Civil Engineering Department for their technical assistance at various stages of this work. I express my sincere appreciation to all the members of the Fluidization Laboratory for all the useful discussions and suggestions.

The financial assistance from the Department of Chemical Engineering is gratefully acknowledged.

DEDICATION

This work is dedicated to

My Parents

TABLE OF CONTENTS

PERMISSION FOR USE	i
ABSTRACT	ii
ACKNOWLEDGMENT	iv
DEDICATION	v
TABLE OF CONTENTS	vi
LIST OF TABLES	ix
LIST OF FIGURES	x
NOMENCLATURE	xii
1 INTRODUCTION	1
1.1 Background	1
1.2 Literature review	5
1.2.1 Importance of powder flow in the pharmaceutical industry	6
1.2.2 Flowability indicators used in industries	7
1.2.2.1 Shear strength measurements	7
1.2.2.2 Density measurements	9
1.2.2.3 Angle of repose	10
1.2.2.4 Process analytical technology (PAT)	12
1.2.3 Powder properties affecting flowability	12
1.2.4 Knowledge gap	15
1.3 Research objectives and approach	16
1.3.1 Phase I: Physical properties characterization	17
1.3.2 Phase II: Powder flowability measurement	17
1.3.3 Phase III: Comparison of powder physical properties and flowability indicators	17
2 EXPERIMENTAL SETUP AND METHODOLOGY	18
2.1 Test Powders	18
2.2 Measurement of powder physical properties	19
2.2.1 Particle size and size distribution using laser diffraction method	19
2.2.2 Moisture content	20
2.2.3 Density measurements	21
2.2.4 Image analysis	22
2.2.4.1 Image analysis equipment	22
2.2.4.2 Stereomicroscopy and SEM image analysis	24

2.2.4.3	Selection of suitable shape descriptors	25
2.3	Measurement of powder flowability	27
2.3.1	Angle of repose	28
2.3.1.1	Measurement of static angle of repose	29
2.3.1.2	Measurement of dynamic angle of repose	30
2.3.2	Density measurements	36
2.3.2.1	Tapped density tester equipment and operation	37
2.3.3	Flowability based on the shear characteristics of a powder	38
2.3.3.1	Construction of parallel plate shear tester	38
2.3.3.2	Operating procedure and calculations	39
3	RESULTS AND DISCUSSION	44
3.1	Fine powder physical properties characterization	44
3.1.1	Particle size distribution from the laser diffraction method	44
3.1.2	Moisture content from halogen moisture analyzer	46
3.1.3	Density measurements	47
3.1.4	Particle shape analysis	48
3.1.5	Frequency distribution	52
3.1.5.1	Equivalent circle diameter	53
3.1.5.2	Shape factors	53
3.2	Flowability measurements	55
3.2.1	Shear measurements	55
3.2.2	Density measurements	58
3.2.3	Angle of repose measurements	61
3.2.3.1	Static angle of repose	61
3.2.3.2	Dynamic angle of repose	61
3.3	Comparison of powder physical properties with flow indicators	65
3.3.1	Relationship between mean particle size and flowability indicators	65
3.3.1.1	Relationship between mean particle size and the angle of repose	66
3.3.1.2	Relationship between Hausner Ratio, cohesion, flow index and mean particle size	67
3.3.2	Relationship between flowability indicators and various shape parameters	69
3.4	Summary of results	76
4	CONCLUSIONS	78
5	RECOMMENDATIONS	81
	REFERENCES	82
	APPENDICES	87
	Appendix A: Results from Malvern Mastersizer- S long bench	87
	Appendix B1: Experimental results for dynamic angle of repose.	88
	Appendix B2: Dynamic angle of repose for test powders at 10 RPM.	88

Appendix B3: Dynamic angle of repose for test powders at 20 RPM.	89
Appendix B4: Dynamic angle of repose for test powders at 30 RPM.	89
Appendix B5: Dynamic angle of repose for test powders at 40 RPM.	90
Appendix C1: Frequency distributions of equivalent circle diameters for various test powders.	91
Appendix C2: Frequency distributions of roundness factor for various test powders.	92
Appendix C3: Frequency distributions of aspect ratio for various test powders.	93
Appendix C4: Frequency distributions of irregularity for various test powders.	94
Appendix D1: Shear stress vs. applied strain for aspartame	95
Appendix D2: Shear stress vs. applied strain for ML001	96
Appendix D3: Shear stress vs. applied strain for lactose	98
Appendix D4: Shear stress vs. applied strain for flour	99
Appendix D5: Shear stress vs. applied strain for HPMC	101
Appendix D6: Shear stress vs. applied strain for placebo granulates	102
Appendix D7: Yield locus for test powders at different preshear stresses	104
Appendix D8: Various flow indicators obtained from shear cell experiments.	107

LIST OF TABLES

Table 1-1 Classification of bulk material (Cain, 2002)	8
Table 2-1 Carr classification of powder flowability based on angle of repose	28
Table 2-2 Jenike classification of powder flowability based on flow index (Teunou and Fitzpatrick, 2000)	43
Table 3-1 Physical properties of test powders	45
Table 3-2 Values of various particle shape parameters from image analysis	50
Table 3-3 Particle shape attributes of test powders	54
Table 3-4 Flow index values for all test powders	56
Table 3-5 Hausner Ratio and Carr Index for test powders	58
Table 3-6 Values of static angle of repose for test samples	61

LIST OF FIGURES

Figure 1-1	Flow chart of pharmaceutical tablet production	1
Figure 1-2	Rathole formation	2
Figure 2-1	Digital image of flour particles obtained after processing from stereomicroscope	25
Figure 2-2	Characteristic dimensions used to calculate aspect ratio, roundness, and irregularity	26
Figure 2-3	Illustration of the maximum and minimum inscribed circle diameter	27
Figure 2-4	Illustration of a)static angle of repose and b)dynamic angle of repose	29
Figure 2-5	Measurement of static angle of repose	29
Figure 2-6	Sample image used to determine the static angle of repose (α) for aspartame	30
Figure 2-7	Dynamic angle of repose (Castellanos and Valverde, 1999)	31
Figure 2-8	Electrical Capacitance Tomography equipment (PCECT, 1998)	34
Figure 2-9	Equipment used to measure dynamic angle of repose	35
Figure 2-10	ECT image used to determine the dynamic angle of repose	36
Figure 2-11	Tapped density meter	37
Figure 2-12	Parallel plate shear cell	38
Figure 2-13	Shear stress-strain plot for the placebo granulate at 2 kPa preshear normal stress and 1 kPa normal stress	40
Figure 2-14	Typical yield loci (Fitzpatrick et al., 2004)	41
Figure 2-15	Flow function lines (Fitzpatrick et al., 2004)	42
Figure 3-1	Size distributions of the various test powders from laser diffraction method	45
Figure 3-2	Variation of moisture content with time for flour	46
Figure 3-3	Micrographs obtained from stereomicroscopy: a) Flour; b) HPMC; c) Aspartame; d) Respitose ML001; e) Alpha-D-Lactose monohydrate; f) Placebo granulate	48
Figure 3-4	SEM micrographs for aspartame at different magnifications	49
Figure 3-5	Comparison of mean diameters obtained from image analysis and laser diffraction method	51
Figure 3-6	Frequency distribution of equivalent circle diameter for aspartame	53
Figure 3-7	Frequency distributions of (a) roundness factor and (b) aspect ratio for HPMC	54
Figure 3-8	Flow function lines for test powders	56
Figure 3-9	Cohesion values for the test powders at different values of normal stress	57
Figure 3-10	Values of Hausner Ratio for test powders up to 300 tappings	59
Figure 3-11	Values of Carr Index for test powders up to 300 tappings	59
Figure 3-12	Variation of Hausner ratio with number of taps for test powders	60
Figure 3-13	Dynamic angle of repose curve for cohesive powders at 20 RPM	62
Figure 3-14	Dynamic angle of repose curve for free flowing powders at 20 RPM	63
Figure 3-15	Dynamic angle of repose for test powders at different rotational speeds	63

Figure 3-16 Angle of repose (AOR) vs. mean particle diameter for the test powders	66
Figure 3-17 Variation of Hausner Ratio and cohesion with particle diameter	67
Figure 3-18 Variation of flow index with particle diameter	68
Figure 3-19 Relationship between aspect ratio and static angle of repose	70
Figure 3-20 Relationship between roundness and static angle of repose	70
Figure 3-21 Micrograph of aspartame agglomerates from stereomicroscope	71
Figure 3-22 Relationship between aspect ratio and flow indicators	72
Figure 3-23 Relationship between roundness and flow indicators	72
Figure 3-24 Relationship between aspect ratio and flow index	73
Figure 3-25 Relationship between roundness and flow index	73
Figure 3-26 Relationship between irregularity factor and static angle of repose	74
Figure 3-27 Relationship between Hausner ratio and cohesion with irregularity	75
Figure 3-28 Relationship between irregularity factor and flow index	76

NOMENCLATURE

A	Projected area of the particle (μm^2)
A'	Convex area (μm^2)
BD	Loose-packed bulk density (kg/m^3)
b	Minor axis (μm)
C	Cohesion of the powder (kPa)
CA	Concavity based on area
CP	Concavity based on perimeter
CI	Compressibility
D	Maximum inscribed circle diameter (μm)
d	Minimum inscribed circle diameter (μm)
d_i	Particle diameter (μm)
d_{sm}	Sauter mean diameter (μm)
ECD	Equivalent circle diameter (μm)
FF	Flow function
HR	Hausner ratio
IP	Irregularity parameter
I	Irregularity factor
l	Major axis (μm)
MCS	Major consolidating stress (kPa)
P	Perimeter of projection (μm)
P_2	Desired target pressure (Pa)
P_3	Resulting lower pressure (Pa)

R	Roundness
S	Total surface area (μm^2)
s_i	Surface area of particles in the i th interval (μm^2)
T	Tensile stress of the powder material (kPa)
TD	Tapped density (kg/m^3)
UYS	Unconfined yield stress (kPa)
V_p	Sample unknown volume (m^3)
V_c	Sample cell volume (m^3)

Greek Letters:

ϕ_{AR}	aspect ratio
α	Angle of repose (Deg)
δ_e	Effective angle of internal friction (Deg)
δ	Angle of internal friction (Deg)
θ_S	Static angles of repose (Deg)
θ_D	Dynamic angles of repose (Deg)

1 INTRODUCTION

1.1 Background

According to Nelson (2004), 75% of chemical processes involve particulate materials as raw material or final product. In the case of the pharmaceutical industry, most products and the ingredients required for their manufacture are in powder form. Over 80% of pharmaceutical products are sold in solid dosage form (i.e. tablets and capsules). Tablets are manufactured in pharmaceutical industries using three basic types of ingredients: an inert carrier that provides volume for final dosage, a filler to form tablets, and the active ingredient. The following flow diagram (Figure 1-1) shows the two methods used by pharmaceutical industries for manufacturing tablets.

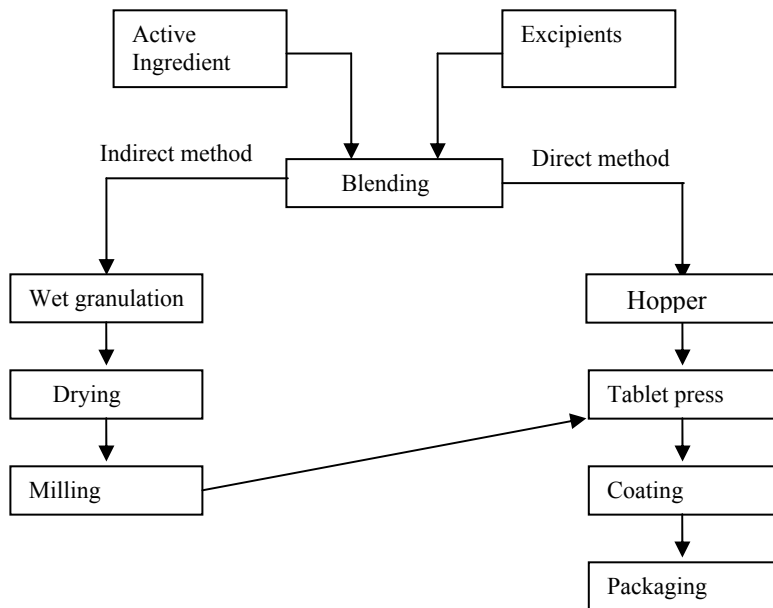


Figure 1-1 Flow chart of pharmaceutical tablet production

The preferred tablet manufacturing method used by the pharmaceutical industry is the direct method (direct compression) as it eliminates additional processing steps and avoids added equipment cost which are required for wet granulation (Prescott and Hossfeld, 1994). In direct compression, ingredients are mixed in a blender and then discharged into a bin or a hopper from where they are fed to the tablet press. Thus, most of the pharmaceutical processes such as mixing, storage, feeding, compaction, transfer and fluidization involve powder handling, which has a direct impact on the quality of the final products in terms of weight and content uniformity. Many of these processes are operated batch-wise, which makes the transportation and storage of ingredients and final product essential. Various types of hoppers, bins or silos are commonly used for the transportation and storage of bulk powders.

Various powder flow problems are commonly encountered in industries handling fine powders. For instance, when flowing out of a storage bin or hopper, fine powders may form a rathole, which is a self-supporting vertical channel extending from the outlet to the top surface of the powder, as seen in Figure 1-2.

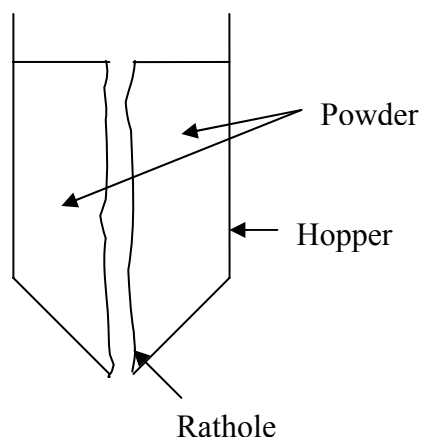


Figure 1-2 Rathole formation

Sometimes, arches are formed at the hopper outlet, leading to intermittent flow or a no flow scenario. Arches can form in bulk solids because of two reasons: particle interlocking or an increase in cohesive strength. Particle interlocking occurs when particles lock together mechanically at the outlet. Particles with irregular shapes have a greater chance of forming arches. Cohesive arches can form where particles bond together physically, chemically or electrostatically. The exposure of the bulk materials to humid air causes an increase in the moisture content, especially if the material is hygroscopic. This leads to a gain in the cohesive strength because of the formation of liquid bridges between neighbouring particles, causing difficulties in flow. Another problem related to fine powder flow is flooding caused by either sudden breakage of an arch or bridge of material in a hopper that is partially or entirely empty, leading to uncontrollable flow of powder through the system. This might affect the downstream equipment and cause spillage of powder material.

During continuous flow, most of the material might flow quite easily; however, if the flow is stopped because of equipment shut down or some other reason, the material will sit at rest in a bin or silo for a period of time, ranging from a few hours to a few months. After this time has elapsed, the particles may rearrange themselves and become more tightly packed together, thus leading to flow problems.

In direct compression tableting, dry powder blends must flow uniformly into the tablet dies to obtain a uniform product. Prescott and Hossfeld (1994) describe the segregation of powder blends and interruptions of flow when the powder is transferred from a bin or hopper to a tablet press as the main problem encountered in direct compression tableting. Particle segregation occurs if the ingredients have different particle properties, particularly, particle size, causing product variation in the form of

pockets of segregated material at the tableting press at regular intervals. This is an important issue because it adversely affects product quality, leading to rejection of batches worth hundreds of thousands of dollars at the production scale, and may result in costly cleanup. Also, flow problems result in downtime, lost production hours and more importantly low quality drugs that may pose health risks to end users.

According to Freeman (2000), powder flowability is a consequence of the combined effects of various physical, chemical and environmental variables. Improper equipment geometry, particle size, shape, surface texture, size distribution, moisture content, compaction condition, storage time, etc. have an impact on powder flow. Physical properties of the powder are found to have more impact on its flowability as compared to chemical properties. The powder flow properties such as compressibility, cohesive strength and friction result from collective forces such as particle interlocking, particle-particle friction, cohesive forces, etc. on individual particles. The cohesive nature of fine powders is due to the presence of a cohesive component to their shear strength in addition to a frictional component. The cohesive component is enhanced in presence of moisture.

Powder flowability also depends upon the geometry of the equipment used for handling, storing or processing the material. Although standards exist for design of equipment for mass flow, it is generally seen in industries handling a variety of powders with different properties that equipment designed for a particular powder is not suitable for handling a different powder. The equipment designs are based on some theoretical equations which do not take into account the effect of various particle properties having an influence on powder flowability.

Although it is known from the literature that powder flowability decreases as the particle size becomes smaller, sometimes similar sized particles are found to have contrasting flowability. The reason for this might be because of differences in powder properties. Some studies indicate that powders containing spherical particles show good flowability as compared to those with elongated or irregular particles. Elongated or irregular particles might tend to mechanically interlock or entangle with each other, thus obstructing powder flow and reducing flowability.

Thus, flowability issues are generally attributed to the cohesive nature of fine powders or to the mechanical interlocking of powders with irregular shapes. It has been suggested by Prescott and Barnum (2000) that, “much proven scientific understanding of bulk powder flow has not been used fully by the pharmaceutical industry”. However, the current understanding of the shear strength of fine powders, which is the main reason for flow stoppages in hoppers, does not include the influence of powder shape, size distribution or powder storage in any systematic way. Thus, the aim of the present study was to improve this lack of understanding.

1.2 Literature review

A detailed study of literature involving the impact of powder flowability in various industries, different flowability indicators used in industry, the various powder properties affecting flowability, and the knowledge gap was done and is presented in this section.

1.2.1 Importance of powder flow in the pharmaceutical industry

According to Prescott and Barnum (2000), several processes used to manufacture solid dosage form pharmaceuticals involve powder handling. The quality of the final product depends upon complex powder flow during manufacturing. The flow of a blend during formulation development affects excipient selection and may dictate whether compression or some form of granulation is required. Problems such as arching, rathole formation, flooding and segregation can develop in equipment handling fine powders. Muzzio et al. (2001) emphasized the importance of powder technology operations in manufacturing pharmaceutical products such as tablets, capsules, aerosols, injectable products and suspensions. Needle-shaped powders have also been shown to adversely impact drug delivery from dry-powder inhalers, presumably due to their poorer flow characteristics (Larhrib et al., 2003). Thalberg et al. (2004) suggested that for successful product development for inhalation, it is important to adjust and control the flow properties of fine powders during processing and formulation.

According to Fitzpatrick et al. (2004), powder properties affect powder behaviour during storage, handling and processing. Flow problems are often connected to the flow pattern inside the vessel. Particle segregation and material flow interruptions are major problems faced during direct-compression tableting operations because of the wide particle size distribution encountered (Prescott and Hossfeld, 1994). Storage of bulk solids in an improperly designed hopper can lead to flow problems such as arching, ratholing and segregation (Behera et al., 2002).

1.2.2 Flowability indicators used in industries

Schwedes and Schulze (1990), in their review of powder flowability test methods, stated that the first step in designing handling equipment for mass flow is to measure the flow properties of the bulk powder. Prescott and Barnum (2000) indicated that powder flowability is a combined result of the influence of material physical properties and the equipment used for handling, storing or processing the material. Shear strength measurement, density measurement and the measurement of angle of repose are some of the common techniques used to establish the potential flowability of powder materials. Each of these will be discussed in the next sections.

1.2.2.1 Shear strength measurements

According to Bell (1999), storage bins or hoppers were historically designed largely by guess work, until the research of Janssen in 1895, followed by that of Jenike in the 1964. Jenike's theory, based on the shear strength of the material, remains the basis for determining powder flowability, the design of silos for mass flow, and the sizing of silo outlets to prevent arching and ratholing. The shear strength is the resistance of a bulk material against failure or flow.

ANSI/CEMA Standard 550 utilizes the four flowability categories defined by Jenike as a measure of the cohesive nature of granular materials (Table 1-1).

Table 1-1 Classification of bulk material (Cain, 2002)

Level of Cohesiveness	ANSI/CEMA Standard 550 Flow Rating	Jenike Flow Factor (FF) Range
Very Free Flowing	1	> 10
Free Flowing	2	4-10
Cohesive	3	2-4
Very Cohesive (Non-Flowing)	4	< 2

The Jenike flow factor is obtained using a Jenike shear cell, which measures variation in shear stress required to produce flow with changes in normal stress in bulk materials. According to Bell (1999), Jenike's shear testing methods have proven to be valid and reproducible for a broad range of powders. The Jenike shear cell provides measurements of powder cohesive properties that can be used to design a hopper to prevent arching and rathole formation (Behera et al., 2002). They used the Jenike shear cell to obtain critical minimum hopper outlet diameter and hopper half angle for the design of a mass flow hopper for five different bulk materials.

They found that the hopper opening diameter needed to be larger for cohesive powders because of the greater cohesion and lower flow functions of these powders. However, it has been reported that applying this analysis can occasionally produce unexpected values for hopper opening size (Fitzpatrick et al., 2004). Also, this procedure is time consuming and requires several-hundred grams of potentially high value product, and results depend upon the skills of the operator (Bell, 1999).

1.2.2.2 Density measurements

Carr (1965) suggested the compressibility of a powder material as an indicator of the tendency of the powder to flow. This is often expressed in terms of Hausner ratio (HR), which is the ratio between the tapped density (TD) and the loose-packed bulk density (BD) of powder (Thalberg et al., 2004) (equation 1.1). Riley and Hausner (1970) were the first to point out the significance of the Hausner ratio. A related indicator calculated from densities is the Carr index (equation 1.2) which is the ratio of the difference between the tapped bulk density and the aerated bulk density to the tapped bulk density.

$$HR = \frac{TD}{BD} \quad (1.1)$$

$$CI = \frac{(TD - BD)}{TD} \times 100 \quad (1.2)$$

Cohesive materials have a Hausner ratio greater than 1.4 (Cain, 2002). According to Carr (1965), materials having Carr Index greater than 20 to 25 % are classified as non-free-flowing.

Cain (2002) demonstrated that a significant correlation existed between the ANSI/CEMA standard 550 flowability rating based on Jenike shear data (Table 1-1) and the Cain-Lairmore model. The Cain-Lairmore model which was based on the Hausner ratio, mean particle size, and the angle of repose was found to be an accurate predictor of bulk material cohesiveness. Thalberg et al. (2004) used a modified Hausner ratio for evaluating the flowability of different formulations. They used a compressed bulk density instead of tap density, as it required less power to achieve a maximum packing condition. Santomaso et al. (2003) suggested a new flowability criterion based on a

novel technique to measure the high packing density. Wouters and Geldart (1996) suggested that the ratio of the angle of repose to aerated bulk density, called the weighted angle of repose provides a more sensitive way of predicting changes in powder flowability with time. They observed a gradual change in weighted angle of repose for the various mean sizes of the materials.

1.2.2.3 Angle of repose

ISO Standard 3435 indicates the use of the angle of repose for quantifying the cohesiveness of a granular material (Cain, 2002). The static angle of repose is the angle made by a pile of material with the horizontal, and the dynamic angle of repose is the angle made by the inclined surface of powder material with the horizontal when rotated in a drum. Unlike the Jenike procedure, the measurement of angle of repose can be completed in less time. Riley et al. (1978) used the tilting box method and the fixed cone method to determine the angle of repose. As the angle of repose for cohesive material cannot be determined easily, they used an admixture with a free flowing material. Determining the angle of repose at different compositions and then extrapolating the angle-composition plot enabled them to obtain a theoretical angle for cohesive powders (Riley et al., 1978). Wouters and Geldart (1996) and Dury and Ristow (1998) listed a number of methods used to measure the angle of repose and the various parameters influencing it.

Dury and Ristow (1998) observed that the dynamic angle of repose is up to 5° higher at the end caps of a rotating drum because of the boundary friction. Thus, methods that measure the angle of repose at the end of the horizontal drum may give faulty results. Yamane et al. (1995) studied particulate flows in a rotating cylinder using

DEM (Distinct Element Method) simulation and non-invasive MRI (Magnetic Resonance Imaging). They observed a linear increase in dynamic angle of repose with the rotation speed for all degrees of non-sphericity. The results from DEM and MRI were found to be in agreement. Yang et al. (2003) did similar studies of microdynamic analysis of particle flow in a horizontal rotating drum using DEM and compared these results with the results from positron emission particle tracking (PEPT). They analysed the results in terms of porosity and coordination number, and explained the effect of rotational speed on agglomeration of particles. Porosity was taken as the voidage in the powder bed and coordination number was taken as the number of particles in contact with a considered particle. A linear increase in dynamic angle of repose with rotational speed was observed.

Lindberg et al. (2004) did flowability studies on four different tablet formulations using five different techniques: Hausner ratio, avalanching behaviour, FT3 powder RheometerTM, uniaxial tester and Jenike shear cell. They used the TSI Aero-FlowTM automated powder flowability analyzer which uses mean time to avalanche as a function of powder flowability. The powder sample is placed inside a slowly rotating cavity disk, the powder rotates with it, building up to an unstable condition, and then slides down. This avalanching is detected and measured photoelectrically. Free flowing powders exhibit a shorter time to avalanche than less flowable powders. FT3 powder Rheometer measures the forces required for powder deformation and flow and uses these energy profiles to characterise flowability (Freeman, 2000).

They found that the flow properties measured by these techniques reflected the behaviour during processing of the powder mixtures during emptying of the mixer and the tableting process. Hausner ratio reflected how well the particles packed together

during tableting, avalanching measurements indicated the powder behaviour in the mixer and the FT3 powder Rheometer indicated the energy required during mixing, whereas the uniaxial and Jenike shear cell reflected the behaviour of powder in a tablet press under compression.

1.2.2.4 Process analytical technology (PAT)

Peschl and Sigulinski (1990) illustrated the importance of controlling the key properties of powder in all phases of the production process for good quality of the final product. According to Balboni (2003) pharmaceutical companies are beginning to use process analytical technology (PAT) to ensure acceptable end-products. PAT is a system of analysis and control of manufacturing process based on the measurements of key parameters of raw materials and in-process materials so as to identify and eliminate potential problems early in the manufacturing process. PAT uses various sophisticated techniques such as Near-Infrared Absorption Spectroscopy (NIR), Raman spectroscopy, and chemical imaging technology (Lawrence et al., 2003).

1.2.3 Powder properties affecting flowability

According to Freeman (2000), Cain (2002), Behera et al. (2002) and Juliano et al. (2006), cohesive behavior in bulk solids is caused by numerous mechanisms such as the presence of moisture (humidity effects, free liquid, moisture ingress, etc.), interparticle forces (Van der Waals, electrostatic forces, moisture, etc.), time consolidation and geometrical interlocking of granular materials. According to Seville et al. (1997), the interparticle forces may potentially exceed particle weight for particles below about 1 mm in size. Van der Waals force is an attractive force between atoms or nonpolar

molecules caused by a temporary change in dipole moment arising from a brief shift of orbital electrons to one side of one atom or molecule, creating a similar shift in adjacent atoms or molecules. Hygroscopic materials are known to form strong interparticle bonds in the form of liquid bridges. Measurement of cohesive forces in fine powders is very difficult and is beyond the scope of the present work.

Yamane et al. (1995) performed DEM and MRI studies of particulate flows in a rotating drum using non-spherical mustard seed. They observed that non-sphericity of particles causes a steeper dynamic angle of repose for a given rotational speed. Surface structure or roughness was found to have a major impact on flowability in comparison to particle shape and size distribution in studies done by Popov et al. (1996) and Oshima et al. (1995).

Lahdenpää et al. (1996) studied the basic properties of three grades of microcrystalline cellulose after storing them under controlled conditions of temperature and humidity. They observed a lower bulk density and poorer flowability with an increase in the amount of irregular, rod-shaped particles in the powder mixture. They also reported that the cellulose containing larger particles flowed better, and that better flow properties were achieved by mixing the three grades in certain proportions. However, they failed to relate the flowability to the Hausner ratio because of the complicated packing arising from differences in particle size and shape.

Wouters and Geldart (1996) explained the mechanical interlocking of irregular particles to be the reason for poor flow. They observed a clear inverse relationship between the angle of repose and the mean particle diameter. Zou and Yu (1996) performed experimental studies to investigate the effect of packing characteristics such as porosity on particle shape. They observed a decrease in Hausner ratio with an increase

in sphericity. Chan and Page (1997) observed similar results when performing flowability studies on powders of various shapes. They observed that irregular shaped copper powder exhibited lower packing densities, lower flowability, higher Hausner ratios and higher coefficient of internal friction. They explained this behavior of irregular particles as being due to temporary adherence or interlocking between particles, which prevents their motion and hence increases interparticle friction during powder flow.

Iida et al. (1997) observed an increase in flowability and a decrease in cohesion as the particle shape of cellulose powders approached that of a sphere. Dury and Ristow (1998) found that the angle of repose was higher for non-spherical particles as the rotations were more suppressed resulting in a higher coefficient of friction. Jensen et al. (1999) performed DEM simulations to compare the shear strength of clustered and non-clustered particles having varying surface roughness. They demonstrated that particle rotations were reduced in clustered particles due to particle interlocking, thus increasing the shear strength as compared to non-clustered particles.

Cain (2002) observed a decrease in the value of the flowability rating (Table 1-1) with an increase in mean particle size, indicating an increase in flowability. His flowability rating was based on a correlation equation involving the Hausner ratio, the mean particle size and the angle of repose. Mullarney et al. (2003) stated that a high tablet variation, blend non-uniformity and difficulty in filling containers and dies could result if the amount of elongated and small particles in the formulation exceeded 10%. They observed that the compacts made from needle shaped aspartame powders were stronger than any other sweeteners having regular shapes due to particle interactions increasing interparticulate bonding and hence improving tensile strength. Tensile

strength is the maximum amount of stress that can be subjected on bulk material before failure. Tensile strength is proportional to the tablet crushing strength (Mullarney et al., 2003). Kaerger et al. (2004) found that pharmaceutical blends containing small spherical particles exhibited increased bulk and tapped density and hence improved flow.

Fitzpatrick et al. (2004) did flowability studies on food powders having different physical properties. They observed no strong relationship between measured powder physical properties and their flowability indices. The theory of critical state soil mechanics 1968, as described by Juliano et al. (2006), recognizes that the peak strength in soils is due to friction and interlocking forces between particles. Juliano et al. (2006) did flowability studies on food powders using shear measurements and observed higher angles of internal friction, mainly due to interlocking among the particles during shear tests.

While the cited studies confirm an influence of size, size distribution, shape, and surface roughness, they are for specific powders and there is at present no systematic method to predict the way a given powder will flow based on the measurement of these properties.

1.2.4 Knowledge gap

It appears from the literature review that there is at present no general systematic relationship between primary properties such as powder size, shape, moisture content, and surface texture and powder flowability as quantified by properties like shear strength, Hausner ratio and angle of repose. It is known from the available literature on food and metal powders that elongated and irregularly shaped particles cause mechanical interlocking between particles and hence reduce the flowability. However, no

quantitative study on pharmaceutical powders has been done relative to the elongated or irregularly shaped particles of a powder to its resulting flowability.

Limited information is available in literature regarding the effect of particle size distribution on the flowability of pharmaceutical powders. The effect of a wide distribution of particle shapes and sizes on Hausner ratio is not well understood. A better understanding of the relationship between particle shape, size, size distribution and density to the powder flowability could help to eliminate potential flow problems and aid in the selection of proper ingredients for manufacture.

The literature also indicates that the techniques used to measure the dynamic angle of repose are either too complicated or give incorrect results because of the effect of end caps. Thus there is need of a technique to measure the dynamic angle of repose and avalanching behaviour. The technique should be simple to use and should not suffer from the effect of end caps. These led to the following research objectives and approach for the present work.

1.3 Research objectives and approach

The objective of the proposed research program was as follows:

To study the relationship between fine pharmaceutical powder flowability as quantified by measuring powder shear characteristics, dynamic and static angles of repose, Hausner ratio and compressibility, and the fine powder physical properties of mean size and size distribution, density, and shape.

Achieving this objective required careful experimentation followed by careful analysis of the results. The overall objective was achieved in the various phases of research program as described below:

1.3.1 Phase I: Physical properties characterization

The objective of this phase was to determine the powder physical properties of mean size and size distribution, particle shape, moisture content and density. Six different powders of varying shapes and sizes were characterized using different techniques such as laser diffraction method, image analysis, pycnometry and halogen moisture analysis.

1.3.2 Phase II: Powder flowability measurement

The objective of this phase was to determine the flowability of test powders using different techniques such as measurement of shear strength, measurement of angle of repose, and measurement of powder compressibility using Hausner ratio and Carr index. A parallel plate shear cell was used to measure the shear strength of test powders. A novel method to determine the dynamic angle of repose was developed in the present study using electrical capacitance tomography. A tapped density meter was used in the evaluation of Hausner ratio and Carr Index.

1.3.3 Phase III: Comparison of powder physical properties and flowability indicators

In this phase the effect of variation of mean particle size, size distribution, shape and shape distribution on the various flowability indicators was studied.

2 EXPERIMENTAL SETUP AND METHODOLOGY

This chapter describes the methods used in the present study to measure the powder physical properties and powder flowability. The selected test powders and reasons for choosing them are also discussed.

2.1 Test Powders

Six powders spanning a range of particle shapes and sizes were used in this study. All powders were sourced from commercial suppliers. The powders tested were: the NutraSweet® Brand sweetener (Aspartame) from The NutraSweet Company, GA, USA; Respitose ML001 from DMV International, NY, USA; Alpha-D-Lactose monohydrate from Fisher Scientific, NJ, USA; the pharmaceutical binder Methocel (R) F50 Premium Hydroxypropyl Methylcellulose (HPMC) from Dow Chemical, USA; a pre-dried placebo pharmaceutical granulate from Merck Frosst Canada Ltd., ON, Canada; and common pastry flour from Robin Hood Multifoods Inc., SK, Canada. Aspartame was chosen for study because it consists of needle-like particles and has been reported to exhibit poor flow characteristics (Mullarney et. al., 2003). The other pharmaceutical powders (Lactose monohydrate, ML001, and HPMC) were chosen because they are common ingredients in solid dosage form pharmaceuticals. Flour was considered in this study because it is well known from the fluidization literature as a Geldart C powder that is very cohesive (Geldart, 1973). It has also been used by Fitzpatrick et al. (2004) in their study on food powder flowability. Finally, the placebo granulate was used as a

reference powder since it was expected to be free flowing. One of the main reasons for granulation is to produce particles that flow more readily than the individual fine powders from which the granule is made.

2.2 Measurement of powder physical properties

Powders were characterized based on the physical properties of mean size, size distribution, moisture content, density and shape. The different techniques used for characterization included laser diffraction, image analysis, loss-on-drying using a halogen moisture balance, pycnometry and tapped density measurement. These techniques are briefly described in the following sections.

2.2.1 Particle size and size distribution using laser diffraction method

The size distribution of the test powders was measured by the laser diffraction method using the Mastersizer-S Long Bench (Malvern Instruments Ltd., Malvern, UK). The Mastersizer essentially consists of a laser transmitter and a receiver (300 RF lens) unit, detectors and a dry powder feeder unit. A representative powder sample is placed in the feeder unit and a vacuum is switched on. The vacuum draws the powder sample into the instrument where the dispersed powder passes through the laser beam. The dispersed powder scatters laser light at angles that are inversely proportional to the size of the particles, i.e. large particles scatter light at small forward angles, whereas small particles scatter light at wider angles. This scattering is captured by an array of detectors. Hence, there is a direct relationship between the distribution of the scattered light energy on these detectors and the particle size distribution. In the present study, measurements were repeated three times for each powder material and a mean particle size distribution

was calculated. The laser diffraction method measures the volume mean diameter. Assuming that powder density is not a function of size, the volume mean diameter can reliably be converted to the mass mean diameter. The Mastersizer software also gives the value of Sauter mean diameter (d_{sm}), which is the diameter of a sphere having the same surface to volume ratio as the particle (equation 2.1) (Seville et al., 1997):

$$d_{sm} = \frac{\sum s_i d_i}{S} \quad (2.1)$$

where s_i is the surface area of particles in the i th interval, S is the total surface area and d_i is the particle diameter. It is important to note that diameters from the laser diffraction method are calculated assuming spherical particles, so incorrect values may be obtained for irregular or needle-shaped particles. Thus the size distribution for all the test powders was checked by image analysis using a scanning electron microscope and a stereomicroscope, as discussed later in section 2.2.4.

2.2.2 Moisture content

Moisture content by weight was determined using a Halogen Moisture Analyzer HB43 (Mettler Toledo, OH, USA.). The analyzer consists of a halogen heating unit, a sample plate and an electronic weighing balance. The instrument works on the thermogravimetric principle: the moisture analyzer determines the weight of the sample at the start, the sample is then quickly heated by the integral halogen heating module and the moisture vaporizes. During the drying process, the instrument continually measures the weight of the sample and displays the reduction in moisture. Once the drying has been completed as indicated by no further reduction in sample weight, the moisture or

solids content of the sample is displayed as the final result. The measurements were carried out in triplicate and an average value was determined.

2.2.3 Density measurements

The loose-packed bulk density of the test powders was measured by a device according to the specifications of ISO 3923/1 standard as mentioned by Wong (2000). The opening of a conical funnel was blocked with a plug and powder material was charged in it. A graduated cylinder was placed exactly below the funnel opening. When the plug from the funnel was removed, the powder filled the cylinder directly underneath it. Care was taken not to impose any stress on the powder in the cylinder and excess powder was removed from the cylinder. The loose-packed bulk density was calculated from the ratio of the mass of powder in the graduated cylinder to the powder volume.

Skeletal density (also known as solid density) was measured using the Ultrapycnometer (Quantachrome, FL, USA) which works on the basis of gas displacement. The instrument determines the true (skeletal) density of solid objects or powders based on the following equation assuming an ideal gas:

$$V_p = V_c + \frac{V_a}{1 - \frac{P_2}{P_3}} \quad (2.2)$$

The general principle is that the solid powder sample of unknown volume V_p is placed in a known sample cell volume V_c , and pressurized with helium gas to the desired target pressure P_2 . The ultrapycnometer has an internal “added volume” chamber (V_a) which is added to the cell volume by opening a valve between the two chambers. The resulting lower pressure P_3 is then recorded, allowing the calculation of V_p . The ultrapycnometer is programmed to perform the above pressurizations and valve

openings automatically. V_a and V_c are known through accurate calibration using the provided calibration spheres. The helium is able to fill all spaces open to the atmosphere, including the pores inside the powder sample. The skeletal density is calculated from the volume of sample and the known sample mass. The instrument reports an average value from the number of runs specified by the user. The specified number of runs is input with a numeric keypad on the front of the Ultrapycnometer.

2.2.4 Image analysis

The image analysis method determines particle size and shape parameters based on two dimensional images of powder samples. This section gives a brief description of the instruments used for capturing images, the processing and handling procedures, and the selection of suitable descriptors to define powder shape.

2.2.4.1 Image analysis equipment

The stereomicroscope and the scanning electron microscope (SEM) used in the present study are powerful tools for the determination of powder properties such as diameter, projected surface area, perimeter and circularity based on two-dimensional data from a projected or sectioned image of a powder sample.

Stereomicroscope:

The Olympus SZ61 Stereomicroscope equipped with a microscope digital camera DP12 (housed in the University of Saskatchewan Toxicology Centre) was used for image analysis in the present study. The microscope creates magnified images (up to 90X magnification) of powder samples, and transfers them to a personal computer for further image analysis. The powder samples were taken from different locations in the

powder container so as to obtain a representative sample. To generate an image of a powder sample, the powder sample was sprinkled on a Petri dish to form an array of non-overlapping particles such that only individual particles were analyzed. The Petri dish was then positioned under the microscope equipped with an illumination source from the bottom to provide a good contrast between dish background and the particle boundary. As mentioned by Li et al. (2002), an average number of at least 500 particles or 5-20 micrographs are recommended by ASTM Standard E1382 for the determination of representative particle size or shape. Thus, 20 optical microscopic images from different regions in the dish and different samples were acquired by the digital camera at a magnification of 90X, with approximately 500 particles detected for each sample. The magnifications were calibrated by the Image-pro Discovery software using an image of a small graduated scale at the same magnification. The software was available from the toxicology centre, University of Saskatchewan.

Scanning electron microscope:

The JEOL 840A scanning electron microscope (SEM) (housed in the University of Saskatchewan, Department of Geological Sciences) was required in the present study for image analysis of aspartame powder as the limited magnification of the stereomicroscope failed to resolve the fine aspartame particles. SEM creates magnified images of powders by scanning their surfaces with electrons, rather than light waves. Because the SEM illuminates samples with electrons, the samples are required to conduct electricity. Therefore, SEM samples are coated with a very thin layer of gold by a machine called a sputter coater. The sample is then placed inside the vacuum column of the microscope through an air-tight door. After the air is pumped out of the column, an electron gun from the top emits a beam of high energy electrons. This beam travels

downward through a series of magnetic lenses designed to focus the electrons on a very small spot. Near the bottom, a set of scanning coils moves the focused beam back and forth across the specimen, row by row. As the electron beam hits each spot on the sample, secondary electrons are loosened from its surface. A detector counts these electrons and sends the signals to an amplifier. The final image is built up from the number of electrons emitted from each spot on the sample (Oatley, 1972).

2.2.4.2 Stereomicroscopy and SEM image analysis

Digital images of the test powders obtained from stereomicroscopy and SEM were processed using Image-pro Discovery software. The software is used to acquire, enhance and process the images. It also measures, analyzes and creates customized reports with images, data and text.

Particle shape parameters were evaluated based on the projected images of randomly positioned particles. Figure 2-1 shows a representative digital image of flour particles obtained from post-processing with the image analysis software. Individual particles were first labelled manually for future reference. The software measured the projected perimeter (P), counting all the pixels on the particle outline and the projected area (A), counting all the pixels inside the particle boundary. A circle inscribing the particle and the major and minor axes was drawn manually. The major axis (l) is a straight line connecting the two most distant points of the projection area; the minor axis (b) is a straight line perpendicular to the major axis which connects the two most distant points in that direction (Bouwman et al., 2004; Ulusoy et al., 2003). The geometrical parameters obtained were: the projected area (A) of the particle, the area of a circle

surrounding the particle boundary or convex area (A'), the perimeter (P) of projection, the major axis (l) and the minor axis (b).

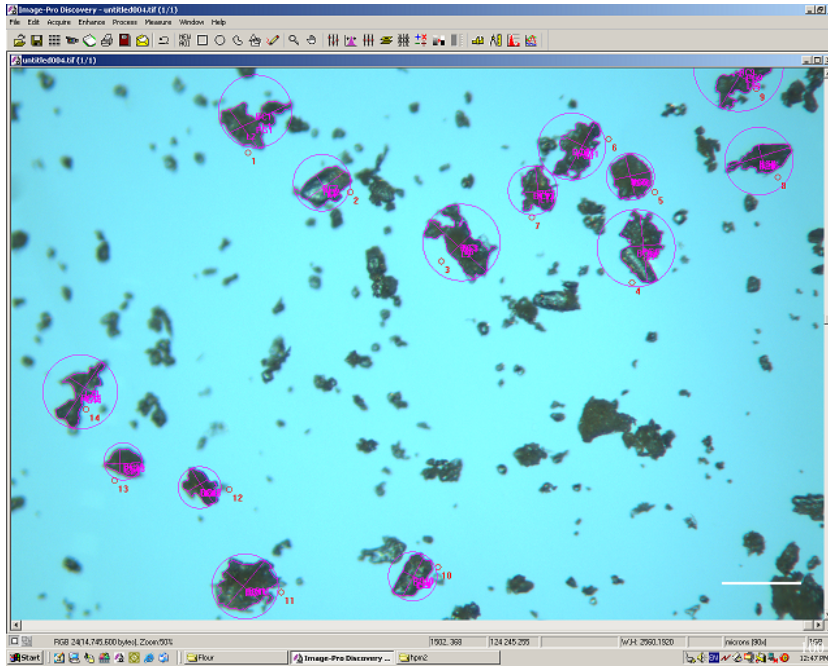


Figure 2-1 Digital image of flour particles obtained after processing from stereomicroscope

2.2.4.3 Selection of suitable shape descriptors

A variety of methods may be used to quantify powder shape, and according to Ulusoy et al. (2003), there is no universally accepted shape factor. Each factor will be sensitive to a specific attribute of shape depending on the parameters selected for its calculation. A common shape factor (and one of the earliest known) is the aspect ratio (ϕ_{AR}), which is the ratio of the length of the minor axis to the length of the major axis (Figure 2-2).

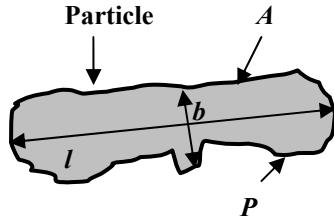


Figure 2-2 Characteristic dimensions used to calculate aspect ratio, roundness, and irregularity

$$\varphi_{AR} = \frac{b}{l} \quad (2.3)$$

Small values of the aspect ratio correspond to elongated particles. The aspect ratio only reflects the elongation of a particle, thus its usefulness is limited. Cox, as mentioned by Li et al. (2002) described a shape factor called circularity ($\varphi_{circularity}$) or roundness (R), which is based on the projected area (A) of the particle and the overall perimeter of the projection (P) according to the following equation,

$$R = \frac{4\pi A}{P^2} \quad (2.4)$$

The values of both the aspect ratio and the roundness approach unity for a perfectly spherical particle and 0 for an extremely elongated particle. Another descriptor, known as the irregularity factor (I), is the ratio of the projected perimeter of the particle to the major axis. According to Podczek (1997), elongation causes the value of this ratio to decrease, whereas irregularities cause an increase in this value.

$$I = \frac{P}{l} \quad (2.5)$$

Particle size and size distribution may be obtained from image analysis by using equivalent circle diameter (ECD), which is the diameter of a circle that has an area equal to the area of the particle (Li et al., 2002):

$$ECD = 2 \times \sqrt{\frac{A}{\pi}} \quad (2.6)$$

Various other shape factors reported in the literature were also calculated in the present study. These were: concavity based on area (CA), concavity based on perimeter (CP) and irregularity parameter (IP) calculated from the ratio of diameters of maximum inscribed (D) to minimum circumscribed circles (d) (Mikli et al., 2001). A' and P' are the area and the perimeter respectively of the maximum inscribed circle (Figure 2-3).

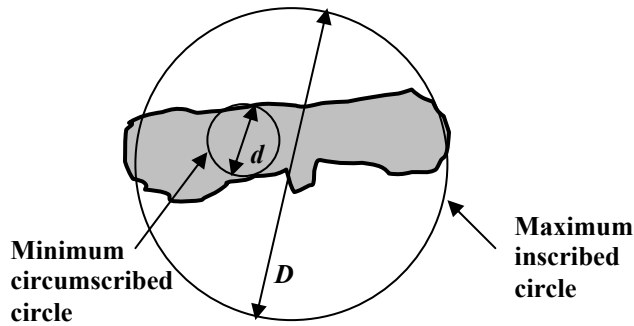


Figure 2-3 Illustration of the maximum and minimum inscribed circle diameter

$$CA = \frac{A' - A}{A'} \quad (2.7)$$

$$CP = \frac{P - P'}{P'} \quad (2.8)$$

$$IP = \frac{D}{d} \quad (2.9)$$

2.3 Measurement of powder flowability

In the present study, powder flowability was quantified based on the angle of repose, the shear strength and the tapped density. These flowability indicators were selected in this study as each of them represents a particular state of the powder material

generally found in process plants that handle them. Static angle of repose represents the state of powder in a heap, dynamic angle of repose represents a powder in motion, and Hausner Ratio, Carr index, and shear strength represents a powder in a compressed or consolidated state. This section briefly describes the equipment, calculations and the methods of operation associated with the various flowability tests.

2.3.1 Angle of repose

The angle of repose provides a reliable, quick and simple method to measure the flowability of different powders. Lower angles of repose correspond to freely flowing powders, whereas higher angles indicate a cohesive or poor flowing material. ISO 3435 utilizes this technique for quantifying the cohesiveness of the bulk material (Cain, 2002). Carr as mentioned by Riley et al. (1978), classified powders according to their flowability using the angle of repose, as indicated in Table 2-1.

Table 2-1 Carr classification of powder flowability based on angle of repose

Description	Angle of repose
Very free flowing	25-30°
Free flowing	30-38°
Fair to passable flow	38-45°
Cohesive	45-55°
Very cohesive	>55°

Values of the angle of repose reported by different researchers are difficult to compare since a range of equipment and methods have been used to evaluate them. Fayed and Otten, as mentioned by Wouters and Geldart (1996), defined the angle of repose as “the angle formed between the horizontal plane and a sloped line extending along the face of a heap formed by pouring material onto the horizontal surface”. This

angle is also known as the static angle of repose, as shown in Figure 2-4a. The dynamic angle of repose is measured in a rotating cylinder, as shown in Figure 2-4b.

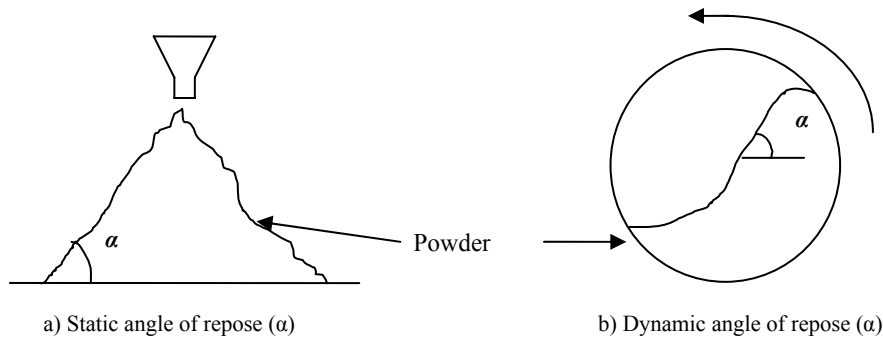


Figure 2-4 Illustration of a) static angle of repose and b) dynamic angle of repose

2.3.1.1 Measurement of static angle of repose

The device used to measure the static angle of repose in the current study consisted of a glass conical funnel, with an outlet diameter of 0.9 cm, fixed on a metal stand, as shown in Figure 2-5. The funnel outlet was kept at a height of 6 cm above the base as per ISO 3435/1. A digital camera was positioned exactly in front of the funnel to take digital images, which were then analyzed for static angle of repose using the computer software ‘Scion Image’ (www.scioncorp.com).

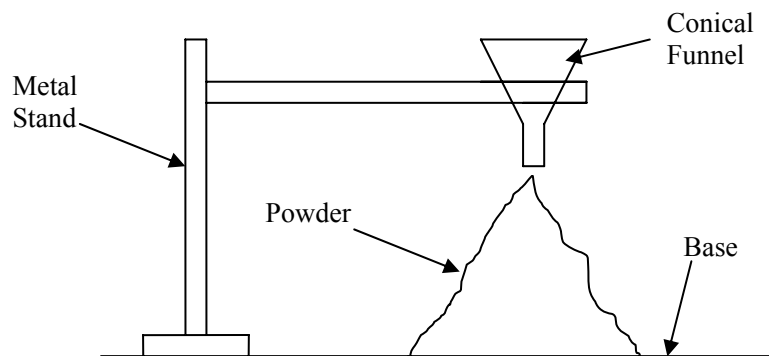


Figure 2-5 Measurement of static angle of repose

The funnel outlet was closed and 200 g of powder sample was poured in. Once the outlet was opened, the powder material flowed out to form a cone on the base. Still photographs were captured using the camera and then fed to the computer program for determining static angle of repose. This procedure was repeated four times for each powder sample and an average value was calculated. Figure 2-6 shows a sample digital image of the aspartame powder used in calculation of the static angle of repose.

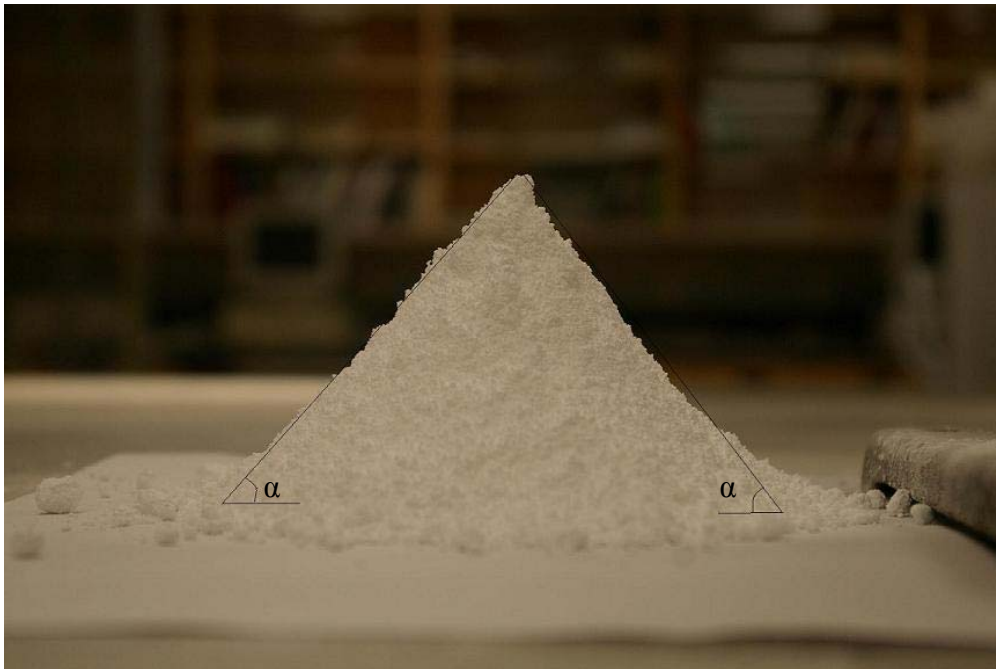


Figure 2-6 Sample image used to determine the static angle of repose (α) for aspartame

2.3.1.2 Measurement of dynamic angle of repose

A novel method to measure the dynamic angle of repose using electrical capacitance tomography (ECT) was developed in the present study. This section gives a brief description of the equipment and method of operation for determining the dynamic angle of repose using ECT.

As per Dury and Ristow (1998), when granular materials are put in a rotating drum, avalanches are observed along the surface of the granular bulk. As the rotation

speed increases, these intermittent avalanches give way to a continuous surface which may be used to define the dynamic angle of repose. The dynamic angle of repose is the angle formed by the inclined surface of a powder with the horizontal when rotating in a cylinder (see Figure 2-7a). Increasing the rotation speed further deforms the flat surface to an *S* shaped profile (Castellanos and Valverde, 1999; Yamane et al., 1995). The deformation starts mostly from the lower boundary inwards and can be well approximated by two straight lines with different slopes. The line with higher slope, as shown in Figure 2-7b, is taken for measurement of the dynamic angle of repose (Dury and Ristow, 1998; Carr, 1965). The greater the angle of repose, the greater is the cohesiveness of the powder, whereas the lower the angle of repose, the more free flowing the bulk material will be (Wouters and Geldart, 1996).

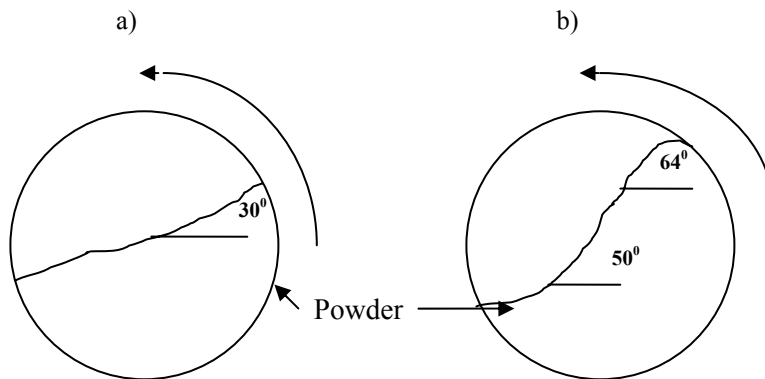


Figure 2-7 Dynamic angle of repose (Castellanos and Valverde, 1999)

Various methods have been used in previous studies to measure the dynamic angle of repose. One of the most common method is to use a horizontal cylindrical drum, designed to rotate around its horizontal axis (Castellanos and Valverde, 1999). A video camera connected to a computer and placed at one of the end of the drum is used to record the movement of powder inside the cylinder and perform the image analysis. This procedure is quite simple to use, but has the disadvantage of the effect of end caps.

It has been found that the dynamic angle of repose is up to 5° higher at the end caps of the drum due to boundary friction (Dury and Ristow, 1998), which thus gives incorrect measurements. The TSI Aero-flow™ automated powder flowability analyzer described in chapter 1 may also suffer from the end cap effect. Furthermore, the commercial TSI Aeroflow device relies on a complex off-line analysis for calculating the angle of repose.

DEM (Distinct Element Method) and non-invasive MRI (Magnetic Resonance Imaging) methods have been used to study particulate flows in a partially-filled, horizontal rotating cylinder and for measuring the dynamic angle of repose (Yamane et al., 1995, Yang et al., 2003). In DEM simulation, the motion of every particle is calculated from equations of motion and the contact forces between particles are modeled using springs, dash-pots and a friction slider. In MRI experiments, protons (nuclei of hydrogen atoms) are usually used because of their high sensitivity and abundance in nature. Other methods commonly used to study particle flow in a horizontal rotating drum include Positron Emission Topography (PET) and Positron Emission Particle Tracking (PEPT) (Yang et al., 2003).

According to Fitzpatrick and Ahrne (2005) it might take many years before these techniques will be useful for design involving real powders. Cohesive powders involve many parameters which affect powder flowability. Such parameters are difficult to quantify both analytically and experimentally due to difficulties in describing multibody interactions and in measuring interparticle forces in such dynamic environment.

ECT system to measure dynamic angle of repose:

A novel approach to determine the dynamic angle of repose using electrical capacitance tomography was used in the present study. Electrical capacitance tomography (ECT) is a non-intrusive imaging technique based on differences in the

permittivity or dielectric constants of air and granular material (McKeen and Pugsley, 2002). ECT gives a cross-sectional image of the process vessel based on the rapid measurement of electrical capacitance between all unique combinations of electrodes wrapped around the periphery of the cross-section of the vessel to be imaged. These capacitance data are then transformed into the permittivity distribution over the given cross-section. Spatial information are obtained by processing these quantities, which gives the cross sectional images. Various image reconstruction algorithms are available for the processing of capacitance data.

The ECT system shown in Figure 2-8 was used in the present study. This system, which was supplied by PTL (Process Tomography Limited, UK), consists of a single-plane capacitance sensor unit, a data acquisition module and a personal computer equipped with custom communication hardware. The capacitance sensor unit consists of a copper foil wrapped around the outside of a 7.6-cm inside-diameter Plexiglas pipe. Twelve electrodes, 10 cm long are etched into the copper sheet. The sensor is connected to the data acquisition module (DAM) which measures the inter-electrode capacitance and which, in turn, is connected to the computer system. The basic measuring circuit works on the charge transfer principle in which one electrode of the pair is the source electrode, while the other is a detector electrode held at ground potential. The electronic controls of the DAM ensure that only one electrode at a time is configured as a source electrode, whereas the remaining ones are detector electrodes (PCECT system operational manual, 1998).

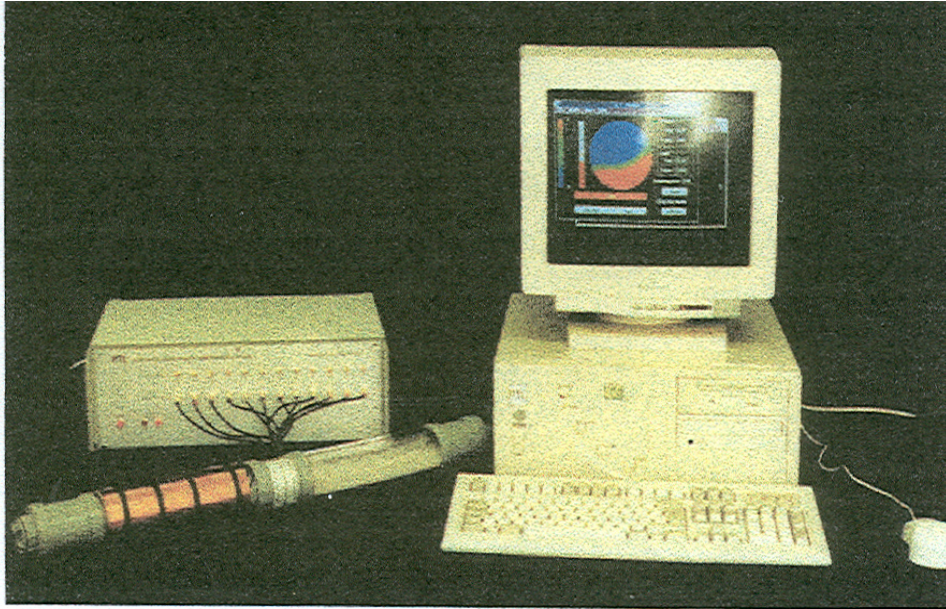


Figure 2-8 Electrical Capacitance Tomography equipment (PCECT, 1998)

A practical limitation of using this equipment to measure the dynamic angle of repose was the twisting of the leads from the sensor to the data acquisition module. Thus a paper towel tube of diameter 4 cm and 31 cm length was inserted inside the sensor tube, and this paper tube was rotated using a variable speed motor. The axis of the paper tube was concentrically aligned with the axis of the sensor tube. The paper tube was selected based on previous studies by McKeen and Pugsley (2002). They observed that the paper tube was not detected by the ECT sensor, thus the flow inside the paper tube becomes visible and can be used to measure the dynamic angle of repose when the paper tube is filled with powder. Both ends of the paper tube were closed using rubber caps. A fine sand paper was glued on the inside of the tube to make it rough so as to prevent the powder from sliding (Thalberg et al., 2004). The ECT set-up for measuring the dynamic angle of repose in the present study is shown in Figure 2-9.

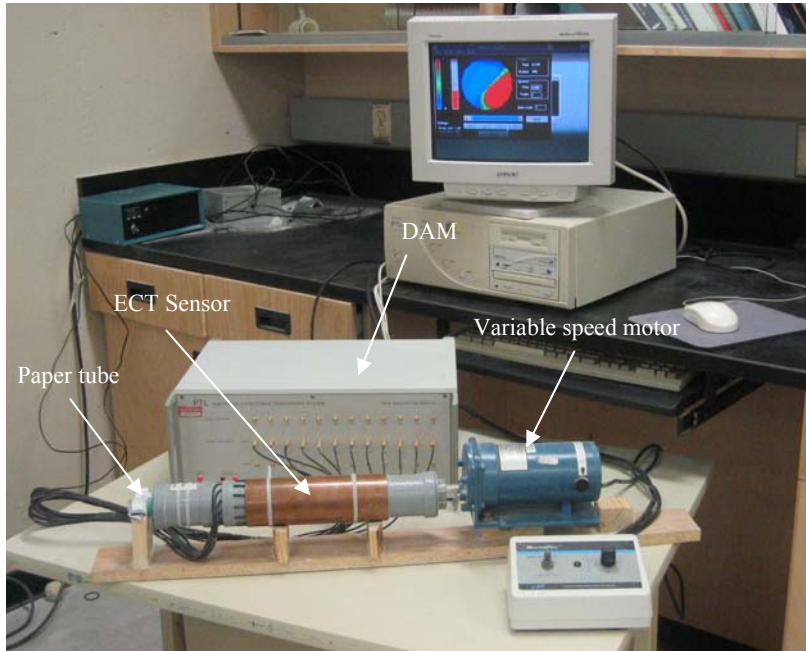


Figure 2-9 Equipment used to measure dynamic angle of repose

The ECT calibration is based on the measurement at two endpoints: the sensor full of low permittivity material (air/sensor empty) and full of high permittivity material (packed bed of powder material in the sensor). After calibration, the paper tube was filled to 30% of its volume with the powder material, closed at the ends with rubber caps and inserted inside the sensor pipe. The amount of powder material to be filled into the paper tube was determined by a trial and error method so as to get a clear ECT image. One end of the paper tube was connected to the variable speed motor by a rod while the other end was placed on a wooden support, as shown in Figure 2-9. The DAM and the computer were turned on and the data collected. Different sets of data were collected by varying the motor rotation speed from 10 RPM to 90 RPM for all powder materials. The iterative linear back projection method with the parallel permittivity model (McKeen and Pugsley, 2002) was used for image reconstruction.

The dynamic angle of repose can be readily determined from the reconstructed ECT image of the air-powder interface inside the tube. ECT images were collected for 15 seconds at a rate of 100 frames per second, or 100 Hz. The angle of repose was measured based on the image collected at every fifth frame using the image analysis software, Scion Image. These images are then fed to a computer program, Platypus Animator, which creates a “movie” file by sequencing the individual images. This file was used to analyze the powder flow qualitatively. ECT gives a cross-sectional image of the centre of the sensor tube, thus the effect of the end caps generally encountered by other methods is eliminated. A typical image taken by ECT to measure the dynamic angle of repose is shown in Figure 2-10.

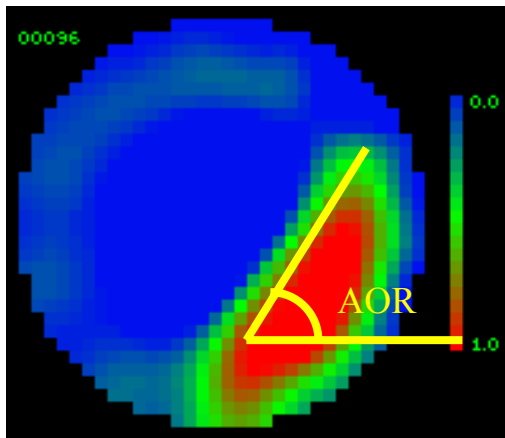


Figure 2-10 ECT image used to determine the dynamic angle of repose

2.3.2 Density measurements

In this study, the loose bulk density was measured according to the ISO 3923/1 standard (Wong, 2000), as mentioned in section 2.2.3. The tapped density was measured using a tapped density tester, as described below. The Hausner ratio and Carr index were determined according to equations 1.1 and 1.2 (Section 1.2.2.2)

2.3.2.1 Tapped density tester equipment and operation

The tapped density was measured using a single platform tapped density tester (Varian Inc., NC, USA), as shown in Figure 2-11.

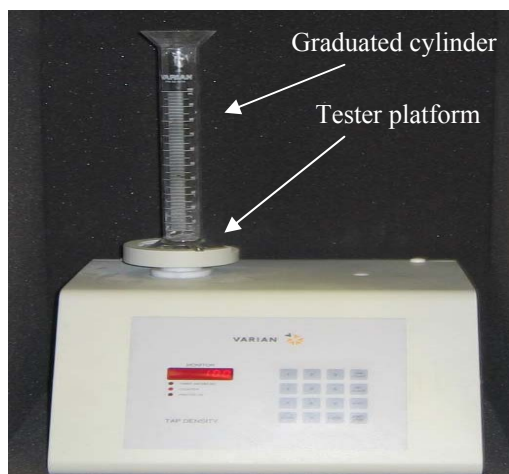


Figure 2-11 Tapped density meter

The tester essentially consists of a graduated cylinder placed on the tester platform. The tapping action is generated by a camshaft which lifts the platform and allows it to drop back to its original position. A shoulder machines into the cam causing the platform to rotate approximately 5-15 times per minute, ensuring an evenly packed surface. The normal speed is 300 taps per minute. The number of taps can be selected from a user interface. In this technique, taps were applied until a maximum packing condition was achieved. The level of powder in the graduated cylinder was checked after every 10 taps till there was no further reduction in level. This was taken as the tapped volume which was used for calculating the tapped density. The measurements were done in triplicate and an average value was reported.

2.3.3 Flowability based on the shear characteristics of a powder

A parallel plate shear cell, which is similar to the Jenike shear cell in its method of operation, was used in this study. This section gives a brief description of the parallel plate shear tester equipment, its operating principle and relevant calculations.

2.3.3.1 Construction of parallel plate shear tester

A parallel plate shear cell is shown in Figure 2-12. The upper shear ring is fixed, whereas the lower base plate can advance either in forward or reverse direction at a fixed shear rate which is controlled by the mechanically driven stem. A normal force is applied at the upper surface of the powder, allowing the shear behaviour of the powder to be determined at various consolidating stresses.

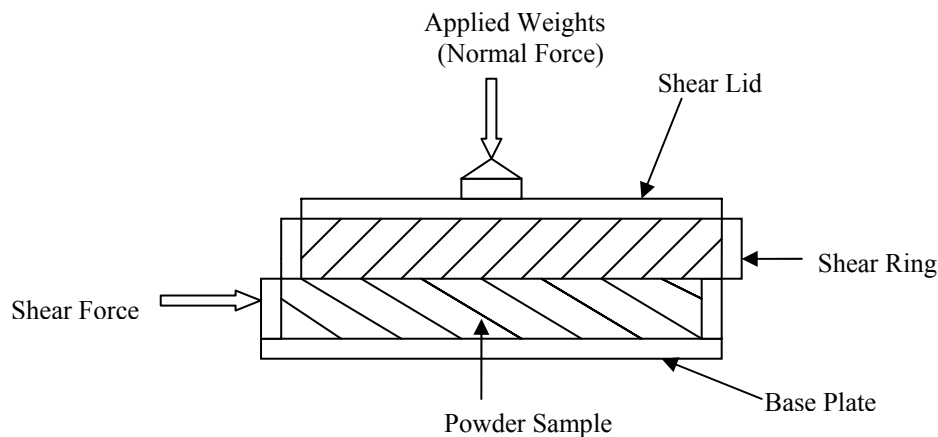


Figure 2-12 Parallel plate shear cell

Along with the shear cell, the tester consists of a load cell to measure the shear force, an amplifier, and a recorder. Data was collected continuously using a data acquisition module connected to a computer, which gives a plot of the shear force versus shearing distance.

2.3.3.2 Operating procedure and calculations

The procedure outlined in the ASTM standard D 6128-00 for the Jenike shear cell was followed for the parallel plate shear cell in the present study. The test sample was loaded into the shear cell without applying any force to the surface of material until the material was over the top of the cell. The excess material was removed using a blade. The weights were placed on the lid and then removed to see if the level of material has dropped. Any empty space was filled with additional powder, and this procedure was repeated until there was no further drop of the powder surface. The shearing procedure involves two steps: preshear and shear.

Preshear: Three normal preshear values of 2 kPa, 4.41 kPa and 6.51 kPa were selected for all test powders. These values were selected in accordance with the ASTM standard values which were based on bulk density of materials. Once the cell was switched on, the shear stress in the powder increased to a steady state value, which was observed in the shear force-shearing distance plot on the computer screen. This constant value was maintained through a relatively short distance and then the cell was reversed until the stem lost contact with the bracket and the value of shear stress was zero.

Shear: For the second stage, three shear normal stress levels within the range of 25 to 80% of the preshear normal stress were selected and shearing was done for a full shear distance of 6 mm. A shear plane developed in the specimen of the powder in the cell. When the stem touched the bracket, the shear force increased to reach a maximum value. The plot of shear force vs. shearing distance was recorded by the computer. This procedure was repeated for all three values of preshear normal stresses.

Figure 2-13 shows a typical plot of shear stress versus displacement (Strain %) for the placebo granulate at 2 kPa normal preshear stress and 1 kPa normal stress. The displacement (Strain %) was taken as the ratio of horizontal displacement of the base plate to the length of the sample along the direction of shear.

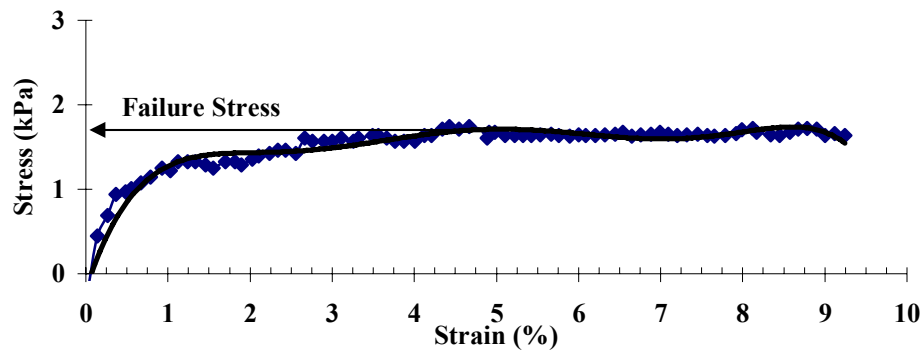


Figure 2-13 Shear stress-strain plot for the placebo granulate at 2 kPa preshear normal stress and 1 kPa normal stress

The failure shear stress point was recorded where the curve reaches a constant value or the maximum value. Three failure shear stress points were recorded at different normal stresses for each powder at given normal preshear stress and plotted against the corresponding normal stress, to give the yield locus for the powder. A typical yield locus is shown in Figure 2-14, where τ is the failure shear stress and σ is the corresponding normal stress.

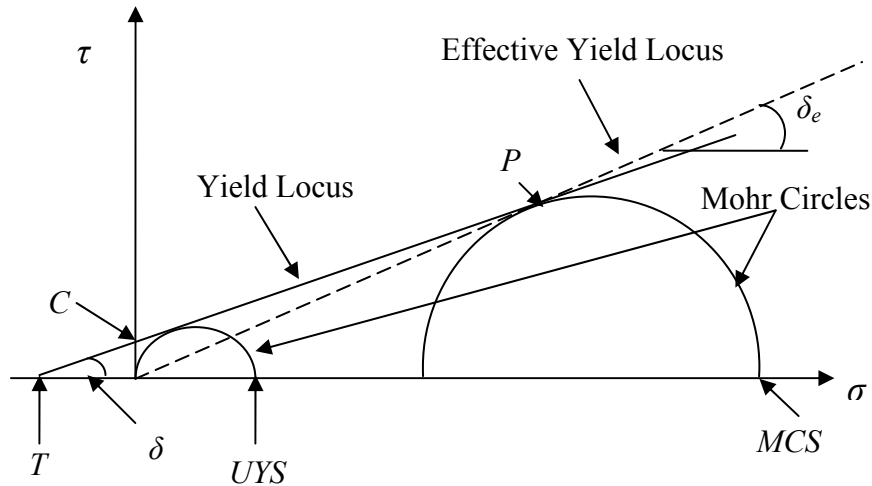


Figure 2-14 Typical yield loci (Fitzpatrick et al., 2004)

Figure 2-14 illustrates some key powder properties that correspond to various points on the graph. C is the cohesion of the powder, and is obtained from the intercept of the yield locus on the shear stress axis. It represents the shear strength of the powder at zero normal stress. T is the tensile stress of the powder material, which is obtained from the intercept of the yield locus with the normal stress axis. A Mohr circle is drawn passing through the origin and tangential to the extrapolated yield locus. The higher point of intersection of this Mohr circle with the normal stress axis gives a value called the unconfined yield stress (UYS). A second Mohr circle tangential to the end point of the yield locus is also drawn. The end point of yield locus corresponds to the value of preshear normal stress (P). The right hand side intercept of this second Mohr circle with the normal stress axis gives a value called as the major consolidating stress (MCS). The effective yield locus line is drawn passing through the origin and tangential to the second Mohr circle. The angle made by this line with the normal axis gives the effective angle of internal friction (δ_e), which is a measure of the friction between the particles

(Fitzpatrick et al., 2004). The angle made by the yield locus with the horizontal is the angle of internal friction (δ).

The corresponding yield loci were obtained by repeating the above procedure for all powders at three different normal preshear stresses, thus three different *UYS* and *MCS* values were obtained for each powder. A plot of *UYS* and *MCS* is called a flow function, and represents the strength developed within the powder when consolidated. It is this strength that must be overcome to make the powder flow (Fitzpatrick et al., 2004). Jenike defines the flow function (*FF*) as (Seville et al., 1997):

$$FF = \frac{\text{Unconfined Yield Strength (UYS)}}{\text{Major Consolidating Strength (MCS)}} \quad (2.12)$$

A typical plot of flow function is shown in Figure 2-15. According to Fitzpatrick et al. (2004) a flow function line located at the bottom of the graph represents easy flowing material, whereas more difficult flow is represented as the flow function line moves in a counterclockwise direction.

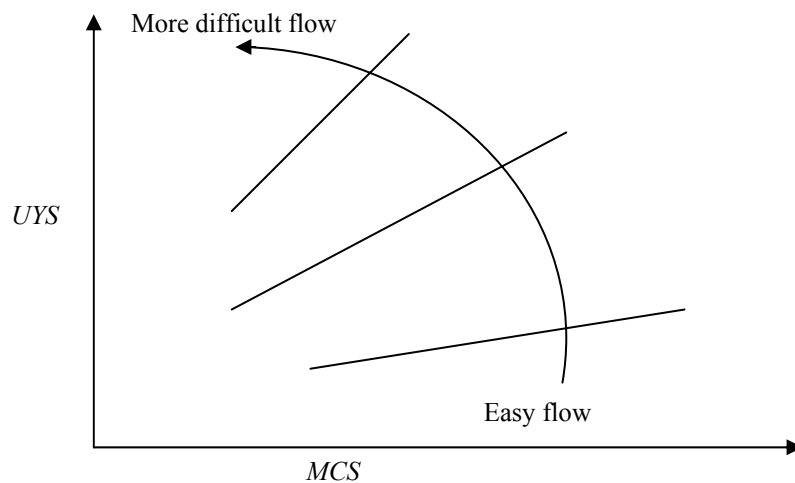


Figure 2-15 Flow function lines (Fitzpatrick et al., 2004)

The flow index obtained from the inverse of the slope of the flow function line was used by Jenike to classify powder flowability as presented in Table 2-2. The greater the flow index, the better the flowability.

Table 2-2 Jenike classification of powder flowability based on flow index (Teunou and Fitzpatrick, 2000)

Flowability	Hardened	Very cohesive	Cohesive	Easy flow	Free flowing
Flow index	<1	<2	<4	<10	>10

3 RESULTS AND DISCUSSION

This chapter describes the various experimental results obtained using the techniques described in chapter 2. Particle size and size distribution were determined using two different techniques. Other powder physical properties analyzed include moisture content, density and shape. The particle shape is quantified from image analysis using different shape factors, with each shape factor indicating a specific shape attribute. The results from the flowability measurements have been presented. Finally, the various flowability indicators are plotted against the powder physical properties in order to better understand their relationship.

3.1 Fine powder physical properties characterization

The fine powders used in the present research work were aspartame, respitose ML001, lactose monohydrate, HPMC, placebo granulate, and pastry flour. The physical properties of particle size, size distribution, shape, moisture content, and density were determined using techniques described in the previous chapter.

3.1.1 Particle size distribution from the laser diffraction method

The size distributions of the various test powders, as measured by laser diffraction with the Malvern Mastersizer-S long bench, are shown in Figure 3-1.

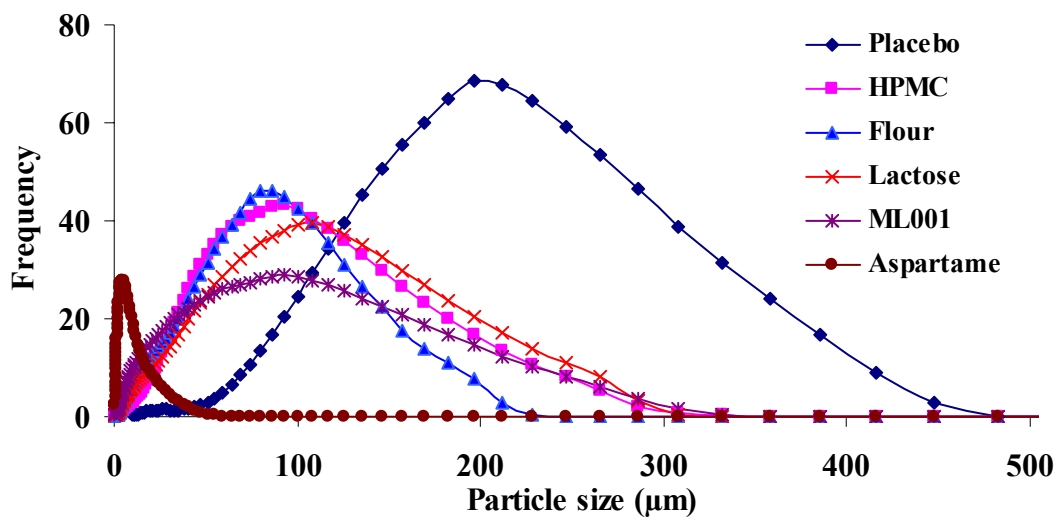


Figure 3-1 Size distributions of the various test powders from laser diffraction method

The placebo granulate had the widest particle size distribution, whereas aspartame had the narrowest distribution. The Sauter mean and volume mean diameter values were smallest for aspartame powder and greatest for the placebo granulate. These values are reported in Table 3-1. Figure 3-1 and Table 3-1 illustrate that the size distributions and mean diameters of the remaining four powders were all in a similar range. Appendix A shows the plot of volume undersize particles versus the particle size.

Table 3-1 Physical properties of test powders

Test powder	Sauter mean diameter (µm)	Volume mean diameter (µm)	Moisture Content (%)	Loose bulk density (kg/m ³)	Skeletal density (kg/m ³)
Aspartame	3	37	3.92	190	1656
ML001	52	110	2.97	610	1531
Lactose	25	89	4.02	675	1550
Flour	27	71	8.58	570	1700
HPMC	36	88	2.72	495	1432
Placebo	163	223	4.84	675	1682

3.1.2 Moisture content from halogen moisture analyzer

The moisture content was determined using the moisture balance described in section 2.2.2. The average moisture contents of the test powders based on three independent moisture measurements on each powder are reported in Table 3-1. The moisture content was found to be lowest for HPMC and highest for the flour powder. Since the moisture content of flour was much higher than that of the other powders, it was deemed necessary to dry the flour sample in advance of the flowability tests. Furthermore, the rate of moisture uptake was determined to see if the flour powder absorbed moisture from the atmosphere during the flowability tests, which would affect the results. This was done by first drying the sample in an oven for 30 minutes until the moisture content in the sample was only 0.17 wt%. The dried sample was exposed to the surrounding environment, and the increase in moisture content was determined at half hour intervals. Figure 3-2 shows a plot of the increase in moisture content with time for flour.

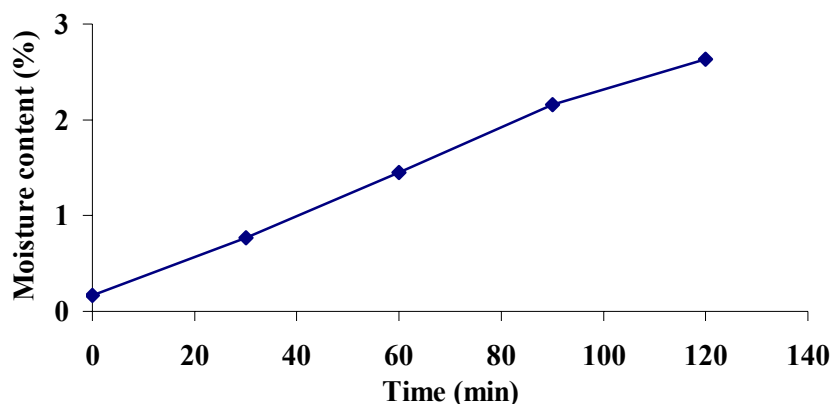


Figure 3-2 Variation of moisture content with time for flour

From this plot, it was concluded that the flowability tests for flour were not significantly influenced by moisture uptake, since each of the tests were carried out in less than 15

minutes using a dried sample. These results may vary depending upon the temperature and humidity of surrounding atmosphere. The moisture contents of the remaining powders were found to be in similar range.

3.1.3 Density measurements

Loose bulk density for the various test powders was measured according to the specifications of ISO 3923/1 standard as discussed in section 2.2.3. The loose bulk density was found to be lowest for the aspartame powder and highest for the lactose powder and placebo granulate. Skeletal density was measured using helium pycnometry as described in section 2.2.3. Skeletal density was highest for flour and lowest for HPMC. These density values are reported in Table 3-1.

3.1.4 Particle shape analysis

The images of the different test powders obtained from the stereomicroscope at 90X magnification are shown in Figure 3-3 below.

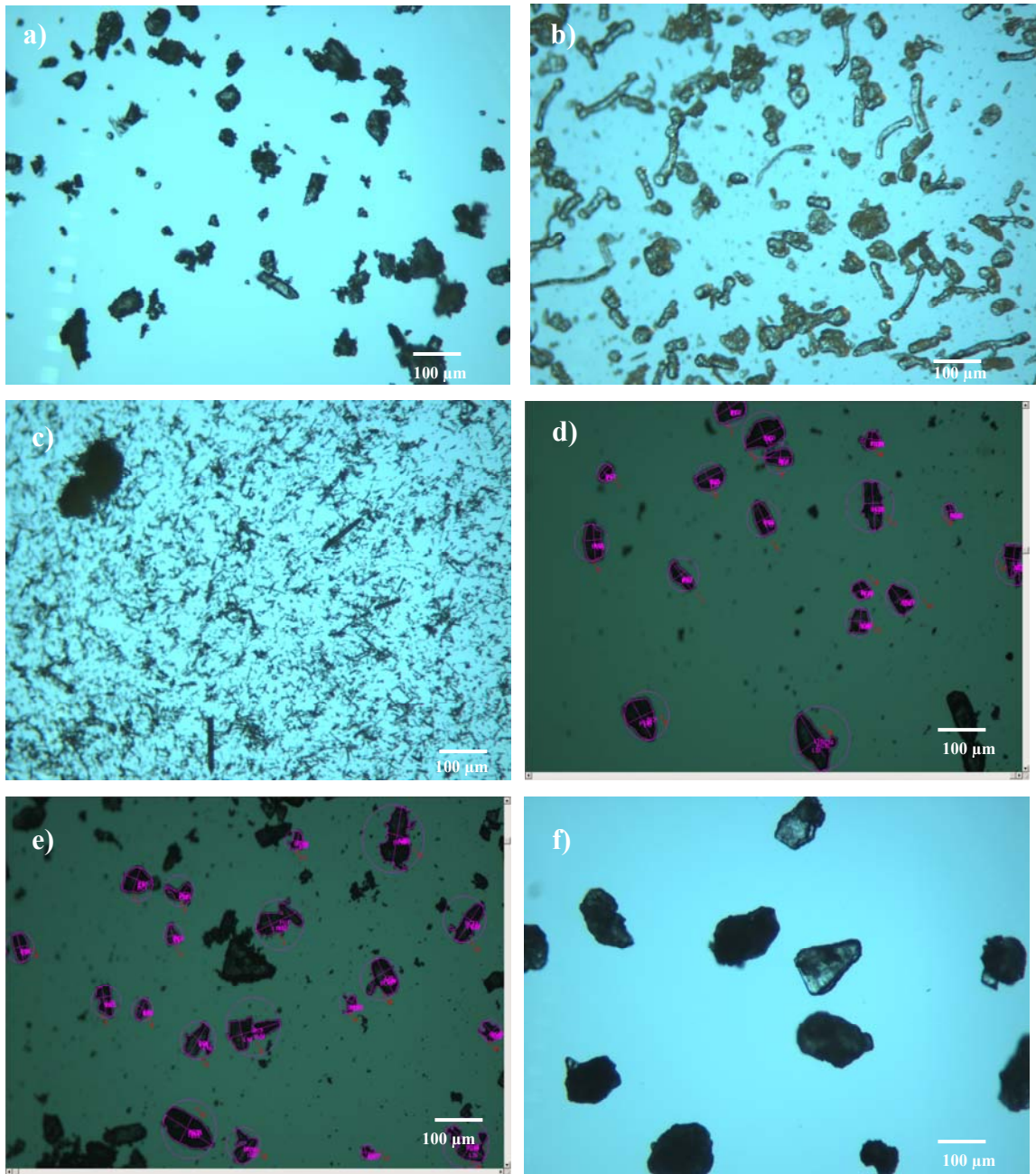


Figure 3-3 Micrographs obtained from stereomicroscopy: a) Flour; b) HPMC; c) Aspartame; d) Respitose ML001; e) Alpha-D-Lactose monohydrate; f) Placebo granulate

From Figure 3-3 it can be observed that the test powders exhibited different shapes and sizes. Flour particles were found to be irregular, HPMC had particles ranging from spheres to elongated shapes with smooth edges, ML001 particles were spherical and irregular, lactose particles were irregular, and the placebo granulate was found to be large and mostly spherical. It can be seen from the micrograph for aspartame (Figure 3-3 c) that the stereomicroscope was not able to resolve the fine aspartame particles because of its limited magnification. Thus a scanning electron microscope (SEM) was used to obtain digital images of aspartame powder at higher magnifications. Figure 3-4 shows the images of aspartame powder at 200X and 500X magnifications. It can be observed from the SEM micrographs for aspartame that these particles were essentially needle-shaped, consisting of small angular fines.

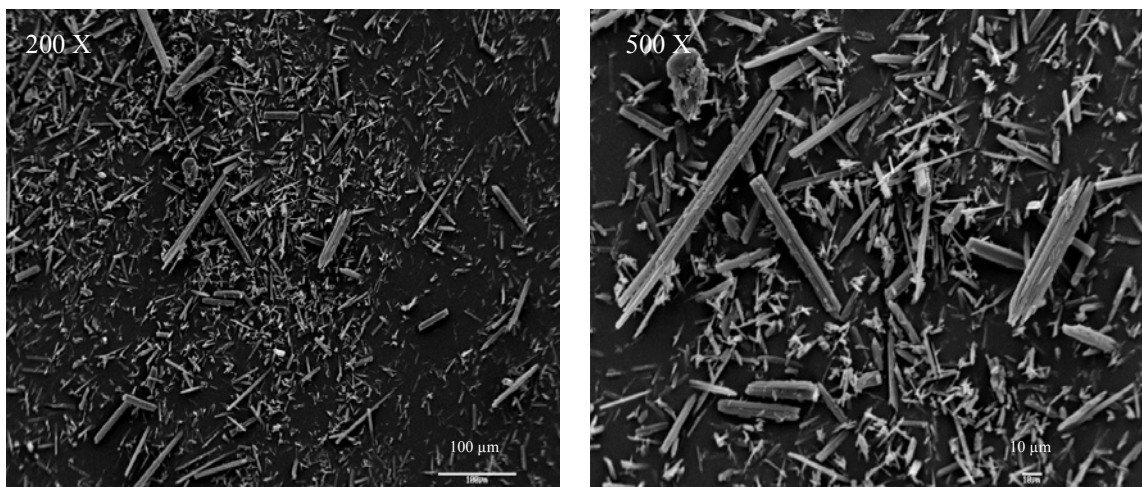


Figure 3-4 SEM micrographs for aspartame at different magnifications

Approximately 20 micrographs for each test powder were obtained from the stereomicroscope and SEM and fed to the computer program ‘Image-Pro discovery’ for obtaining various particle dimensions. Particle shape factors were calculated from the particle dimensions using equations (2.3) to (2.9) and were compared with the observable particle features from the digital images. For characterization of particle

shape, the aspect ratio, roundness and irregularity were found to be the best. Each of these shape factors was found to be sensitive to a specific attribute of particle shape. Aspect ratio gave an indication of the elongation of a particle, roundness indicated how closely the projected area of a particle approached a circle, and irregularity gave an indication of whether or not the particle was elongated or irregular.

Concavity (*CA* and *CP*) were found to be very similar to roundness, while the irregularity parameter (*IP*) failed to distinguish between irregular and elongated particles. Thus, in the present study only the aspect ratio, roundness, irregularity and equivalent circle diameter were used to study the influence of shape. Particle size was determined using equivalent circle diameter as it was based on the true projected area of the particle taking into account the particle shape. The values of the various shape factors are reported in Table 3-2 for each of the powders studied.

Table 3-2 Values of various particle shape parameters from image analysis

Powder material	Aspect ratio (ϕ_{AR})	Roundness (R)	Irregularity (I)	Equivalent circle diameter (ECD) (μm)
Aspartame	0.19	0.28	2.62	3.45
ML001	0.63	0.7	3.96	56
Lactose	0.56	0.55	3.77	71
Flour	0.56	0.47	4.21	107
HPMC	0.44	0.46	3.01	102
Placebo	0.71	0.67	3.3	172

As seen in Table 3-2, the values of aspect ratio for aspartame and HPMC are lower than the other powders, indicating the presence of elongated particles, whereas the roundness factors for the placebo granulate and respitose ML001 are higher, reflecting

their more spherical shape. The elongated shape of aspartame and HPMC particles is also confirmed by the lower values of irregularity factor as seen in Table 3-2. Higher values of the irregularity factor for flour, lactose and ML001 suggest that they are irregular in shape since the digital images show that they are not particularly elongated.

Considering the shape parameters in combination can give more detailed information. For instance, ML001 is more spherical and irregular as indicated by the higher values of both roundness and the irregularity factor (Table 3-2).

Aspartame had the smallest equivalent circle diameter as compared to the other powders, whereas the placebo granulate had the largest diameter (Table 3-2). This finding is qualitatively consistent with the results from laser diffraction measurements of particle size. Figure 3-5 shows a comparison of the various mean diameters obtained from image analysis and laser diffraction method.

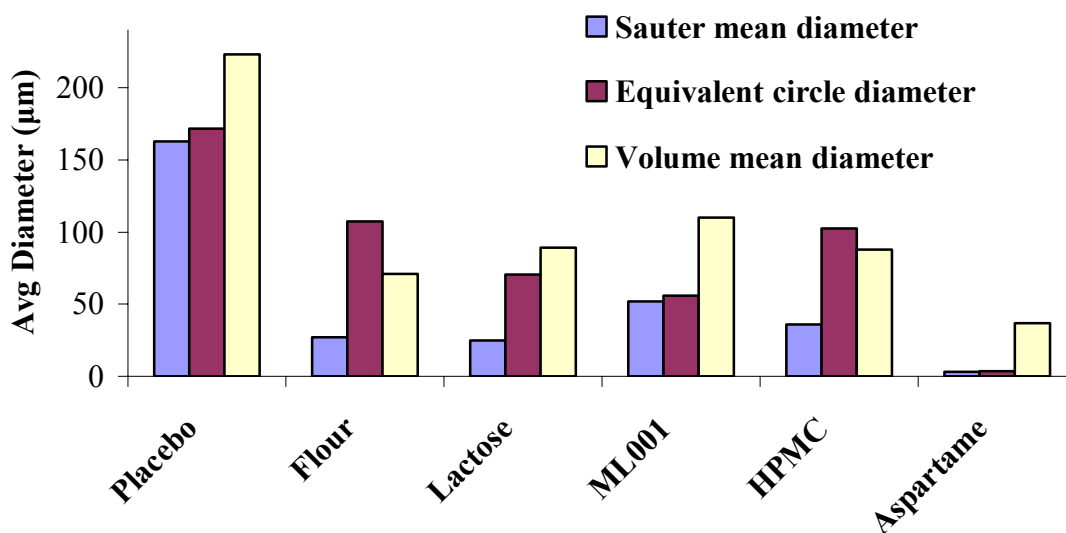


Figure 3-5 Comparison of mean diameters obtained from image analysis and laser diffraction method

It is interesting to note in Figure 3-5 that for some powders (placebo, ML001, and aspartame) the equivalent circle diameter (ECD) agrees closely with the Sauter mean diameter (SMD), whereas for other powders (flour, lactose and HPMC) they are different. ECD and SMD calculations are done assuming that the surface area of a particle is equal to that of a circle and sphere respectively, so they might sometimes have close values (for example for placebo, ML001, and aspartame). However, during the flow of particles through the laser beam in laser diffraction, irregular or elongated particles might align themselves along the direction of flow of the air stream.

Kaye et al. (1999) compared particle size distribution values obtained from different techniques and image analysis and found striking differences in the values for irregular and elongated particles. According to Rawle (1999), each characterization technique measures a different property of a particle and thus will give a different answer from another technique which measures an alternative dimension. Thus, the close agreement in values for some powders may be just coincidence or due to their irregular or elongated shapes. The equivalent circle diameter is based on the area and true shape of the particle, which are known to have an effect on powder flow. Thus, in this study it is considered as a dimension for particle diameter.

3.1.5 Frequency distribution

It should be noted that all the values reported for shape factors and diameter are mean values obtained from the data of 500 particles for each powder material. In order to determine if these values are representative of the entire bulk, frequency distributions were prepared for all shape factors and the equivalent circle diameter. These plots are included in Appendix C for all test powders.

3.1.5.1 Equivalent circle diameter

Frequency distribution plots of equivalent circle diameter for all test powders showed that, all powders with the exception of aspartame, had diameters normally distributed about their mean. The frequency distributions of equivalent circle diameter for all the test powders are included in Appendix C1. Aspartame exhibited a large volume percent of fine particles less than 1 micron as can be clearly seen in Figure 3-6.

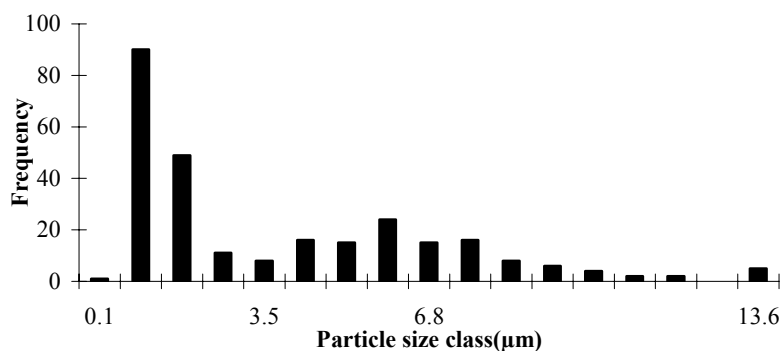


Figure 3-6 Frequency distribution of equivalent circle diameter for aspartame

Aspartame also exhibited a bimodal frequency distribution for the equivalent circle diameter, thus the mean value reported in Table 3-2 was calculated by taking the arithmetic average of the two peak values. A frequency distribution plot of equivalent circle diameter indicates the amount of fines in the powder bulk.

3.1.5.2 Shape factors

A frequency distribution of the shape factors indicates if the powder bulk consists of particles of varying shapes. The frequency distribution of roundness factor and aspect ratio for all the test powders except HPMC exhibited a normal distribution. HPMC had a wide distribution for aspect ratio and roundness factor, as shown in Figures 3-7(a) and 3-7(b).

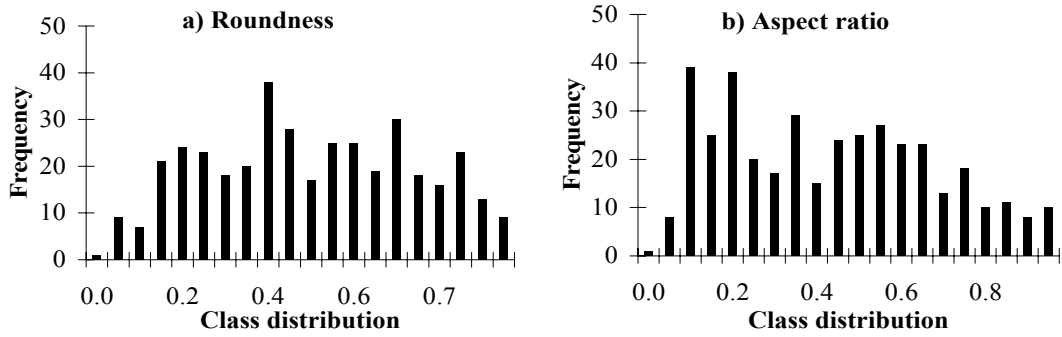


Figure 3-7 Frequency distributions of (a) roundness factor and (b) aspect ratio for HPMC

As can be seen in Figure 3-7, HPMC consists of particles of varying shapes, ranging from spheres to elongated particles as indicated by the broad range in the values of shape factors. The frequency distributions of the irregularity shape factor for all the test powders indicated a nearly normal distribution about the mean. Table 3-3 gives a qualitative summary of the shape attributes for all the test powders obtained from image analysis.

Table 3-3 Particle shape attributes of test powders

Powder	Particle shape
Aspartame	Needle shaped, large percent of fines
ML001	Spherical, but irregular
Lactose	Irregular
Flour	Irregular
HPMC	Small spherical to elongated
Placebo granulate	Large and spherical

3.2 Flowability measurements

Flowability indicators used in the present study included dynamic and static angles of repose, Hausner Ratio, Carr Index and Flow Index. The following sections report the results obtained from the various techniques used to measure the different flowability indicators.

3.2.1 Shear measurements

Three normal preshear stresses of 2 kPa, 4.41 kPa and 6.51 kPa (see section 2.3.3.2) were selected according to the ranges mentioned in ASTM standard D 6128-00, which are based on the bulk density of powders. Shearing was performed using normal stress values in the range of 25-80% of the preshear normal stresses. Three failure shear stress values were obtained for each normal preshear stress and plotted against the corresponding normal stress to give a yield locus. Different key powder properties such as cohesion (C), tensile strength (T), unconfined yield strength (UYS), major consolidating strength (MCS), and angle of internal friction (δ) were obtained from the yield locus. Appendix C reports the values of these powder properties obtained from the yield loci at different normal preshear stresses. A flow function plot was obtained for all the test powders from the values of UYS and MCS . The flow function line represents the strength developed within a powder material when consolidated. The flow function plot for all the test powders is shown in Figure 3-8.

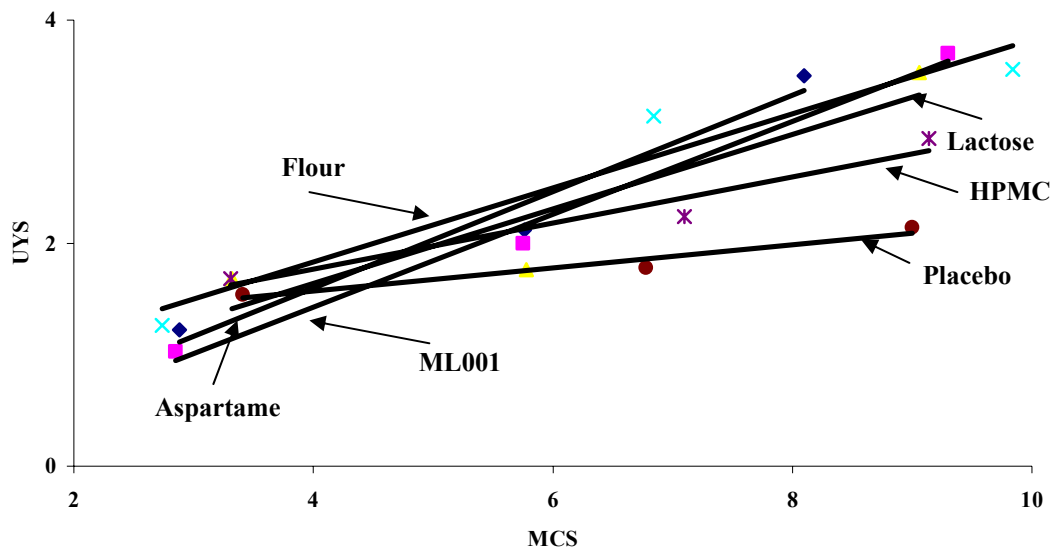


Figure 3-8 Flow function lines for test powders

A flow function line lying towards the bottom of the graph corresponds to powders that flow easily. As the flow function moves upwards in the counterclockwise direction, the corresponding powder flows less freely (Fitzpatrick et al., 2004). Flow function lines for placebo granulate and HPMC lie towards the bottom of the graph, indicating easier flow, whereas those for aspartame, ML001, lactose and flour lie towards the upper portion, indicating difficulties in flow. The flow indexes obtained from the inverse of the slope of the flow function lines for all the test powders are reported in Table 3-4.

Table 3-4 Flow index values for all test powders

Test powder	Aspartame	ML001	Lactose	Flour	HPMC	Placebo
Flow Index	2.31	2.40	2.99	3.01	4.81	9.57

Thus, based on Jenike's classification of powder flowability (see Table 2-2), aspartame, ML001, lactose and flour will not flow easily, whereas HPMC and placebo granulate will be free flowing. The poor flowability of most of these powders is likely due to various factors, including small particle size, wide particle size distribution and particle shape, which will be discussed in section 3.3. Powder cohesion values obtained from the y-axis intercept of the yield locus are presented in Figure 3-9.

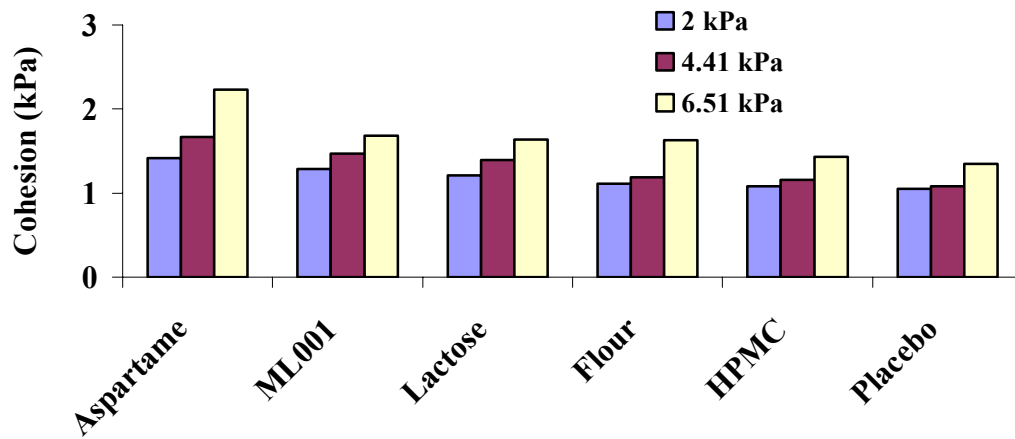


Figure 3-9 Cohesion values for the test powders at different values of normal stress

Cohesion in a powder is a result of either interparticle forces (Van der Waals, electrostatic, moisture, etc.) or mechanical interlocking between adjacent particles.

3.2.2 Density measurements

Table 3-5 reports the values of Hausner Ratio and Carr Index for all test powders.

Table 3-5 Hausner Ratio and Carr Index for test powders

Test material	Hausner Ratio	Carr Index (%)	Loose bulk density (Kg/M ³)	Tapped bulk density (Kg/M ³)
Aspartame	1.92	48	205	395
ML001	1.54	35	610	938
Lactose	1.43	30	680	971
Flour	1.35	26	490	662
HPMC	1.32	24	490	645
Placebo	1.16	14	670	780

The values of Hausner Ratio and Carr Index are highest for aspartame, indicating that it is a highly compressible powder, whereas Hausner Ratio and Carr Index are lowest for the placebo granulate, which indicates its free flowing behaviour. As observed in Figures 3-10 and 3-11, test powders in order of increasing flowability based on Hausner Ratio and Carr Index are: Aspartame>ML001>Lactose Monohydrate>Flour>HPMC>Placebo granulate. The powder volume in the graduated cylinder was recorded after every 10 taps until the powder surface reached a maximum packing condition. As can be observed in Figures 3-10 and 3-11, the Hausner Ratio and Carr Index curves first increase with the number of taps and then reaches a steady value. These values are dependent on factors such as particle size, size distribution and shape. Large spherical particles, such as those of the placebo granulate, reach a maximum packing condition easily with fewer taps as there is no scope for further packing. Thus

they have very close values for tapped and loose bulk density and hence lower compressibility.

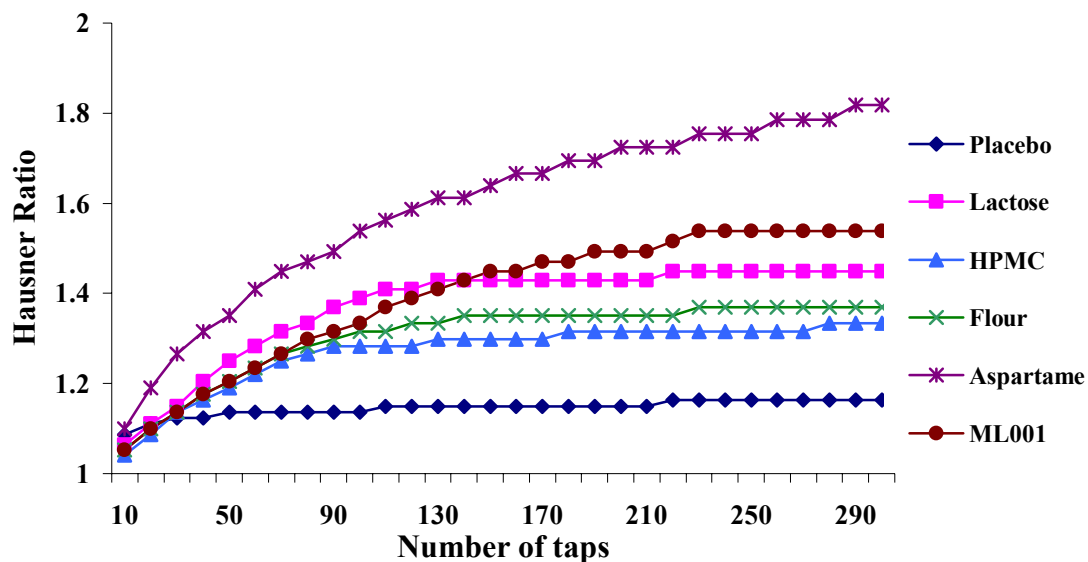


Figure 3-10 Values of Hausner Ratio for test powders up to 300 tappings

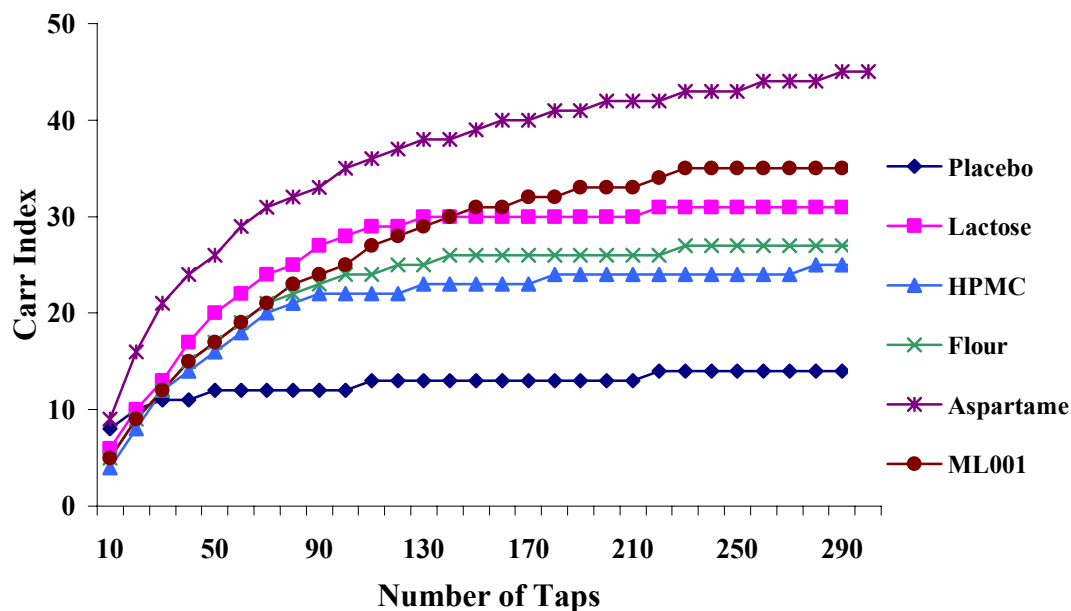


Figure 3-11 Values of Carr Index for test powders up to 300 tappings

It was observed that for all powders, with the exception of aspartame and HPMC, the powder surface reached maximum packing after 300 taps or less. For HPMC it took

600 taps, and for aspartame it took 1200 taps to reach a maximum packing condition, as shown in Figure 3-12.

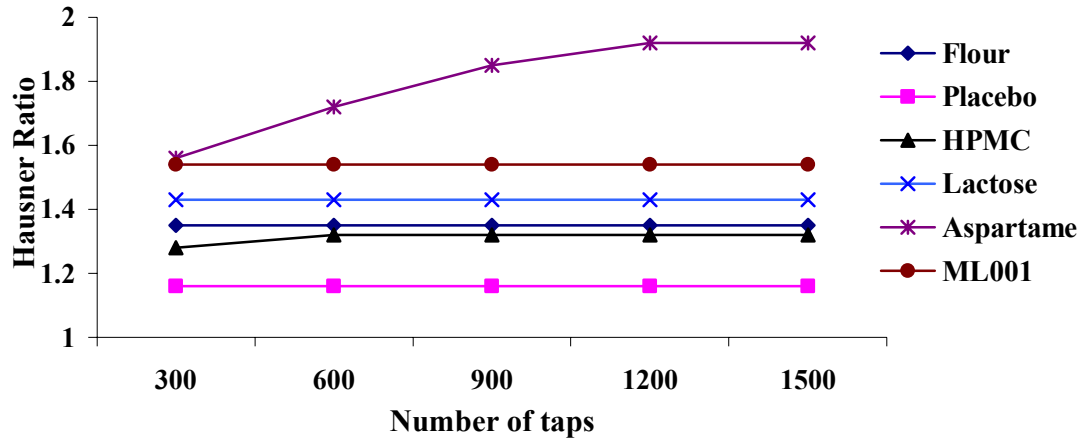


Figure 3-12 Variation of Hausner ratio with number of taps for test powders

The reason for this behaviour is because of the wide distribution of particle size and shape found in aspartame and HPMC. The aspartame powder consists mostly of elongated particles whereas HPMC consists of particles ranging from spheres to needle shaped particles. In a segregating system, when powder is given mobility by tapping, the large and small particles are able to rearrange to form the densest packing (Abdullah and Geldart, 1999). Greater number of large particles will provide more unoccupied voids as most of the small particles would migrate to the bottom of the cup to fill those voids in the lower region. This would leave most of the voids in the middle and upper region of the cup unoccupied. Thus, aspartame and HPMC require a greater number of taps to reach a maximum packing as compared to other test powders, and it was found that the Hausner Ratio and Carr Index are sensitive to differences in particle size and shape distribution. The loose bulk density and tapped density data can be used to gain insight into the packing of the particles in the mixtures.

3.2.3 Angle of repose measurements

The static angle of repose was measured according to the procedure mentioned in section 2.3.1.1, and the dynamic angle of repose was measured using the Electrical Capacitance Tomography (section 2.3.1.2).

3.2.3.1 Static angle of repose

Table 3.5 reports the values obtained for the static angle of repose for the test powders. The results showed a high level of reproducibility, with a standard deviation of 1.67° or less. When comparing the results obtained from the static angle of repose measurements (Table 3-6) with Carr's classification (Table 2-1), it was clear that aspartame, ML001 and lactose monohydrate are cohesive powders, flour exhibits fair to passable flowability, HPMC is free flowing and the placebo granulate is very free flowing.

Table 3-6 Values of static angle of repose for test samples

Test powder	Angle of repose
Aspartame	52°
ML001	50°
Lactose	46°
Flour	43°
HPMC	33°
Placebo	30°

3.2.3.2 Dynamic angle of repose

The dynamic angles of repose for all test powders at rotational speeds from 10 to 90 RPM are reported in Appendix D1. The angle initially goes to a maximum and then decreases, which is consistent with avalanching behaviour. After two or three

avalanches, the angle of repose becomes nearly constant at 10 and 20 RPM. However, beyond 30 RPM, the angle of repose fluctuates between a minimum and maximum value. The mean value of the dynamic angle of repose is calculated by taking the arithmetic average of the measured angles after two avalanches. The dynamic angle of repose curves for test powders are included in Appendix B2 to B5.

The test materials, according to increasing order of flowability based on dynamic angle of repose, are: aspartame>ML001>lactose monohydrate>flour>HPMC>placebo granulate. These results are in agreement with the results from static angle of repose.

A different trend was found between the curves of dynamic angle of repose for cohesive and free flowing powders at all rotation speeds. Figure 3-13 shows the curve for four cohesive powders: aspartame, ML001, lactose monohydrate and flour, and Figure 3-14 shows the curve for free flowing powders: HPMC and the placebo granulate.

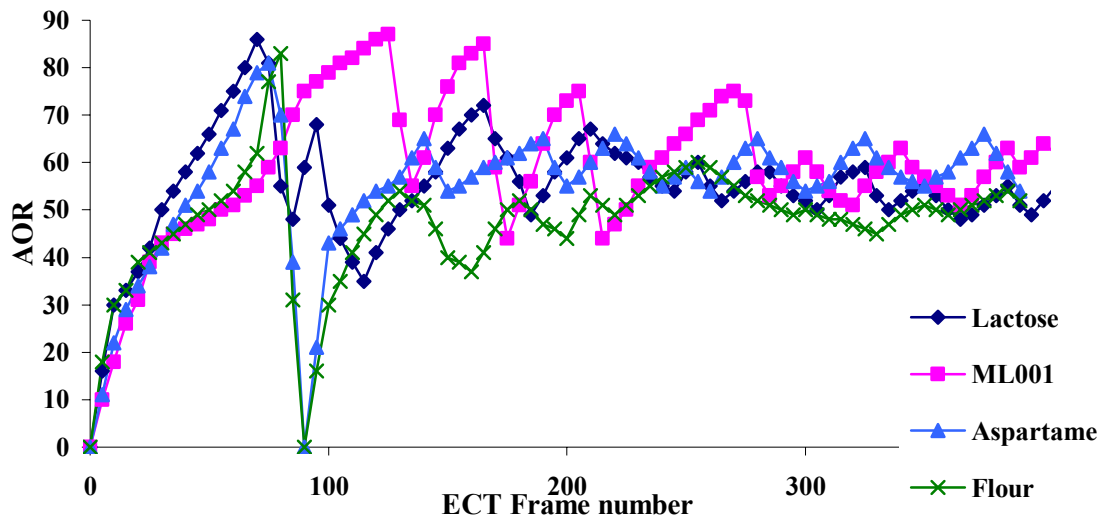


Figure 3-13 Dynamic angle of repose curve for cohesive powders at 20 RPM

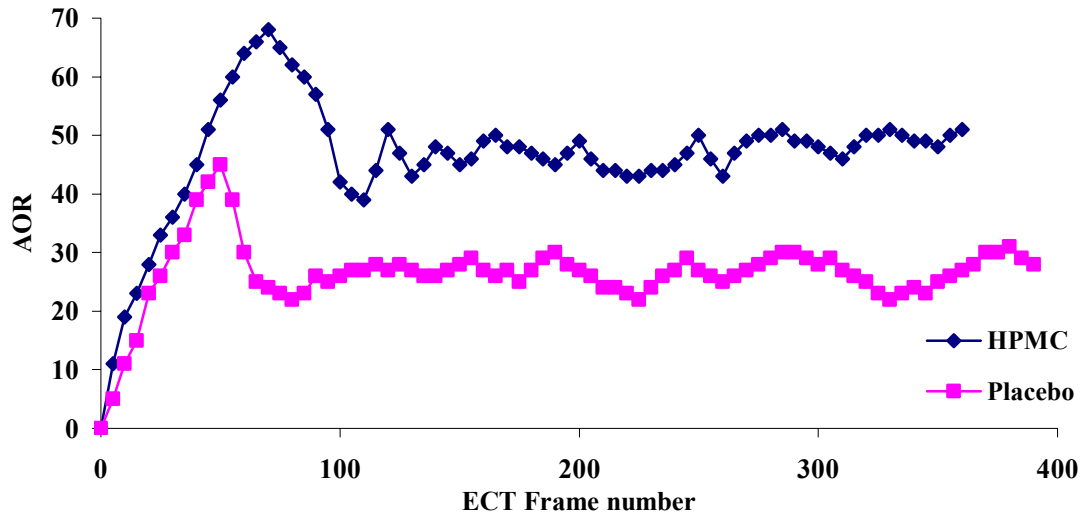


Figure 3-14 Dynamic angle of repose curve for free flowing powders at 20 RPM

As can be noticed in Figure 3-13, cohesive powders tend to experience a greater number of avalanches before the curve fluctuates between a maximum and minimum value as compared to the free flowing powders (Figure 3-14). This behaviour might be because of the differences in powder physical properties such as shape and size distribution. The dynamic angles of repose were plotted at different rotational speeds in order to determine their dependence, as shown in Figure 3-15.

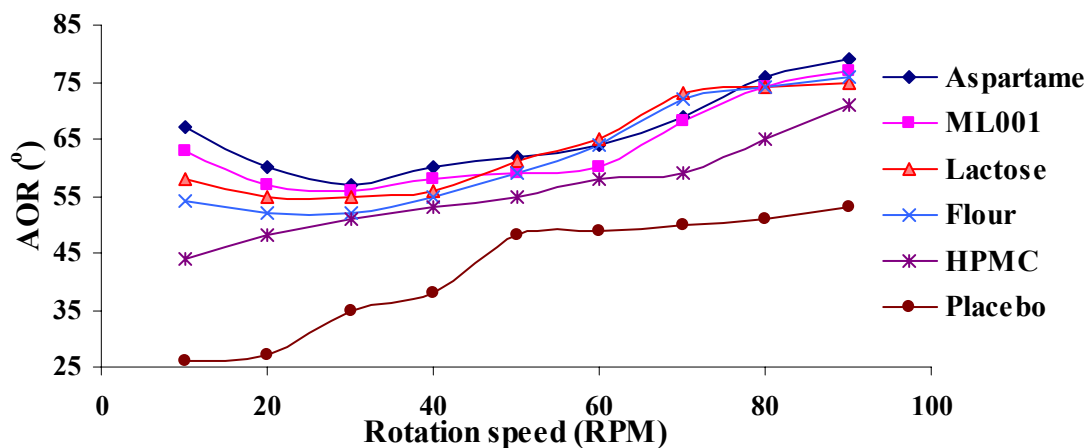


Figure 3-15 Dynamic angle of repose for test powders at different rotational speeds

The dynamic angle of repose increases linearly with rotation speed for free flowing HPMC and placebo granulates. For the cohesive powders (aspartame, ML001, lactose and flour), the dynamic angle of repose falls between 10 and 30 RPM and then increases. Similar results were observed by Castellanos et al. (1999). They compared free flowing sand for which AOR was found to increase with rotation rate and cohesive toner particles for which AOR decreased with rotation rate.

According to Castellanos et al. (1999), granular materials exhibit four different flow regimes: plastic, inertial, fluidized and entrained flow. The plastic regime is characterized by small or zero velocities, small voidage and the stresses are independent of gas velocity. The stresses in the inertial regime are due to transport of momentum by interparticle collisions and voidage is greater than the plastic regime. In the fluidized regime, pressure drop, caused by the gas flow, is sufficient to support the weight of the powder bed. In entrained flow particles are suspended by the gas. The motion of the free flowing powders such as HPMC and placebo in a rotating drum passes from plastic to inertial flow, whereas that for cohesive powders passes from plastic to a fluidized flow with increase in rotation speed (Castellanos et al., 1999). This might explain the difference in the trend of the AOR curve for cohesive and free flowing powders with rotational speed.

After about two avalanches, the dynamic angle of repose curve becomes nearly constant at lower rotation speeds (10 and 20 RPM) for all test powders. However, at higher rotation speeds, the angle of repose curve fluctuates between a minimum and maximum value. The results from the various flowability indicators were found to be very much in agreement, with aspartame powder having the least flowability and placebo granulates having free flowing nature.

3.3 Comparison of powder physical properties with flow indicators

The powder physical properties considered in this study were particle size, size distribution and shape. These properties were selected as they were found to have a major impact on powder flowability according to the literature review presented in Chapter 1. The flowability of test powders was examined based on the static and dynamic angles of repose (θ_s , θ_D), Hausner ratio (HR), Carr Index (CI), flow index and cohesion. This section examines the relationship between the various powder physical properties and the powder flowability indicators.

3.3.1 Relationship between mean particle size and flowability indicators

This section relates the mean particle size to the powder flowability indicators. The equivalent circle diameter obtained from the image analysis was used in the present study to represent the particle size as it reflected the accurate value for particle diameter taking into account the particle shape (Kaye et al., 1999). It is known from work done previously (Cain, 2002; Wouters and Geldart, 1996) that a decrease in the particle size causes a decrease in powder flowability. Similar results were found in the present study when comparing the mean particle size with the various flowability indicators.

3.3.1.1 Relationship between mean particle size and the angle of repose

Figure 3-16 shows the plot of dynamic and static angles of repose as a function of mean particle size.

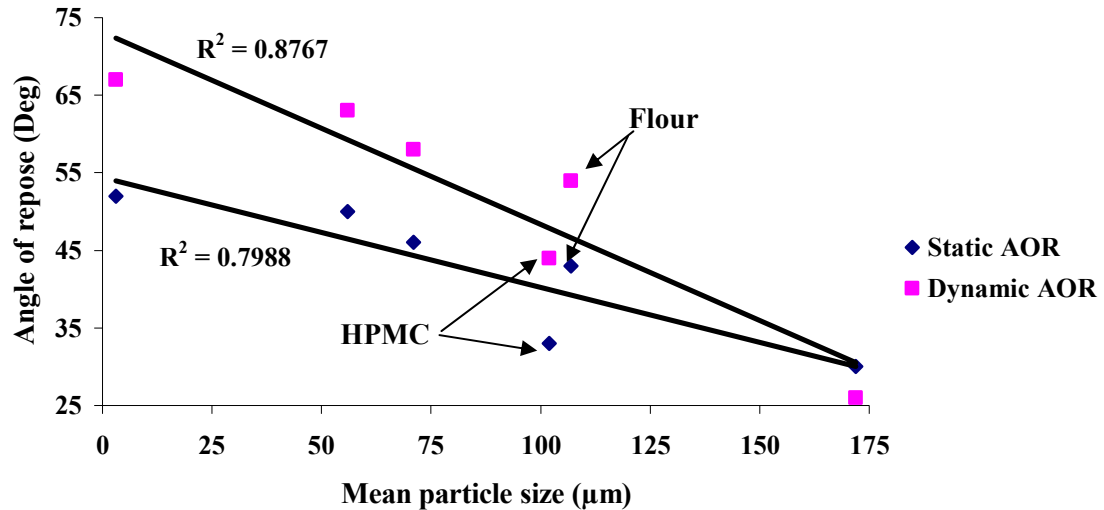


Figure 3-16 Angle of repose (AOR) vs. mean particle diameter for the test powders

The dynamic and static angles of repose decreased with increasing mean particle diameter, indicating easier flow. The placebo granulate had the largest particle diameter and the lowest angle of repose, while the reverse was true for aspartame. Smaller particles tend to have a greater number of contacts with neighbouring particles. Thus, while measuring the static and dynamic angles of repose, small particles are able to form a more dense packing which prevents the particles from rolling and hence increases the angle. Large particles cause failure of the slope by pushing other particles, hence avalanches happen more frequently and therefore lower the angle of repose values. Although, HPMC and flour had mean particle diameters that were very close to each other, flour exhibited a higher angle of repose. This might be because of the differences in particle shape between the two powders.

3.3.1.2 Relationship between Hausner Ratio, cohesion, flow index and mean particle size

Figure 3-17 shows the variation of Hausner Ratio and cohesion with the mean particle diameter.

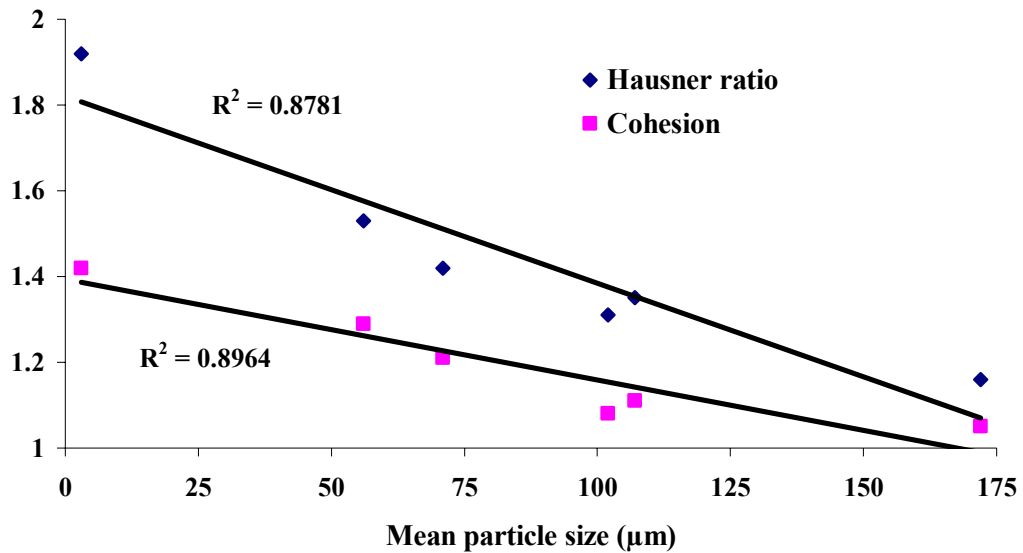


Figure 3-17 Variation of Hausner Ratio and cohesion with particle diameter

Hausner Ratio and cohesion were found to decrease with increase in mean particle diameter indicating difficulties in flow. Similar results were found for the Carr Index. A large mean diameter is an indication of a lesser amount of fines in the powder bulk (Abdullah and Geldart, 1999). Larger particles reach their densest possible packing condition in fewer taps as there is limited scope for further packing. Hence, they have very similar bulk and tapped densities which decrease the values of Hausner Ratio and Carr Index.

On the other hand, small mean particle size suggests the presence of more fines in the powder bulk. Small particles have a greater number of contact points with the neighbouring particles which makes it difficult to rearrange and form a dense packing.

However, when tapping is applied to the powder bulk, small particles roll between the particle voids and reach a maximum packing condition. In loose state, large voids are formed due to arching of particles. These voids collapse when tapping is applied. Thus, there is a large difference between their loose and tapped densities, which increases the value of the Hausner ratio and Carr index.

Figure 3-17 also illustrates that cohesion increases with decreasing particle size. Large size particles have comparatively less number of contact points with neighbouring particles. Thus, when shearing, they are able to easily roll over each other in the shear plane, reducing the cohesion. Small size particles, on the other hand have a larger number of contact points with neighbouring particles, which increases cohesion either due to higher interparticle forces or mechanical interlocking, if the particles are irregular.

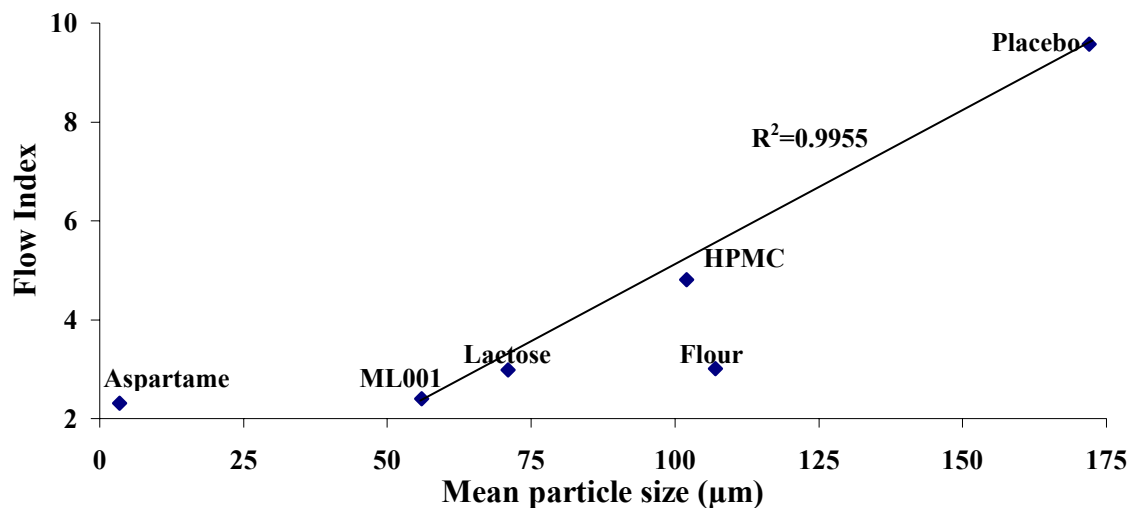


Figure 3-18 Variation of flow index with particle diameter

Figure 3-18 plots the Jenike flow index as a function of mean particle diameter. Also presented on this plot is the linear regression of the flow indices for ML001, lactose

monohydrate, HPMC, and the placebo granulate. With an R^2 value of 0.9955, it is clear that the fit is excellent and thus the flowability of these four powders is a strong function of mean particle diameter.

The outlying values on this plot corresponding to aspartame and flour are due to two different reasons. With respect to aspartame, the behaviour of its flow index reflects the difficulty in performing reliable shear measurements with powders of high aspect ratio. As noted by Bell (2001), it can be nearly impossible to attain a steady-state shear rate for powders that are needle-shaped or in the form of flakes.

Flour is not needle-shaped, but as the SEM images showed, it is irregular. This may be the reason that flour does not follow the linear relationship shown in Figure 3-18. The influence of irregularity on powder flow will be discussed in the next section.

3.3.2 Relationship between flowability indicators and various shape parameters

The particle shape parameters for all test powders are reported in Table 3-2. In this section, the influence of shape on powder flowability was examined by comparing each of the flow indicators with the various shape parameters.

Figures 3-19 and 3-20 show the relationship between shape factors (aspect ratio and roundness) and the static angle of repose.

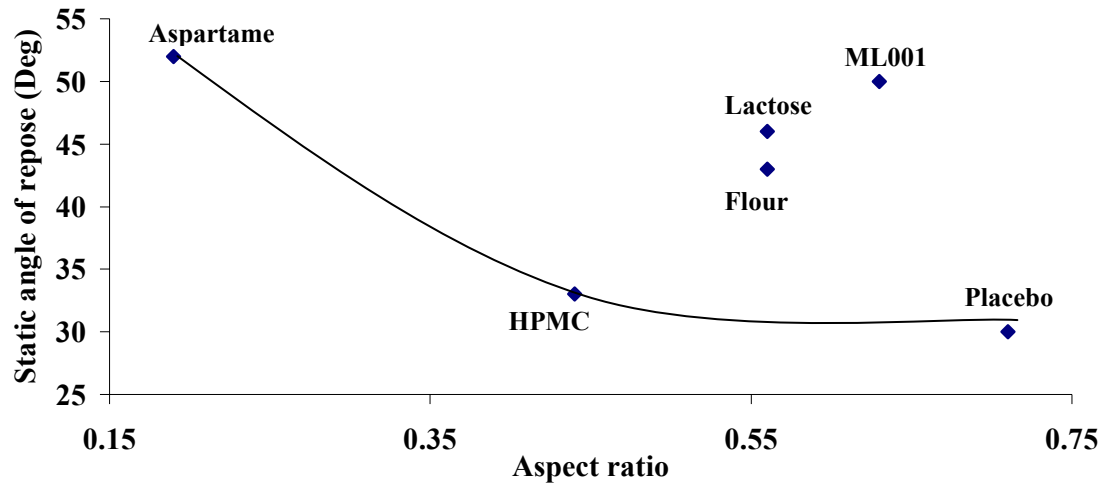


Figure 3-19 Relationship between aspect ratio and static angle of repose

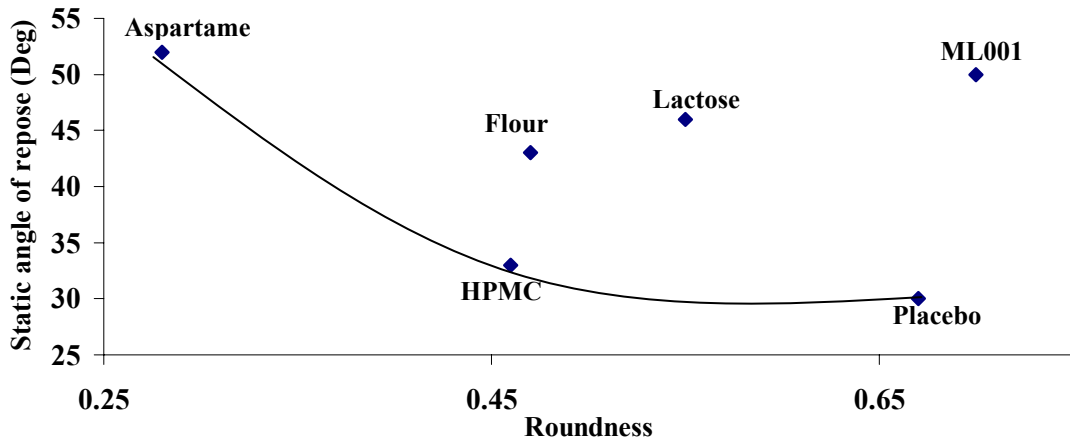


Figure 3-20 Relationship between roundness and static angle of repose

Similar results were found for the dynamic angle of repose. From Figures 3-19 and 3-20, the angle of repose decreases with increasing aspect ratio and roundness values for aspartame, HPMC and the placebo granulate, indicating that the flowability increases as the particles become more spherical. The spherical particles tend to rotate easily in a rotating drum, also spherical particles provide comparatively less resistance to the flow of neighbouring particles. Aspartame powder consists of needle-shaped particles that tend to form agglomerates as shown in Figure 3-21.

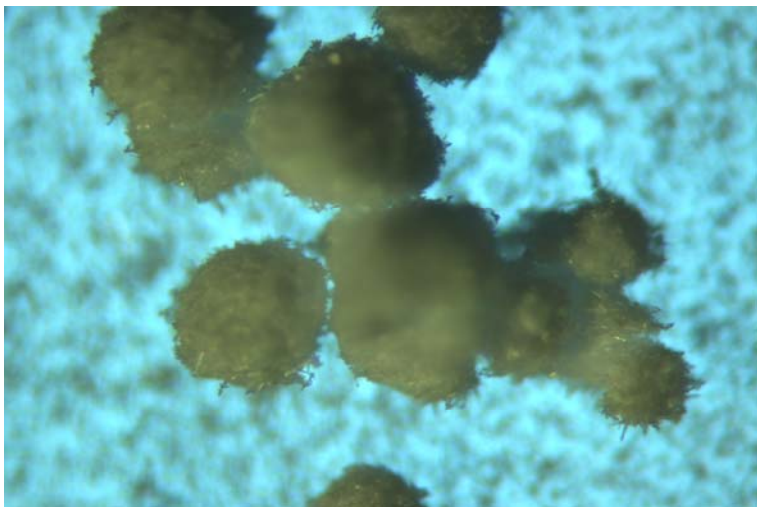


Figure 3-21 Micrograph of aspartame agglomerates from stereomicroscope

This interlocking prevents powder flow and hence, increases the angle of repose. Although HPMC has a lower aspect ratio, indicating elongated particles, it has a lower angle of repose, indicating easier flow. The reason for this may be due to the fact that HPMC bulk shows a wide distribution of particle shapes ranging from small spheres to elongated particles (Figure 3-7), which assist in powder flow. For other powders (ML001, lactose and flour), there is an increase in the angle of repose with an increase in the values of aspect ratio and roundness.

A plot of the other flow indicators, (Hausner Ratio and cohesion), with the aspect ratio and roundness shows similar trends, as seen in Figures 3-22 and 3-23. However, the correlation between these flowability indicators and the aspect ratio is somewhat better than what was seen in Figures 3-19 and 3-20. This trend is consistent with the behaviour of Hausner ratio and cohesion found in the previous section, whereby these two flowability indicators appears to be less sensitive to differences in powder properties and their influence on powder flow.

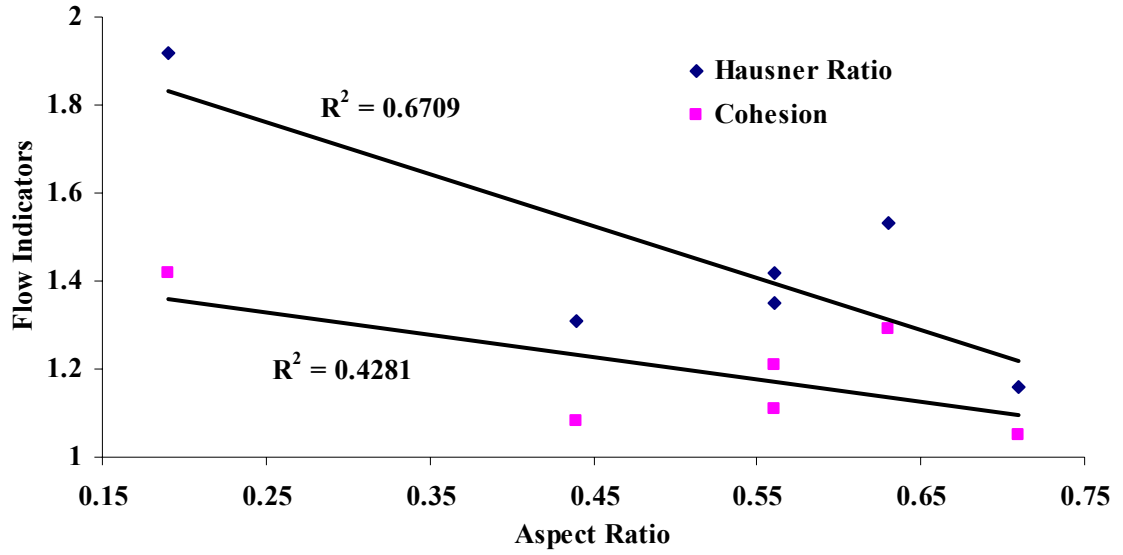


Figure 3-22 Relationship between aspect ratio and flow indicators

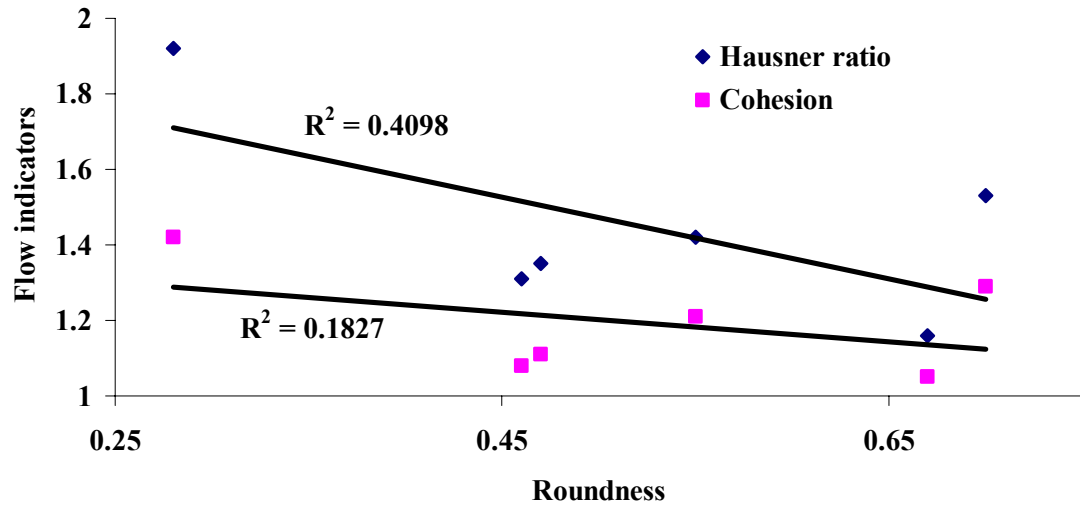


Figure 3-23 Relationship between roundness and flow indicators

Figure 3-24 and 3-25 present plots of flow index vs. aspect ratio and roundness.

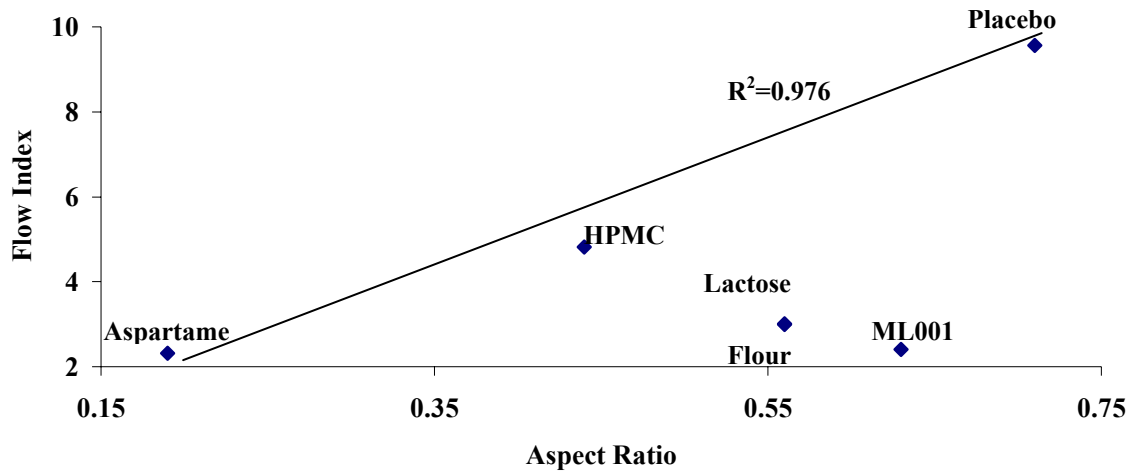


Figure 3-24 Relationship between aspect ratio and flow index

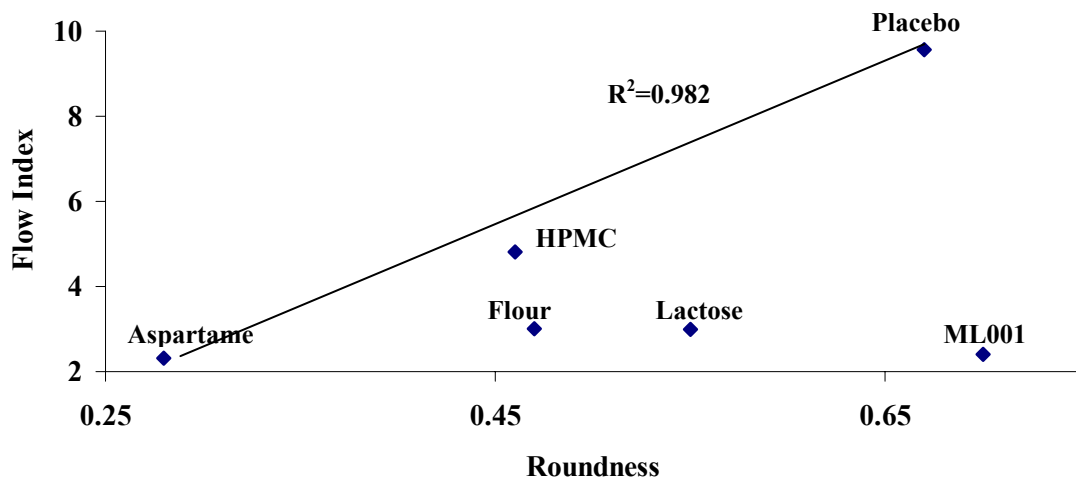


Figure 3-25 Relationship between roundness and flow index

The flow index decreases with decrease in aspect ratio and roundness (Figure 3-24 and Figure 3-25), for placebo, HPMC and aspartame, indicating that powders having elongated particles show lower flowability. Elongated particles such as those of aspartame tend to interlock with each other during shearing, and hence resist the powder flow. Small spherical particles in HPMC bulk cause easy rolling of particles in the shear region during shearing and hence assist in powder flow. Spherical particles provide less

contact points between neighbouring particles as compared to elongated and irregular particles. Thus spherical particles cause less friction and shear and hence assist in flow.

As can be observed from Figures 3-19, 3-20, 3-22, 3-23, 3-24 and 3-25, for flour, lactose, and ML001 there is a decrease in powder flowability with increase in aspect ratio and roundness. This is contrary to what is normally expected, i.e. spherical powders generally will flow better. Thus there seems to be some other particle shape attribute in addition to elongation and sphericity which affects the powder flow. Figure 3-26 shows a plot of irregularity vs. static angle of repose.

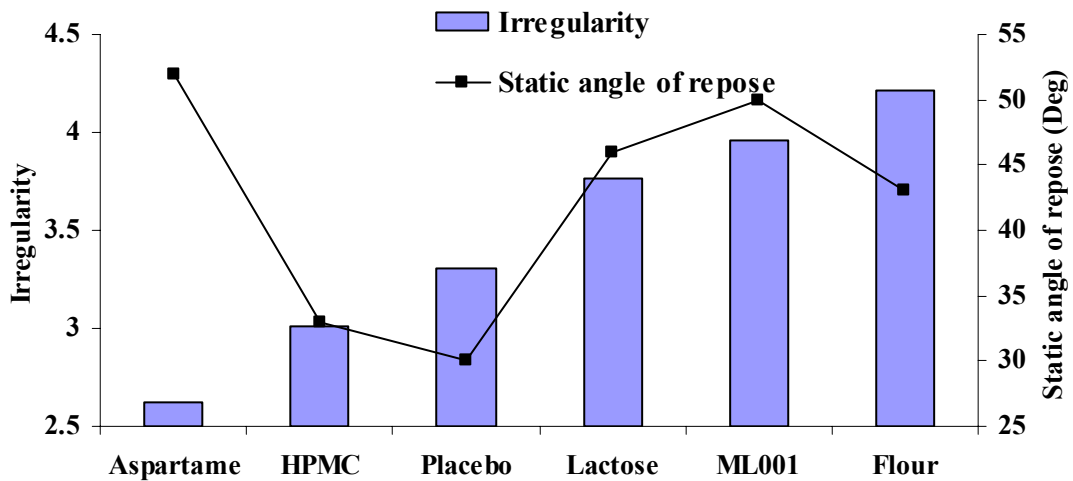


Figure 3-26 Relationship between irregularity factor and static angle of repose

A high value of irregularity factor is an indication of irregular particle whereas a lower value indicates an elongated particle. A value of 3.14 indicates a spherical particle. In the present study, ML001, lactose, and flour were found to have irregular-shaped particles, whereas HPMC and aspartame particles were elongated based on the irregularity factor. It is clear from Figure 3-25 that ML001, lactose, and flour had high values of irregularity factor and angle of repose indicating their cohesive nature. Aspartame has low value of irregularity factor indicating elongated particles and highest

value of angle of repose indicating its cohesive nature. This may be because of the fact that irregular particles tend to mechanically interlock with each other (Cain, 2002: Marinelli and Carson, 1992: Juliano et al., 2006). Thus they are turned up to a steeper angle, increasing the angle of repose. Also, when measuring the static angle of repose, irregular particles interlock with each other, thus preventing any avalanching, resulting in steeper angles.

It can be observed from Figures 3-13 and 3-14 that cohesive powders tend to experience a larger number of avalanches as compared to free flowing powders. This can be explained because of the elongated and irregular particle shape of cohesive powders. Because of the mechanical interlocking between the particles, they are carried up to higher angles and after reaching a maximum angle, they fall down because of the gravitational force. However after a couple of avalanches, the interlocking between the particles breaks and thus the powder attains a nearly constant angle with the horizontal which is taken as the dynamic angle of repose.

Figure 3-27 shows a plot of Hausner ratio and cohesion vs. irregularity.

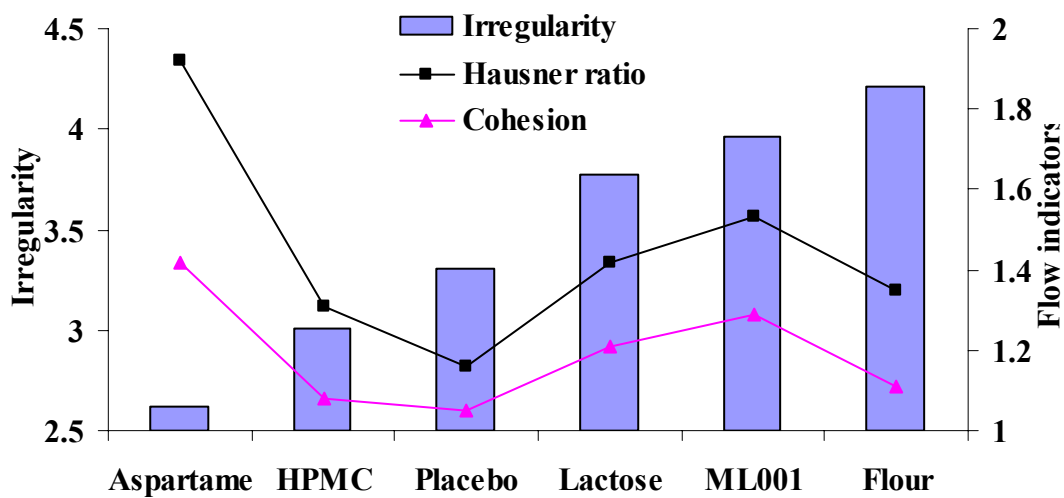


Figure 3-27 Relationship between Hausner ratio and cohesion with irregularity

Irregular particles provide a larger number of unoccupied voids, as small fines find it difficult to roll in between the voids of large particles. This in turn increases the tap density and hence the Hausner ratio.

Figure 3-28 shows the relationship between irregularity factor and flow index.

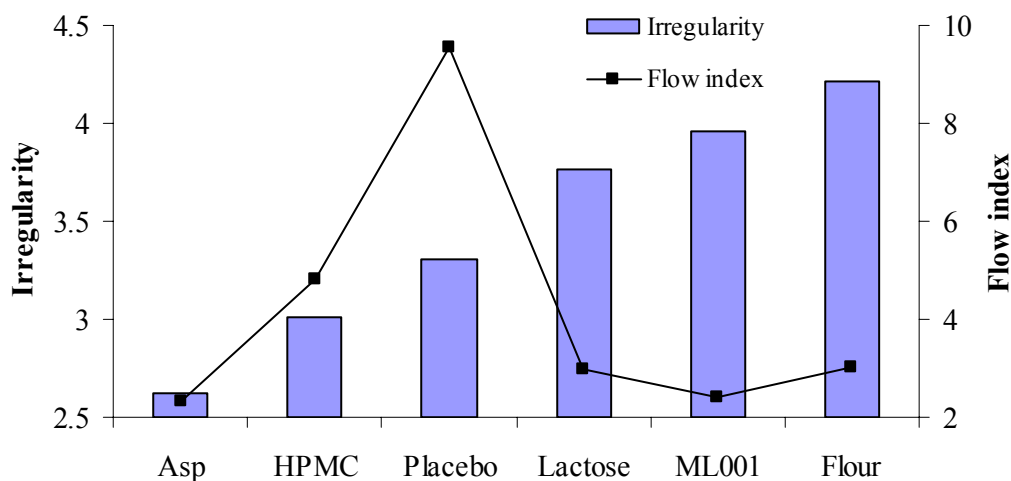


Figure 3-28 Relationship between irregularity factor and flow index

The flow index is lower for elongated and irregular particles of aspartame, ML001, lactose and flour as compared to HPMC and placebo granulates. The elongated and irregular particles interlock with each other increasing the cohesive strength and hence friction. The small spherical particles in HPMC bulk assist the flow and thus reduce the shear. Large spherical placebo granulates have smooth surfaces and edges which make them free flowing.

3.4 Summary of results

The mean particle size was found to be an accurate predictor of powder flowability, with decreasing particle size indicating difficulties in flow. However, certain other powder physical properties such as particle elongation, sphericity, irregularity, size and shape distribution were found to have an influence on powder flowability. These

properties may influence powder flowability either individually or in combination with other properties. In addition to mean particle size, irregularity factor was found to be a good predictor of powder flowability. Flour and HPMC, although having similar particle diameters, exhibited contrasting flowability. Irregular-shaped particles in flour powder lower its flowability, whereas the wide distribution of particle shapes in HPMC assists in its flow. Flour, ML001 and lactose, although having higher values for roundness, exhibited poor flowability because of their irregular shapes.

4 CONCLUSIONS

The objective of the present study was to study the relationship between powder flowability and the powder physical properties. Powder flowability was quantified using various techniques such as shear strength, angle of repose and density measurements. The powder physical properties measured included the particle size, shape, density and moisture content. Finally the influence of powder physical properties on powder flowability was studied. The following conclusions were drawn from the present study:

- Particle size was found to be the most accurate predictor of granular material flowability, with decreasing particle size indicating lower flowability.
- Irregularity factor was found to correlate well with poor flowability of elongated and irregular particles. Particle shape irregularity was found to be the main reason for lower flowability in ML001, lactose and flour. Irregular particles tended to interlock with each other and resisted powder flow. After the passage of time, the particle interlocking may result in strong mechanical bonds between particles which may eventually lead to formation of arches, cakes, and ratholes. This caused an increase in powder cohesion and shear strength.
- Wide distributions of particle shapes and sizes were found to have an impact on powder flowability. Although HPMC consisted of a large number of elongated particles, it demonstrated good flowability. This was because of the fact that HPMC bulk consisted of small spherical particles in addition to elongated particles, which appeared to assist powder flow.

- ECT was found to be a promising non-intrusive tool to measure the dynamic angle of repose effectively, eliminating the effect of end caps as encountered by other methods.
- Image analysis provides an easy and accurate method to define various particle attributes. A variety of shape factors can be used and each descriptor will be sensitive to a specific attribute of shape depending upon the parameters selected for its calculation. Combining the shape parameters can give more detailed information, as in case of ML001 where the roundness factor indicates its spherical shape, whereas the irregularity factor indicates its irregular shape. Thus, while comparing shape parameters with other powder properties, all particle shape attributes should be taken into account.
- The dynamic angle of repose increases linearly with rotation speed for free flowing powders, whereas for cohesive powders, first it decreases till 30 RPM and then increases. The motion of the free flowing powders such as HPMC and placebo in a rotating drum passes from plastic to inertial flow, whereas that for cohesive powders passes from plastic to a fluidized flow with rotation speed, which causes the AOR to first decrease and then increase with rotation speed as it becomes fluidized.
- The present study could be used in process analytical technology (PAT) in pharmaceutical industries to monitor the physical properties of raw and in-process materials so as to predict the potential flowability of materials. Performing image analysis on a representative process sample can yield the values of mean particle size and irregularity factor. A comparison of these values

with the correlations of mean particle size and irregularity factor with flowability indicators from the present study could help in identifying the potential flowability.

5 RECOMMENDATIONS

This project has clearly identified the need for further experimental work to confirm the effect of each particle parameter to the resulting powder flowability. Ideally, it would be desirable to study monodisperse powders, having uniform particle shapes and sizes. Then, it would be much clearer to compare the effect of particular particle property on powder flowability. An easier way to obtain a monodisperse powder having uniform particle size will be by sieving, using a mesh of required size.

In present study, shear strength measurements were carried out mainly to obtain the flow index and cohesion values of test powders, for comparing them with particle properties. Other powder properties such as angle of internal friction, effective angle of internal friction and angle of wall friction can also be obtained from shear strength measurements. A comparison of these properties with powder physical properties can provide more detailed information of powder behavior.

Since particle shape was found to have an effect on powder flowability, particle shape should be characterized using other accurate methods. Fractal dimensional analysis and Fourier analysis are some of the sophisticated and accurate methods used for particle shape analysis.

ECT measurements should be carried out at much lower rotation speeds for studying the avalanching behavior of powders. Typically industry carries out the avalanching measurements at around 0.5 to 2 RPM.

REFERENCES

Abdullah, E. C. and Geldart, D., 'The use of bulk density measurements as flowability indicators', *Powder Technol.*, **102**, 1999, 151-165.

ASTM standard: **D 6128-00**, 'Standard test method for shear testing of bulk solids using the Jenike shear cell'.

ANSI/CEMA Standard: **500-1980**, 'Classification/Definitions of Bulk Material'.

ASTM Standard: **E1382-91**, Standard test methods for determining average grain size using semiautomatic and automatic image analysis. American Society for Testing and Materials, Philadelphia, PA (1991).

Balboni, M. L., 'Process analytical technology- Concepts and principles', *Pharm. Technol.*, Oct 2003, 54-67.

Behera, S., Das, S., Hatvani, Z., and Pahl, M. H., 'Flowability studies of bulk materials for design of hopper using a Jenike shear cell', *Powder Hand. Proc.*, **14 (2)**, 2002, 96-101.

Bell, T. A., 'Industrial needs in solids flow for the 21st century', *Powder Hand. Proc.*, **11 (1)**, 1999, 9-12.

Bell, T. A., 'Solids flowability measurement and interpretation in industry', *Handbook Conv. And Handl. Part. Sol.*, **10**, 2001, 3-13.

Bouwman, A. M., Bosma, J. C., Vonk, P., Weselingh, J. A., and Frijlink, H. W., 'Which shape factor (s) best describe granules?', *Powder Technol.*, **146**, 2004, 66-72.

Cain, J., 'An alternative technique for determining ANSI/CEMA standard 550 flowability ratings for granular materials', *Powder Hand. Proc.*, **14 (3)**, 2002, 218-220.

Carr, R. L., 'Evaluating flow properties of solids', *Chem. Engg.*, **72 (2)**, 1965, 163-169.

Castellanos, A., Valverde, J. M., Perez, A. T., Ramos, A., and Watson, P. K., 'Flow regimes in fine cohesive powders', *Phy. Rev. Let.*, **82 (6)**, 1999, 1156-1159.

Chan, L. C. Y. and Page, N. W., 'Particle fractal and load effects on internal friction in powders', *Powder Technol.*, **90**, 1997, 259-266.

Dury, C. M. and Ristow, G. H., 'Boundary effects on the angle of repose in rotating cylinders', *Phy. Rev. E*, **57 (4)**, 1998, 4491-4497.

Fitzpatrick, J. J., Barringer, S. A., and Iqbal, T., 'Flow property measurement of food powders and sensitivity of Jenike's hopper design methodology to the measured values', *J. Food Engg.*, **61**, 2004, 399-405.

Fitzpatrick, J. J. and Ahrne, L., 'Food powder handling and processing: Industry problems, knowledge barriers and research opportunities', *Chem. Engg. Proc.*, **44 (2)**, 2005, 209-214.

Freeman, R., 'The flowability of powders-an empirical approach', *Int. Conf. Powder & Bulk Solids Handl.*, June 2000, IMechE HQ, London.

Geldart, D., 'Types of gas fluidization', *Powder Technol.*, **7**, 1973, 285-292.

Iida, K., Aoki, K., Danjo, K., Otsuka, A., Chen, C. Y., and Horisawa, E., 'A comparative evaluation of the mechanical properties of various celluloses', *Chem. Pharm. Bull.*, **45 (1)**, 1997, 217-220.

ISO **3435-1977 (E)**, 'Classification and Symbolization of Bulk Materials'.

ISO **3923/1-1979**, 'Determination of apparent density-Funnel method'.

Jenike, A. W., 'Storage and flow of solids', Bulletin 123 of the Univ. of Utah Engr. Experimental Station, 1964.

Juliano, P., Muhunthan, B. and Gustavo, V. B., 'Flow and shear descriptors of preconsolidated food powders', *J. Food Engg.*, **72**, 2006, 157-166.

Jensen, R. P., Bosscher, P. J., Plesha, M. E., and Edil, T. B., 'DEM simulation of granular media structure interface: Effects of surface roughness and particle shape', *Int. J. Numer. Anal. Meth. Geomech.*, **23**, 1999, 531-547.

Kaerger, J. S., Edge, S., and Price, R., 'Influence of particle size and shape on flowability and compactibility of binary mixtures of paracetamol and microcrystalline cellulose', *Eur. J. Pharm. Sci.*, **22**, 2004, 173-179.

Kaye, B. H., Alliet, D., Switzer, L., and Turbitt-Daoust, C., 'The effect of shape on intermethod correlation of techniques for characterizing the size distribution of powder', *Part. Part. Syst. Charact.*, **16**, 1999, 266-273.

Lahdenpää, E., Niskanen, M., and Yliruusi, J., 'Study of some essential physical characteristics of three Avicel PH grades using a mixture design', *Eur. J. Pharm. Biopharm.*, **42 (3)**, 1996, 177-182.

Larhrib, H., Martin, G. P., Prime, D. and Marriott, C., 'Characterisation and deposition studies of engineered lactose crystals with potential for use as a carrier for aerosolised salbutamol sulfate from dry powder inhalers', *Eur. J. Pharm. Sci.*, **19 (4)**, 2003, 211-221.

Lawrence, X. Y., Lionberger, R. A., Raw, A. S., D'Costa, R., Huiquan, W. and Hussain, A. S., 'Applications of process analytical technology to crystallization process', www.fda.gov/cder/OPS/patcrystalSub.pdf (May, 2005)

Li, Z., Yang, J., Xu, X., Yu, W., Yue, X., and Sun, C., 'Particle shape characterization of fluidized catalytic cracking catalyst powders using mean value and distribution of shape factors', *Adv. Powder Technol.*, **13 (3)**, 2002, 249-263.

Lindberg, N., Palsson, M., Phil, A., Freeman, R., Freeman, T., Zetzener, H. and Enstad, G., 'Flowability measurements of pharmaceutical powder mixtures with poor flow using five different techniques', *Drug Dev. Ind. Pharm.*, **30 (7)**, 2004, 785-791.

Marinelli, J. and Carson, J. W., 'Solve solids flow problems in bins, hoppers and feeders', *Chem. Engg. Prog.*, **88 (5)**, 1992, 22-28.

McKeen, T. R. and Pugsley, T. S., 'The influence of permittivity models on phantom images obtained from electrical capacitance tomography', *Meas. Sci. Technol.*, **13**, 2002, 1822-1830.

Mikli, V., Kaerdi, H., Kulu, P., and Besterci, M., 'Characterization of powder particle morphology', *Proc. Estonian Acad. Sci. Eng.*, **7 (1)**, 2001, 22-34.

Mullarney, M. P., Hancock, B. C., Carlson, G. T., Ladipo, D. D., and Langdon, B. A., 'The powder flow and compact mechanical properties of sucrose and three high-intensity sweeteners used in chewable tablets', *Int. J. Pharma.*, **257**, 2003, 227-236.

Muzzio, F. J., Shinbrot, T., and Glasser, B. J., 'Powder technology in the pharmaceutical industry: the need to catch up fast', *Powder Technol.*, **124**, 2001, 1-7.

Nelson, R. D., 'Why Study Particle Science?', www.erpt.org (March, 2004)

Oatley, C. W., 'The Scanning electron microscope', London Cambridge Press, **1**, 1972, 189-192.

Obradovic, M. C., 'The effect of the particle shape and structure on the flowability of electrolytic copper powder. II. The experimental verification of the model of the representative powder particle', *J. Serb. Chem. Soc.*, **68 (10)**, 2003, 779-783.

Oshima, T., Zang, Y. L., Hirota, M., Suzuki, M., and Nakagawa, T., 'The effect of the types of mills on the flowability of ground powders', *Adv. Powder Technol.*, **6 (1)**, 1995, 35-45.

Peschl, I. A. S. Z., and Singulinski, F., 'Flowability tests of powders', *Powder Metl. Int.*, **22 (2)**, 1990, 31-34.

Podczeczek, F., 'A shape factor used to assess the shape of particles using image analysis', *Powder Technol.*, **93**, 1997, 47-53.

Popov, K. I., Pavlovic, M. G., Pavlovic, L. J., Ivanovic, E. R., Krstic, S. B., Zou, R. P. and Yu, A. B., 'Evaluation of the packing characteristics of mono-sized non-spherical particles', *Powder Technol.*, **88**, 1996, 71-79.

Prescott, J. K. and Hossfeld, R. J., 'Maintaining product uniformity and uninterrupted flow to direct-compression tableting presses', *Pharm. Technol.*, **18 (6)**, 1994, 99-114.

Prescott, J. K. and Barnum, R. A., 'On Powder Flowability', *Pharm. Technol.*, Oct 2000, 60-84.

Process Tomography Ltd., **PTL Application Note AN1: Generation of ECT images from capacitance measurements**, March 2001.

Process Tomography Ltd., PCECT system operational manual, 1998

Rawle, A., 'Repeatable particle size analysis', *World Cement*, **30 (6)**, 1999, 56.

Riley, R. E., and Hausner, H. H., 'Effect of particle size distribution on the friction in a powder mass', *Int. J. Powder Met.*, **6 (1)**, 1970, 17-22.

Riley, G. S., Mann, S. and Jesse, R. O., 'Angle of repose of cohesive powders', *J. Powder & Bulk Sol. Technol.*, **2 (4)**, 1978, 15-18.

Santomaso, A., Lazzaro, P., Canu, P., 'Powder flowability and density ratios: the impact of granules packing', *Chem. Eng. Sci.*, **58**, 2003, 2857-2874.

Schofield, A. N. and Wroth, C. P., 'Critical state soil mechanics', New York: McGraw Hill.

Schwedes, J. and Schulze, D., 'Measurement of flow properties of bulk solids', *Powder Technol.*, 1990, **61 (1)**, 59-68.

Seville, J. P. K., Tüzün, U., and Clift, R., 'Processing of particulate solids', *Powder Technol. Ser.*, **IInd Edition**, 1997.

Teunou, E. and Fitzpartick, J. J., 'Effect of storage time and consolidation on food powder flowability', *J. Food. Eng.*, **43 (2)**, 2000, 97-101.

Thalberg, K., Lindholm, D., and Axelsson, A., 'Comparison of different flowability tests for powders for inhalation', *Powder Technol.*, **146**, 2004, 206-213.

Ultrapycnometer Operating Instructions

Ulusoy, U., Yekeler, M., and Hicyilmaz, C., 'Determination of the shape, morphological and wettability properties of quartz and their correlations', *Minerals Engg.*, **16**, 2003, 951-964.

Wong, A. C., 'Characterization of the flowability of glass beads by bulk densities ratio', *Chem. Eng. Sci.*, **55**, 2000, 3855-3859.

Wouters, I. M. F. and Geldart, D., 'Characterizing semi-cohesive powders using angle of repose', *Part. Part. Syst. Charact.*, **13**, 1996, 254-259.

Yamane, K., Tanaka, T. and Tsuji, Y., 'DEM and MRI studies of particulate flows in a rotating cylinder', *Flow Visu. Image Proc. Multiphase Sys.*, **209**, 1995, 225-228.

Yang, R. Y., Zou, R. P. and Yu, A. B., 'Microdynamic analysis of particle flow in a horizontal rotating drum', *Powder Technol.*, **130**, 2003, 138-146.

Zou, R. P. and Yu, A. B., 'Evaluation of the packing characteristics of mono-sized non-spherical particles', *Powder Technol.*, **88 (1)**, 1996, 71-79

APPENDICES

Appendix A: Results from Malvern Mastersizer- S long bench

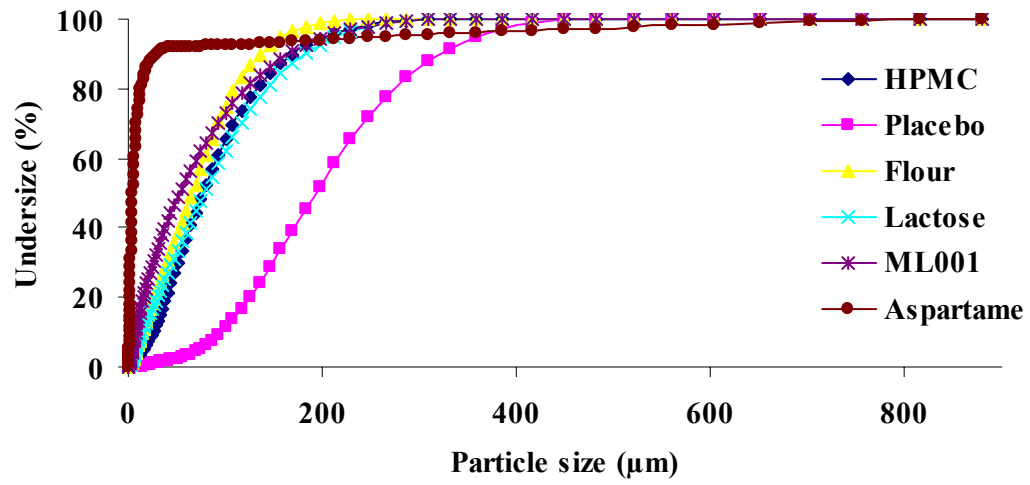


Figure: Volume undersize (%) vs. particle size (µm)

Appendix B1: Experimental results for dynamic angle of repose.

Table: Dynamic angle of repose for test powders at different rotation speeds.

RPM	Aspartame	ML001	Lactose	Flour	HPMC	Placebo
10	67	63	58	54	44	26
20	60	57	55	52	48	27
30	57	56	55	52	51	35
40	60	58	56	55	53	38
50	62	59	61	59	55	48
60	64	60	65	64	58	49
70	69	68	73	72	59	50
80	76	74	74	74	65	51
90	79	77	75	76	71	53

Appendix B2: Dynamic angle of repose for test powders at 10 RPM.

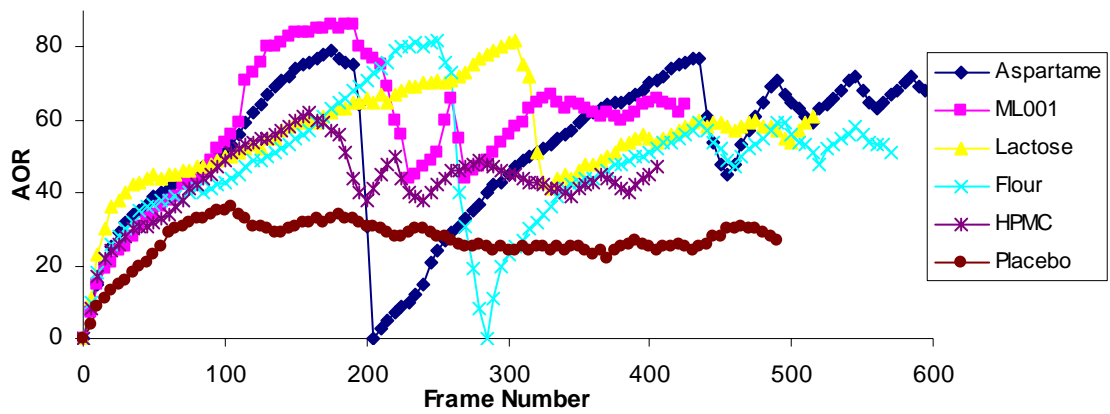


Figure: Dynamic angle of repose at 10 RPM

Appendix B3: Dynamic angle of repose for test powders at 20 RPM.

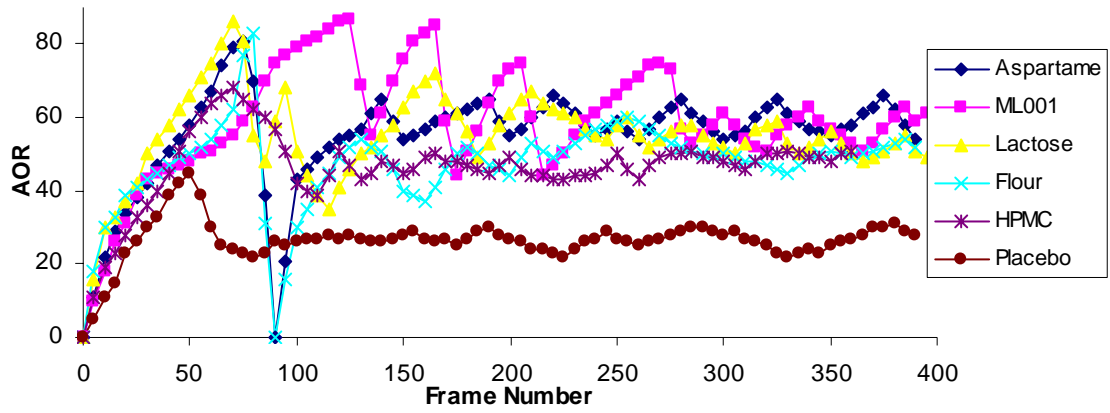


Figure: Dynamic angle of repose at 20 RPM

Appendix B4: Dynamic angle of repose for test powders at 30 RPM.

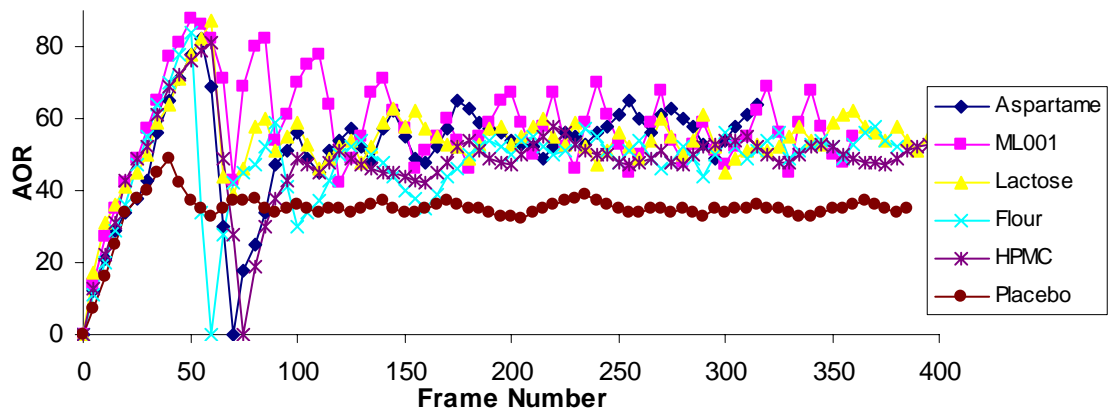


Figure: Dynamic angle of repose at 30 RPM

Appendix B5: Dynamic angle of repose for test powders at 40 RPM.

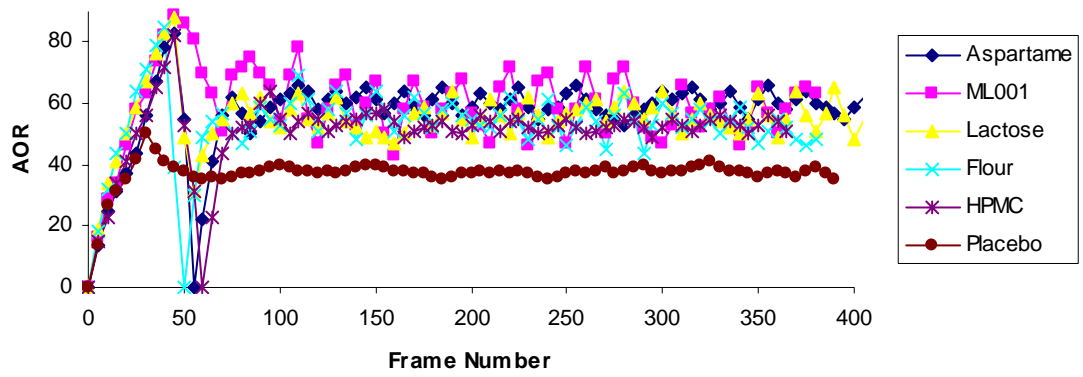


Figure: Dynamic angle of repose at 40 RPM.

Appendix C1: Frequency distributions of equivalent circle diameters for various test powders.

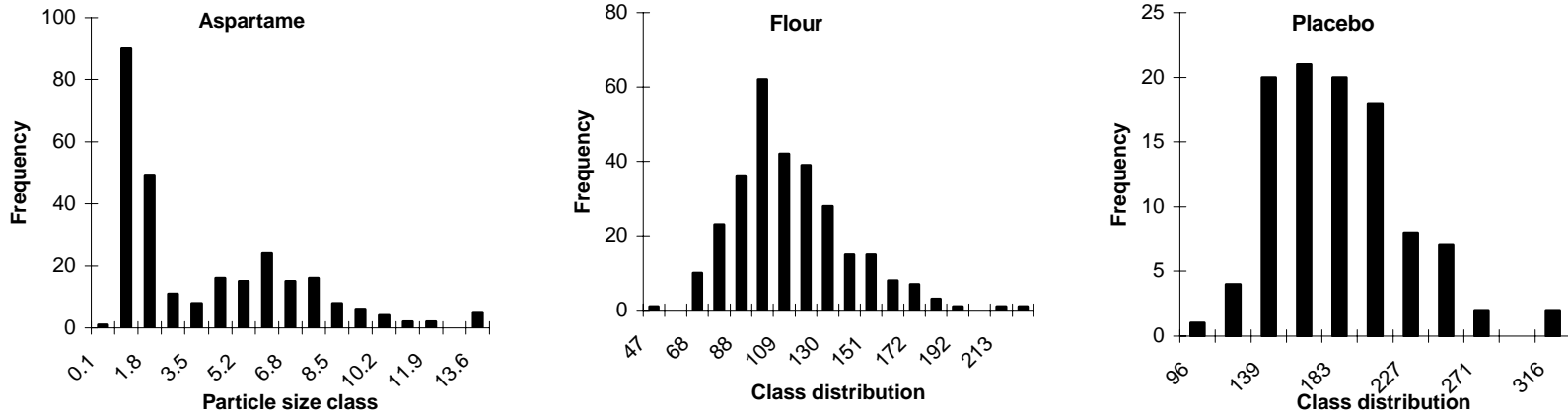


Figure: Frequency distribution of equivalent circle diameter for aspartame, flour, and placebo.

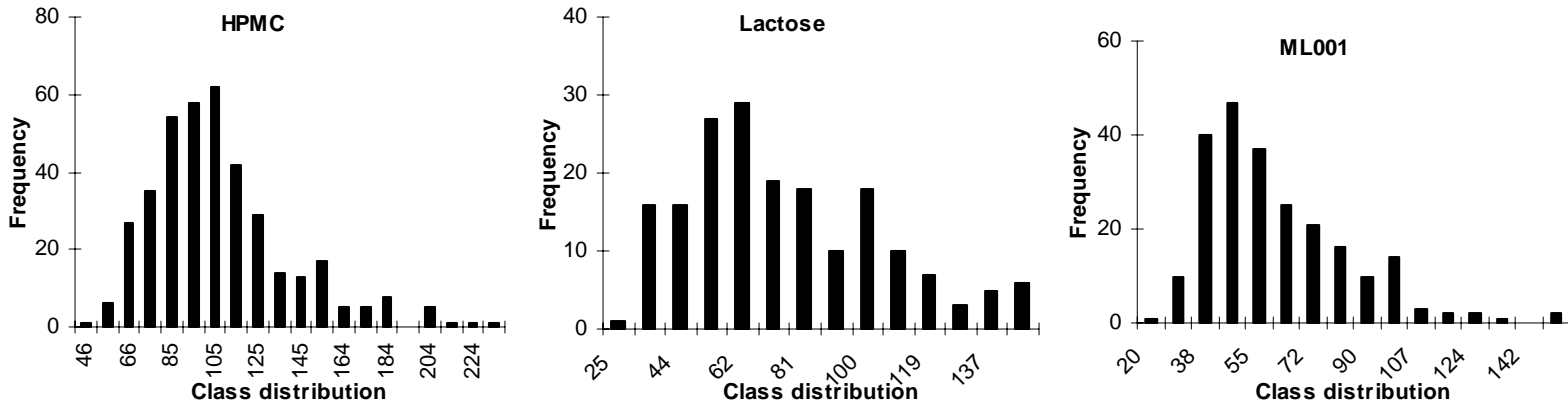


Figure: Frequency distribution of equivalent circle diameter for HPMC, lactose, and ML001 powders.

Appendix C2: Frequency distributions of roundness factor for various test powders.

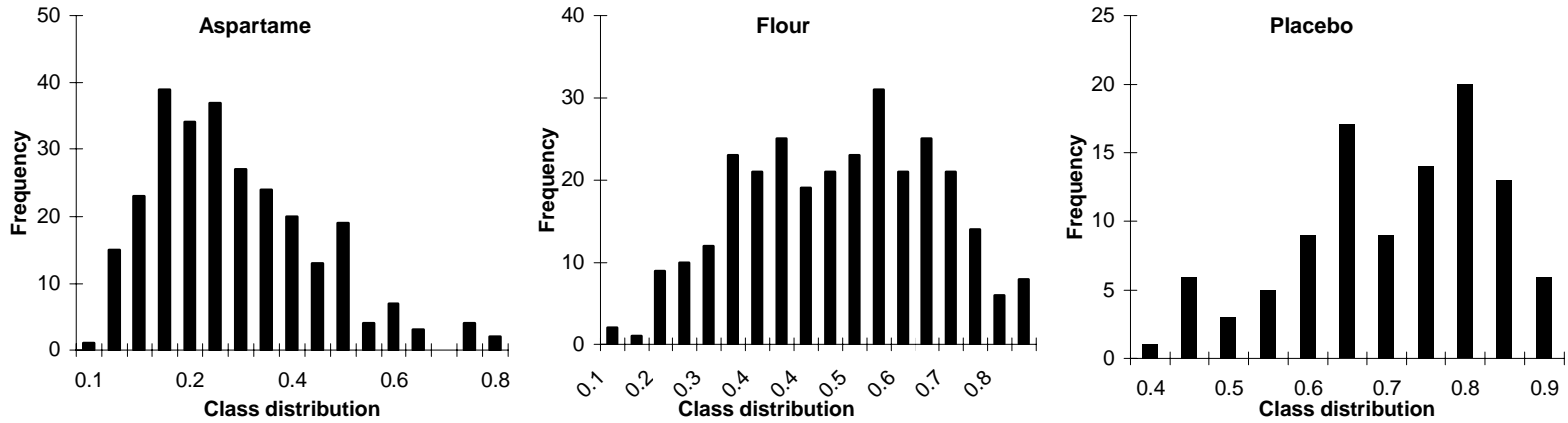


Figure: Frequency distribution of roundness factor for aspartame, flour, and placebo.

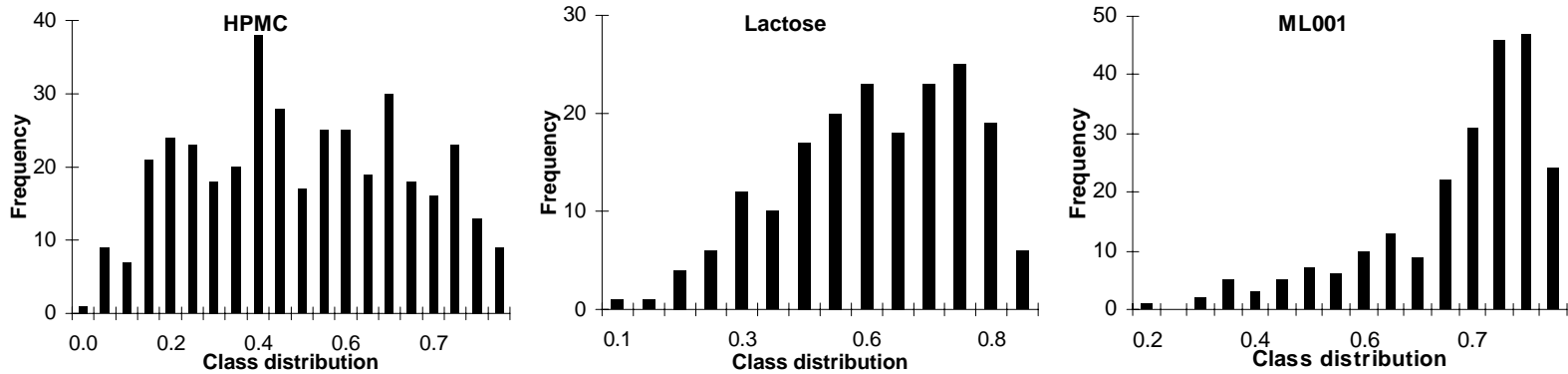


Figure: Frequency distribution of roundness factor for HPMC, lactose, and ML001 powders.

Appendix C3: Frequency distributions of aspect ratio for various test powders.

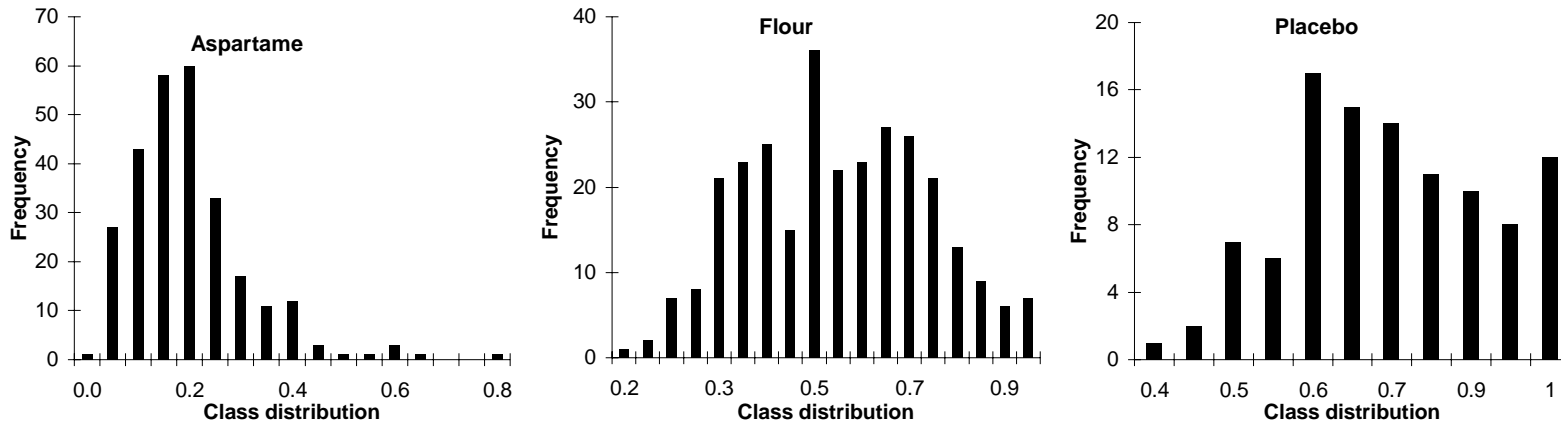


Figure: Frequency distribution of aspect ratio for aspartame, flour, and placebo.

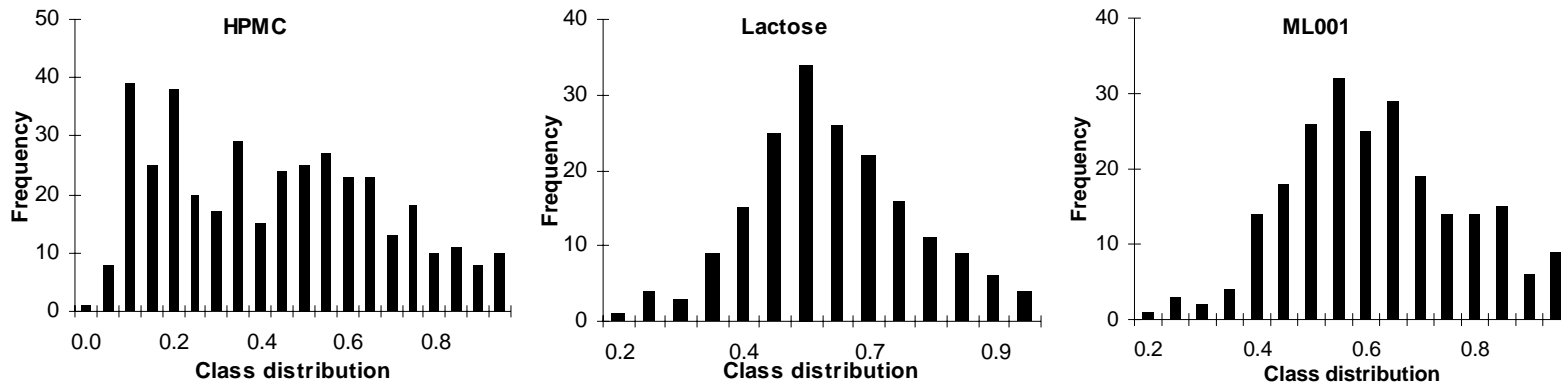


Figure: Frequency distribution of aspect ratio for HPMC, lactose, and ML001 powders.

Appendix C4: Frequency distributions of irregularity for various test powders.

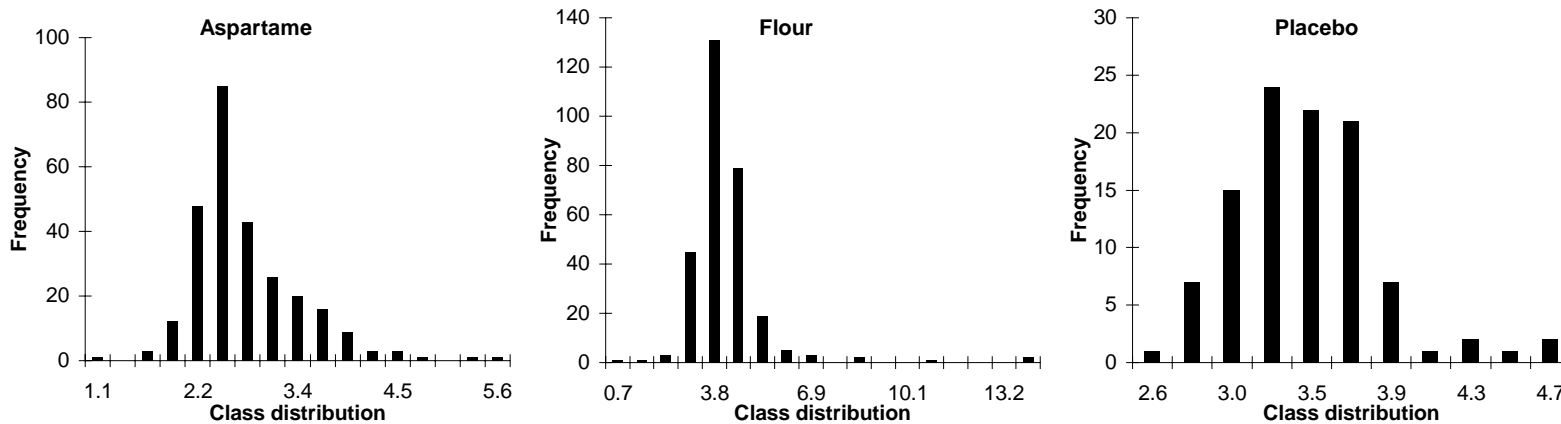


Figure: Frequency distribution of irregularity for aspartame, flour, and placebo.

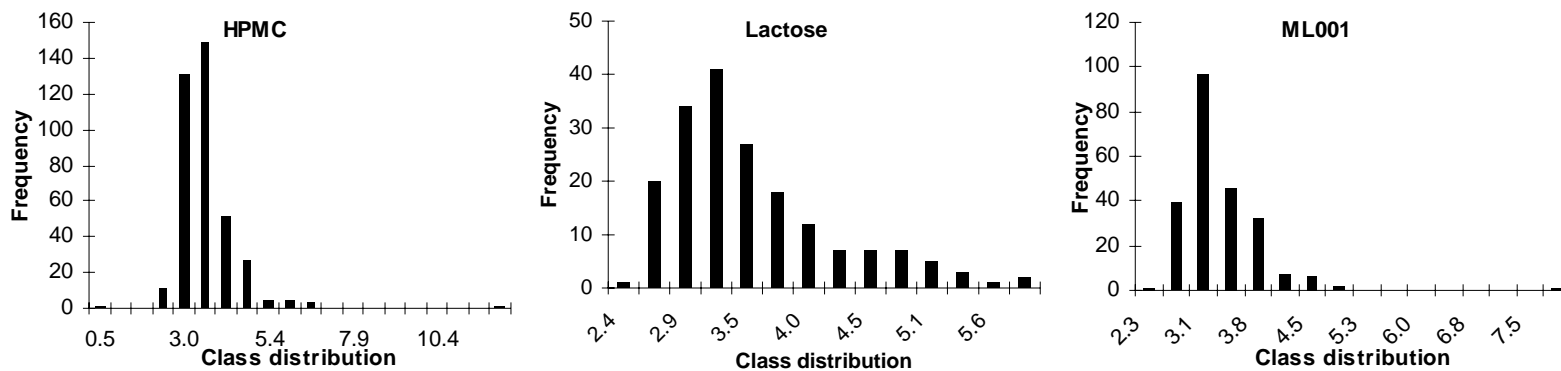


Figure: Frequency distribution of irregularity for HPMC, lactose, and ML001 powders.

Appendix D1: Shear stress vs. applied strain for aspartame

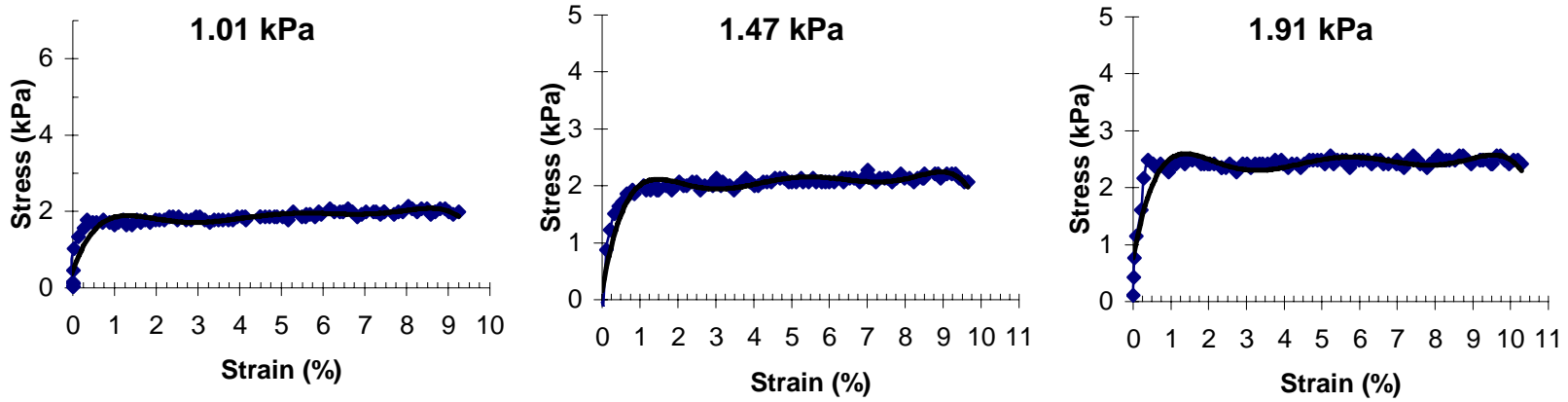


Figure: Shear stress vs. displacement for aspartame at 2 kPa preshear stress.

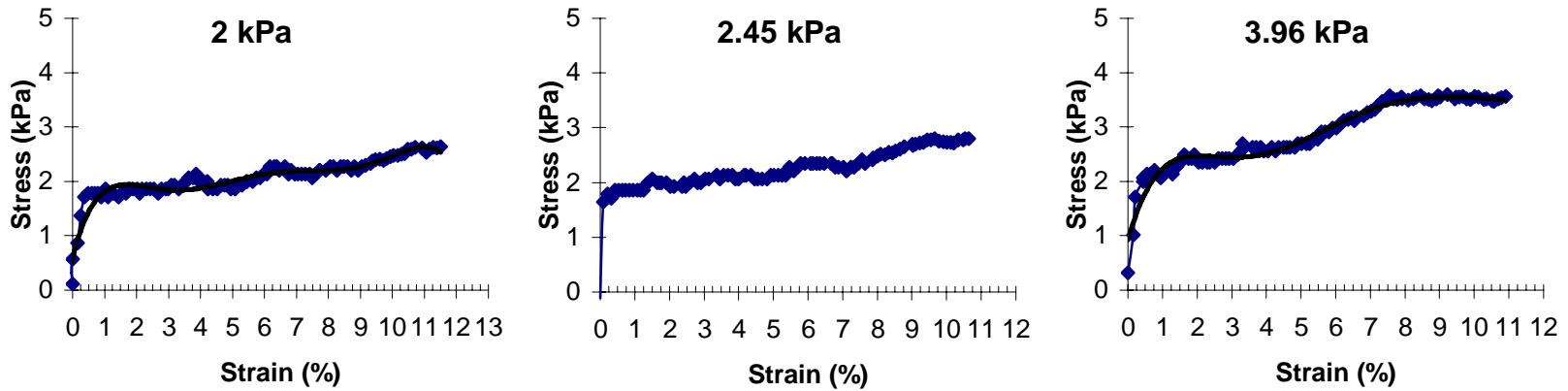


Figure: Shear stress vs. displacement for aspartame at 4.41 kPa preshear stress.

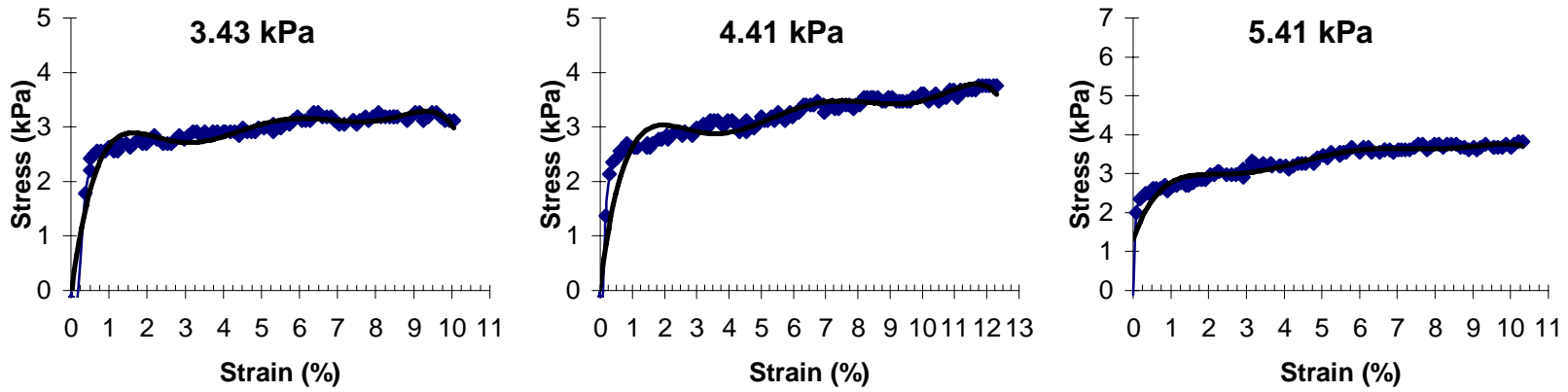


Figure: Shear stress vs. displacement for aspartame at 6.51 kPa preshear stress.

96

Appendix D2: Shear stress vs. applied strain for ML001

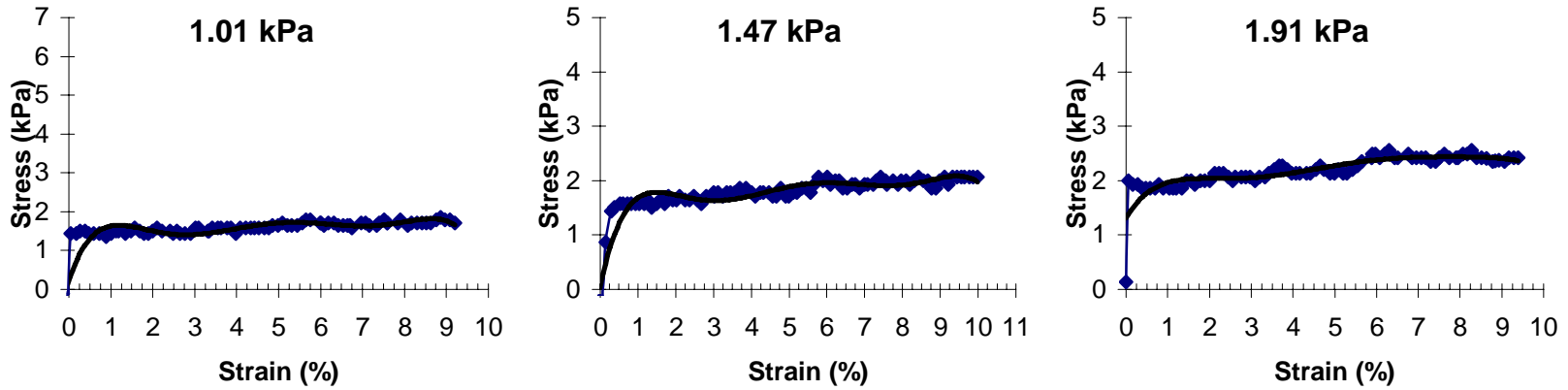


Figure: Shear stress vs. displacement for ML001 at 2 kPa preshear stress.

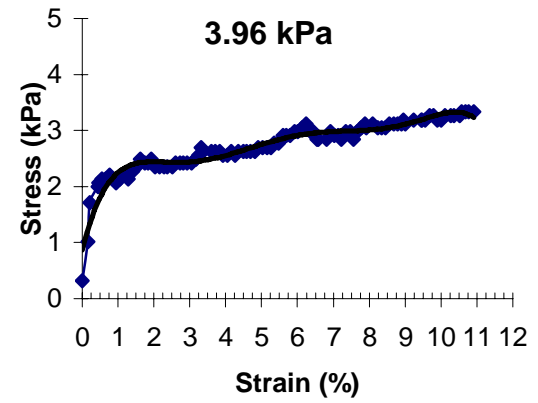
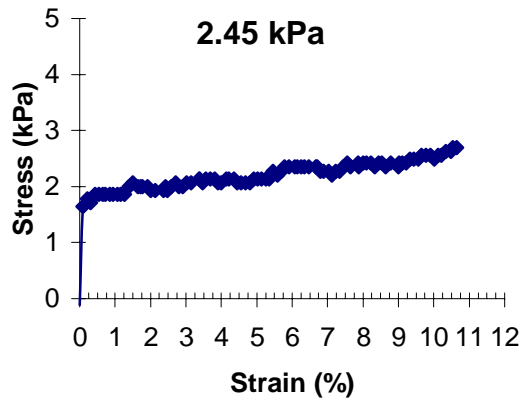
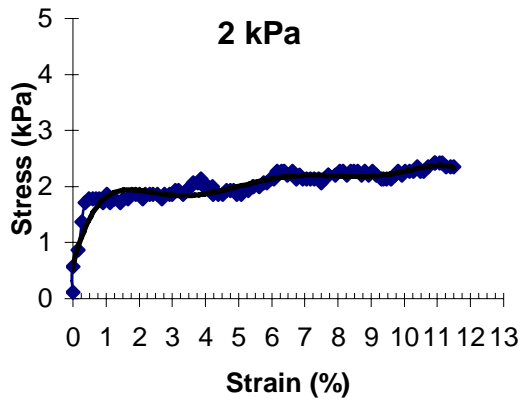


Figure: Shear stress vs. displacement for ML001 at 4.41 kPa preshear stress.

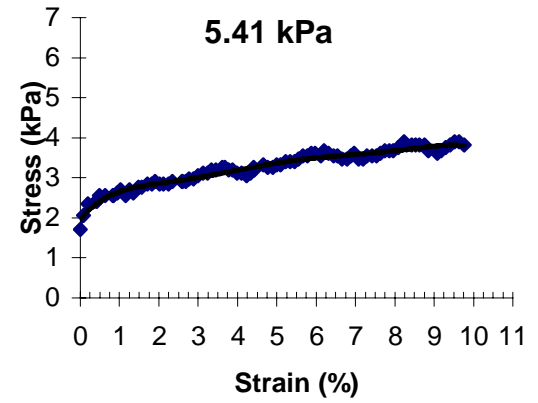
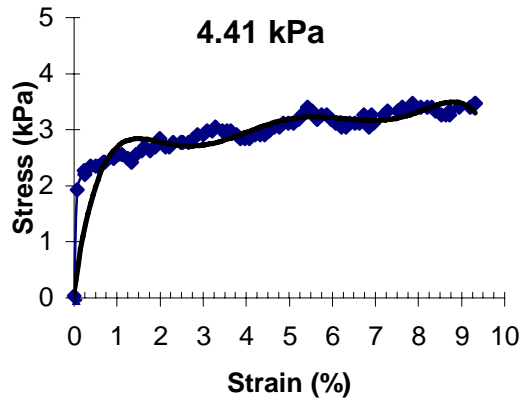
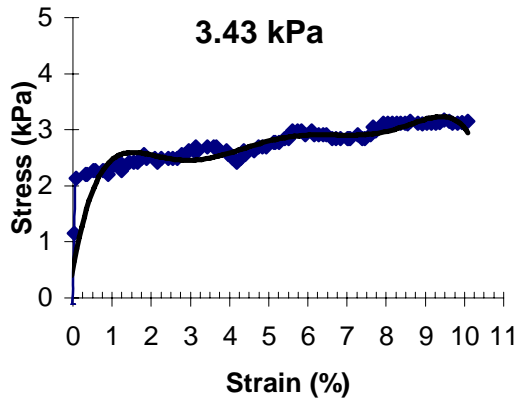
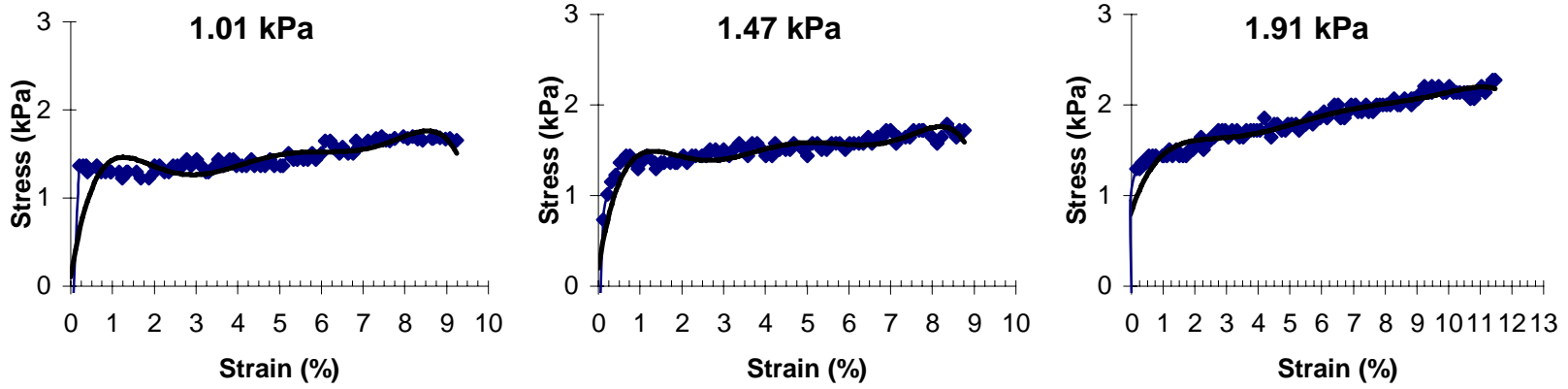


Figure: Shear stress vs. displacement for ML001 at 6.51 kPa preshear stress.

Appendix D3: Shear stress vs. applied strain for lactose



86

Figure: Shear stress vs. displacement for lactose at 2 kPa preshear stress.

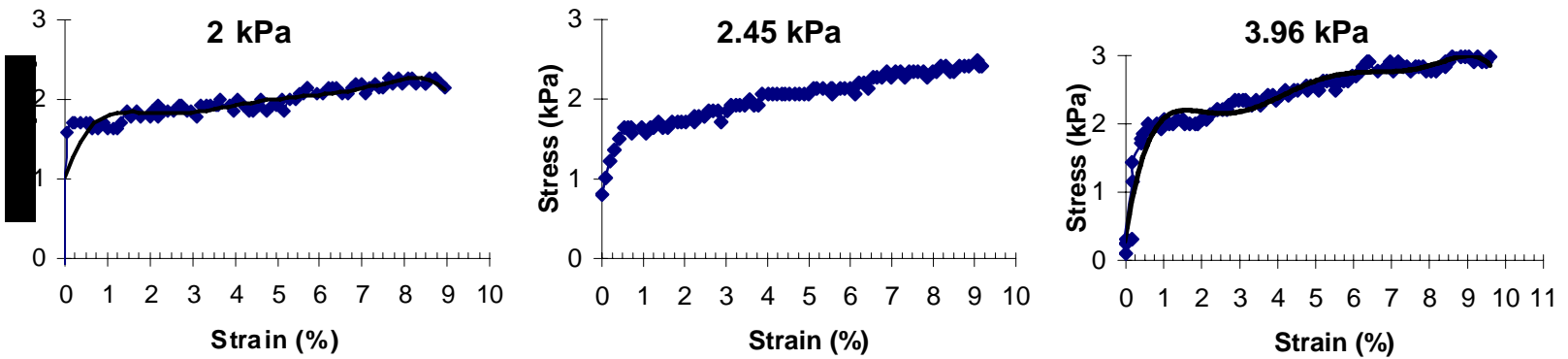


Figure: Shear stress vs. displacement for lactose at 4.41 kPa preshear stress.

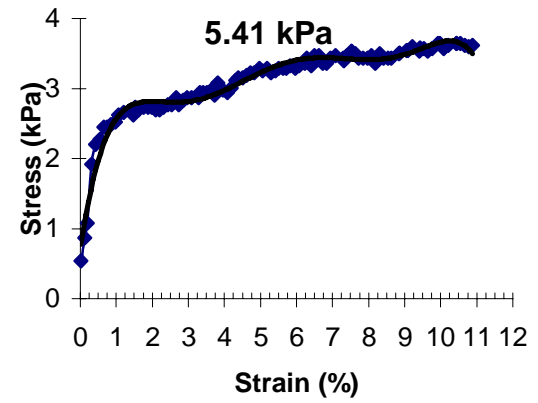
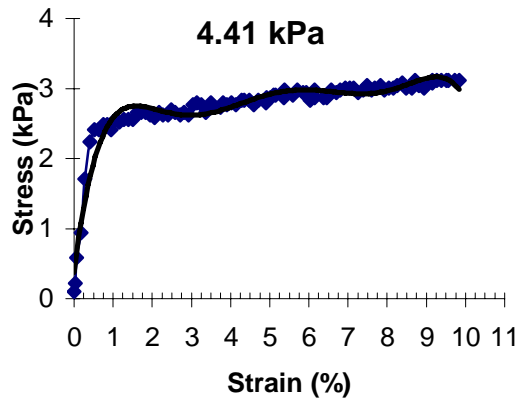
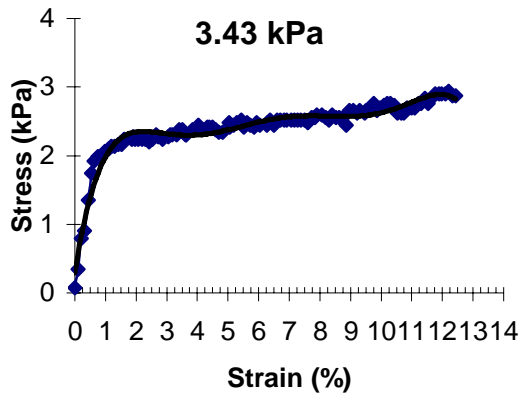


Figure: Shear stress vs. displacement for lactose at 6.51 kPa preshear stress.

66

Appendix D4: Shear stress vs. applied strain for flour

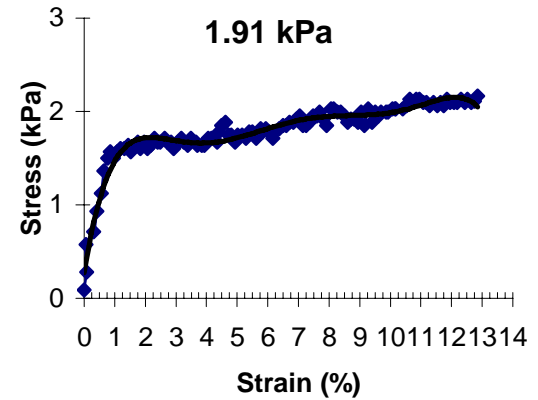
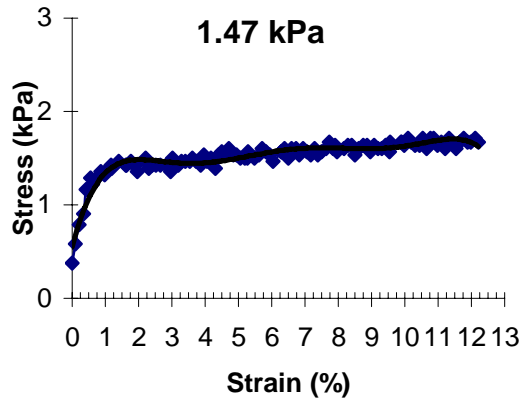
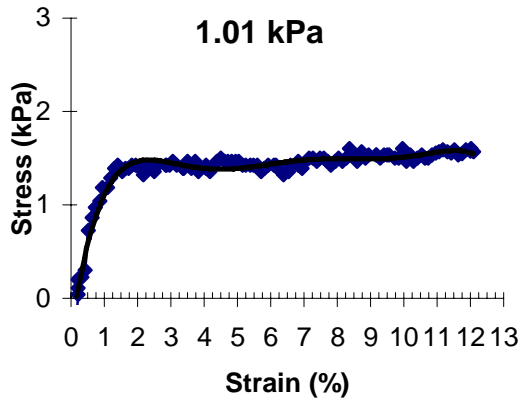


Figure: Shear stress vs. displacement for flour at 2 kPa preshear stress.

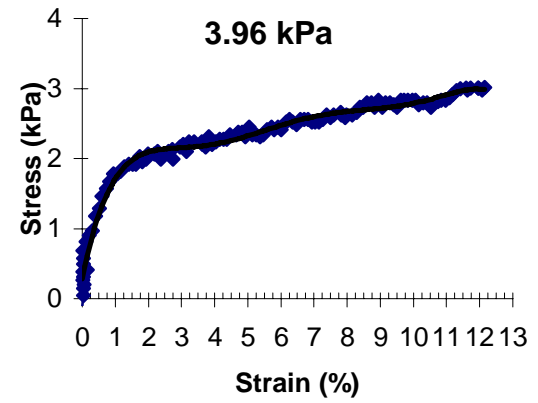
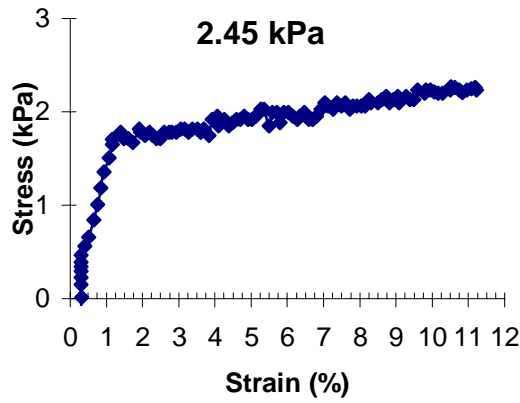
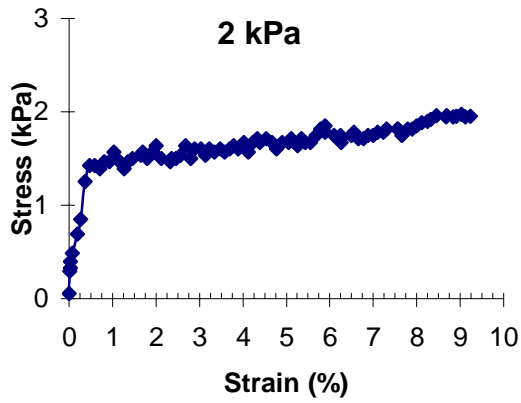


Figure: Shear stress vs. displacement for flour at 4.41 kPa preshear stress.

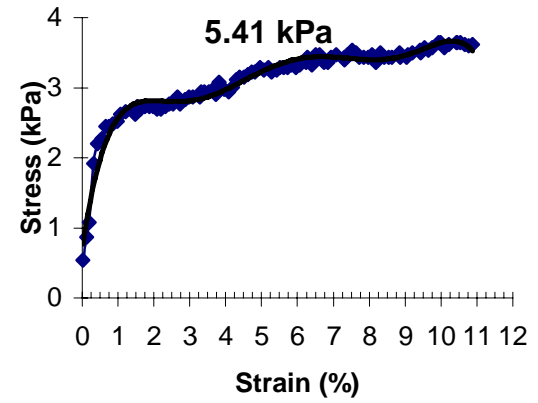
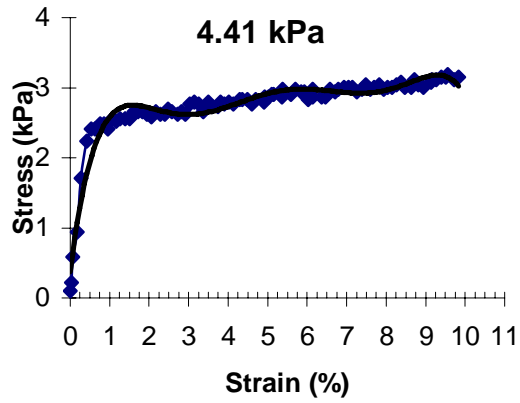
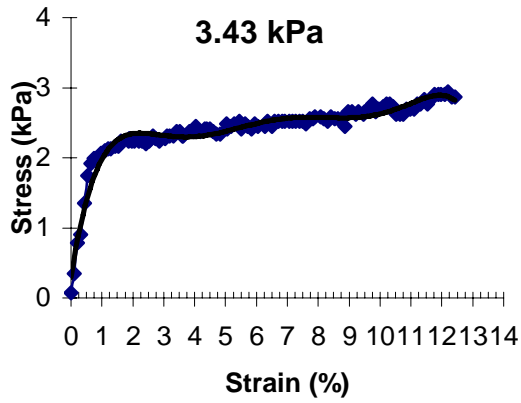


Figure: Shear stress vs. displacement for flour at 6.51 kPa preshear stress.

Appendix D5: Shear stress vs. applied strain for HPMC

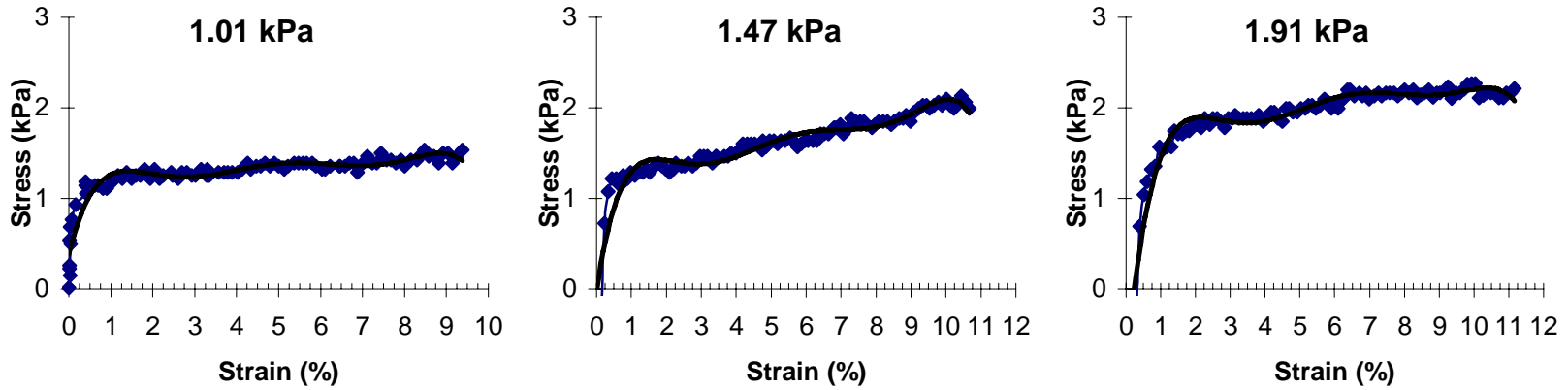


Figure: Shear stress vs. displacement for HPMC at 2 kPa preshear stress.

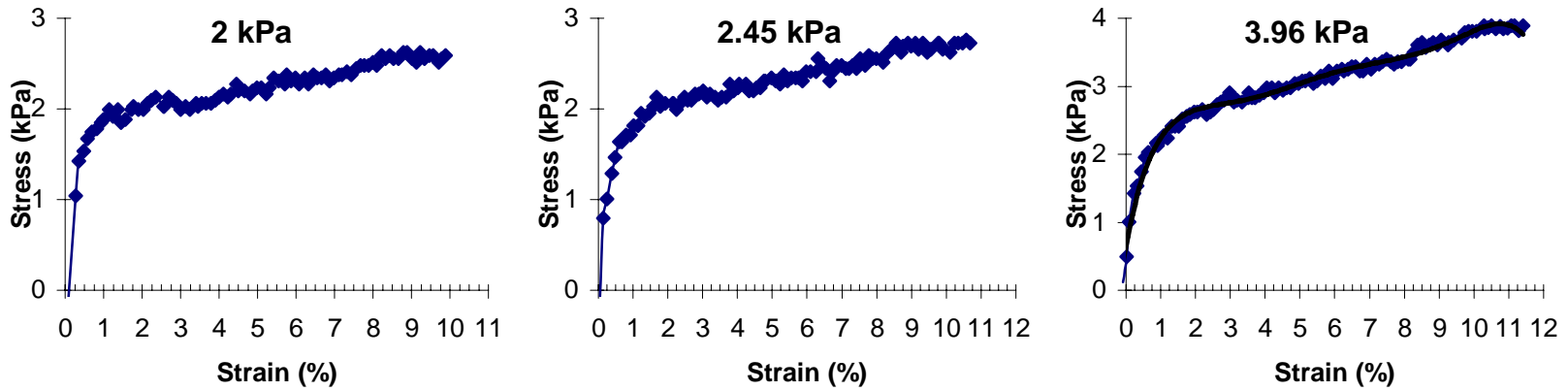


Figure: Shear stress vs. displacement for HPMC at 4.41 kPa preshear stress.

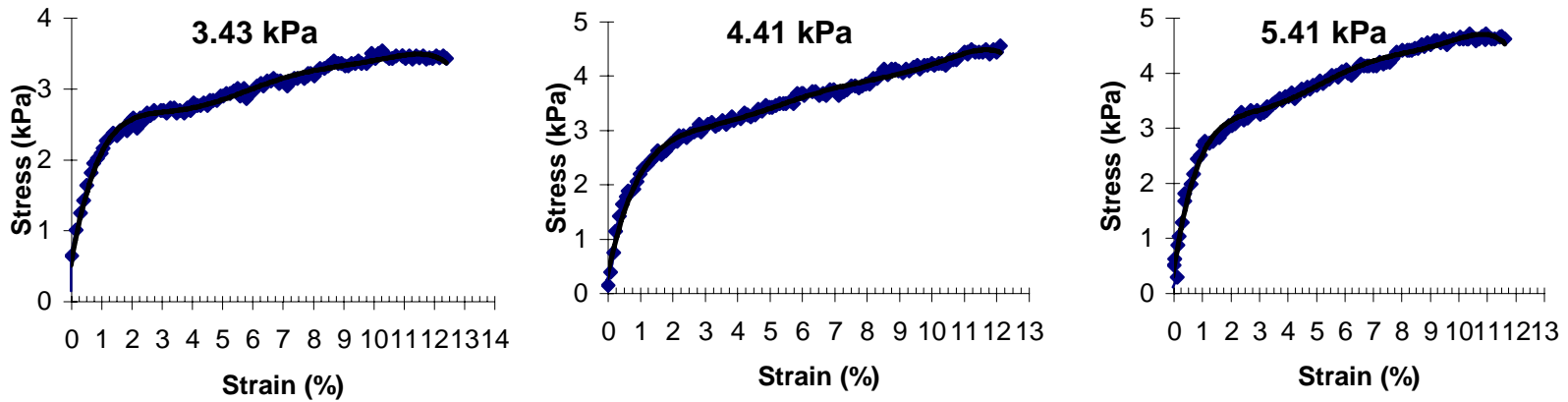


Figure: Shear stress vs. displacement for HPMC at 6.51 kPa preshear stress.

102

Appendix D6: Shear stress vs. applied strain for placebo granulates

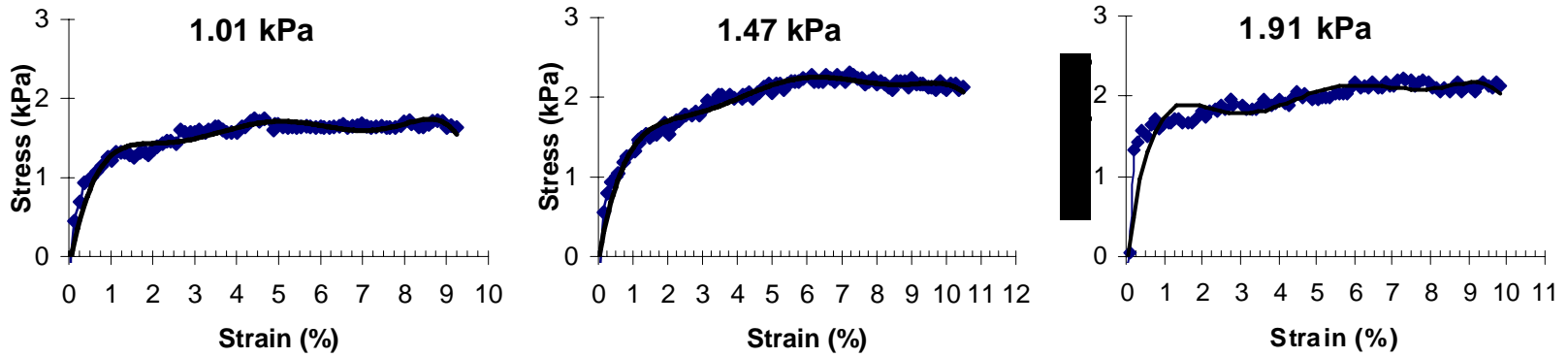


Figure: Shear stress vs. displacement for placebo granulates at 2 kPa preshear stress.

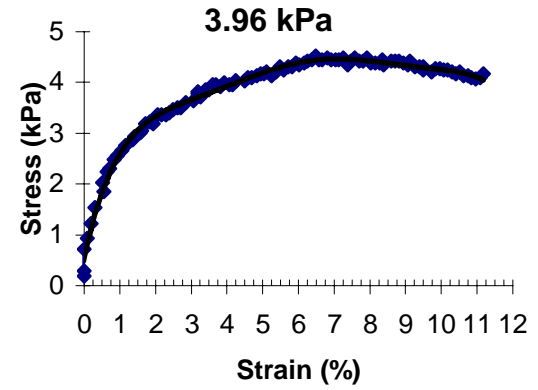
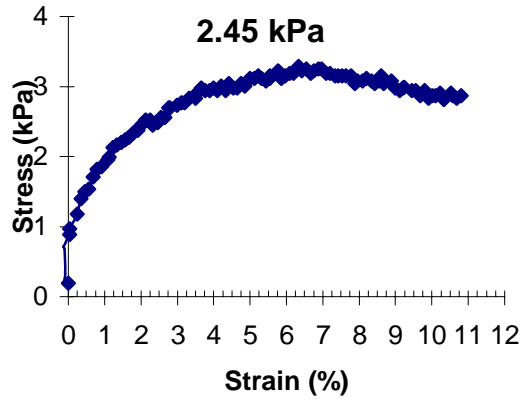
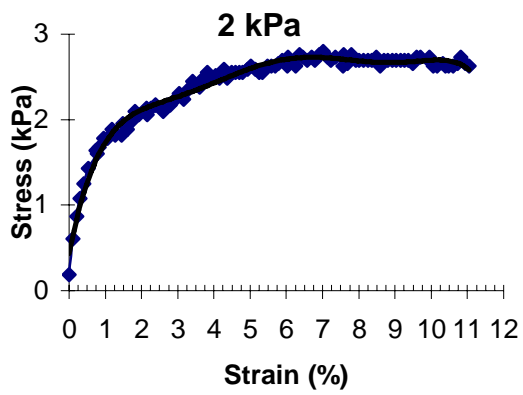


Figure: Shear stress vs. displacement for placebo granulates at 4.41 kPa preshear stress.

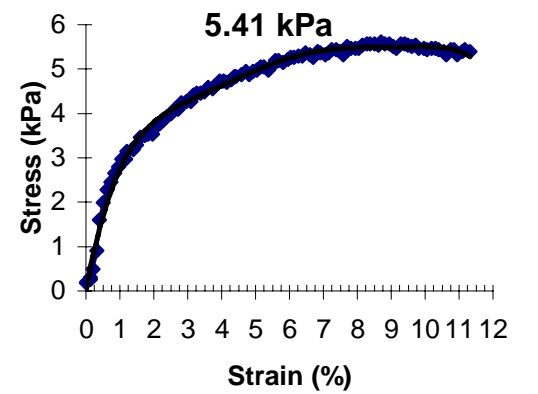
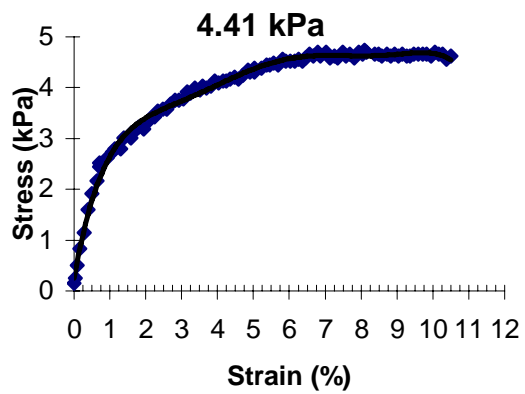
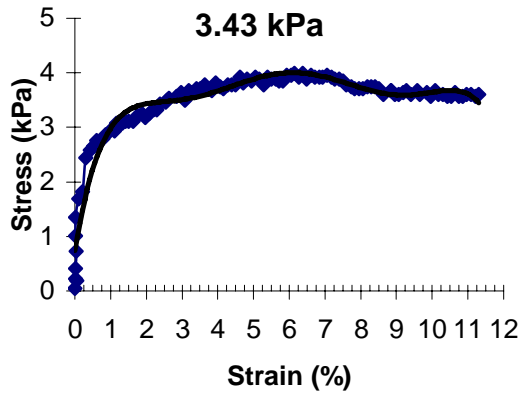


Figure: Shear stress vs. displacement for placebo granulates at 6.51 kPa preshear stress.

Appendix D7: Yield locus for test powders at different preshear stresses

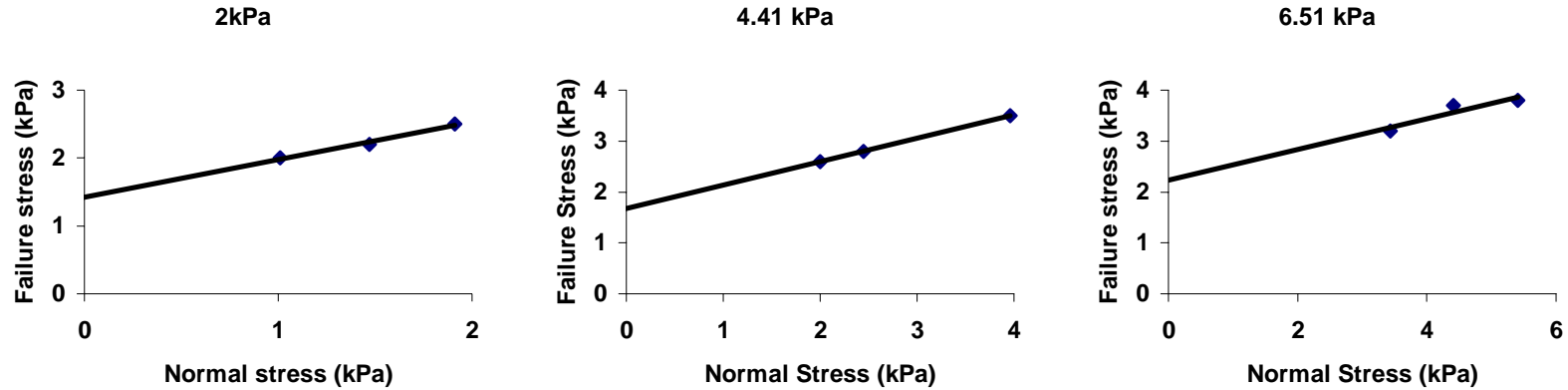


Figure: Obtained yield locus for aspartame powder at different preshear stresses

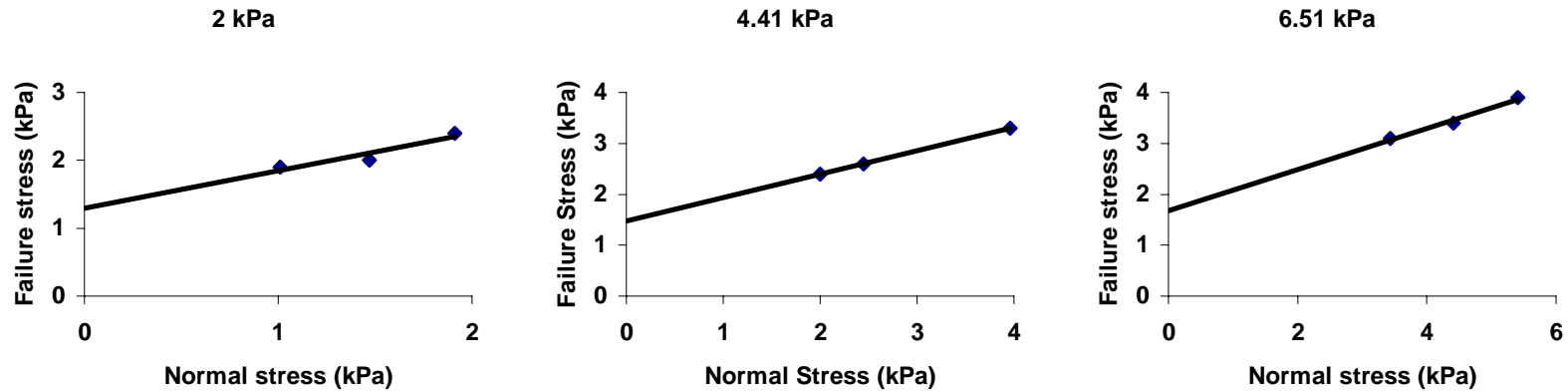


Figure: Obtained yield locus for ML001 powder at different preshear stresses

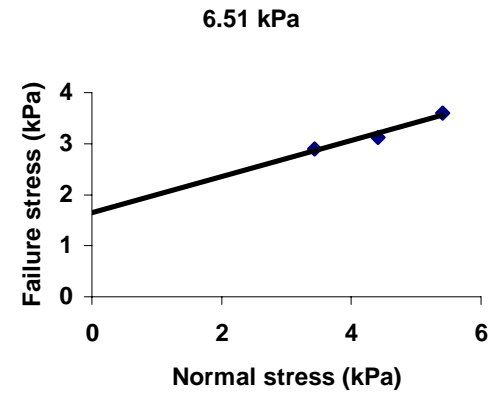
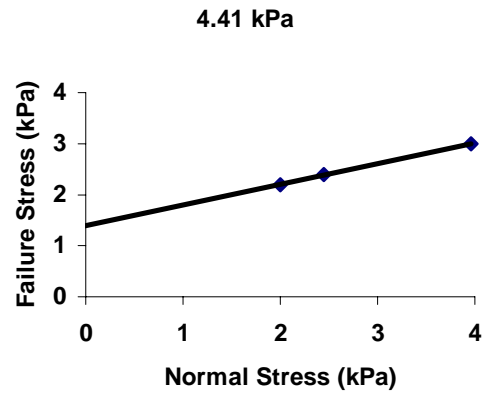
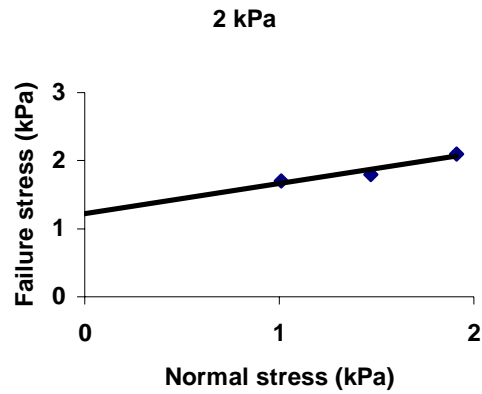


Figure: Obtained yield locus for lactose powder at different preshear stresses

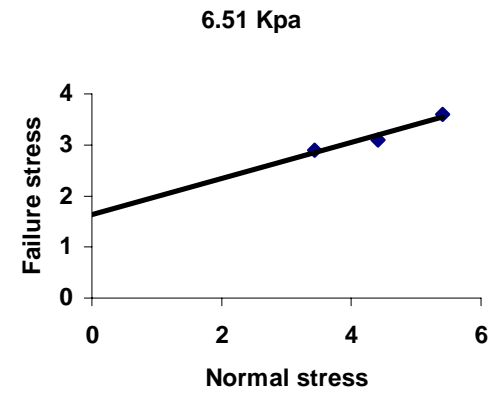
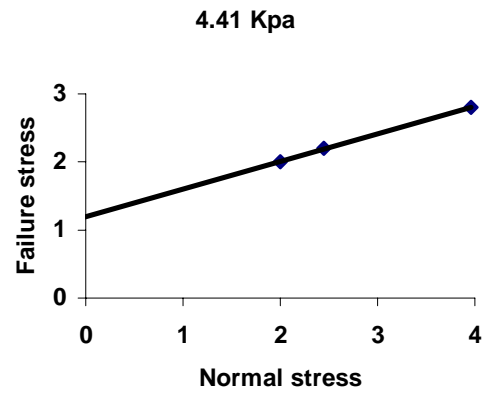
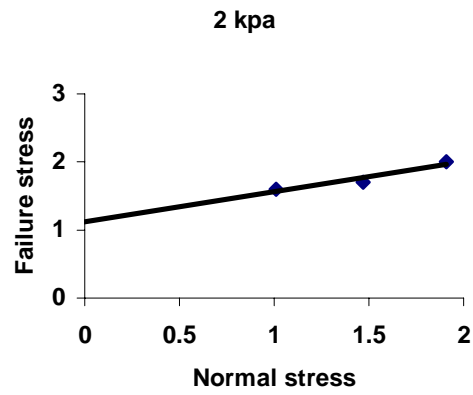


Figure: Obtained yield locus for flour powder at different preshear stresses

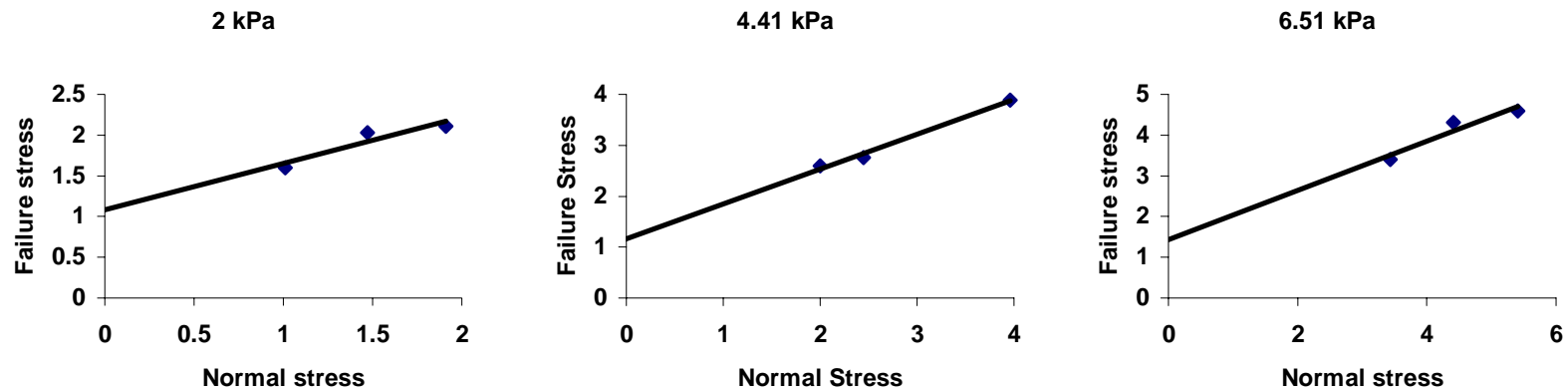


Figure: Obtained yield locus for HPMC powder at different preshear stresses

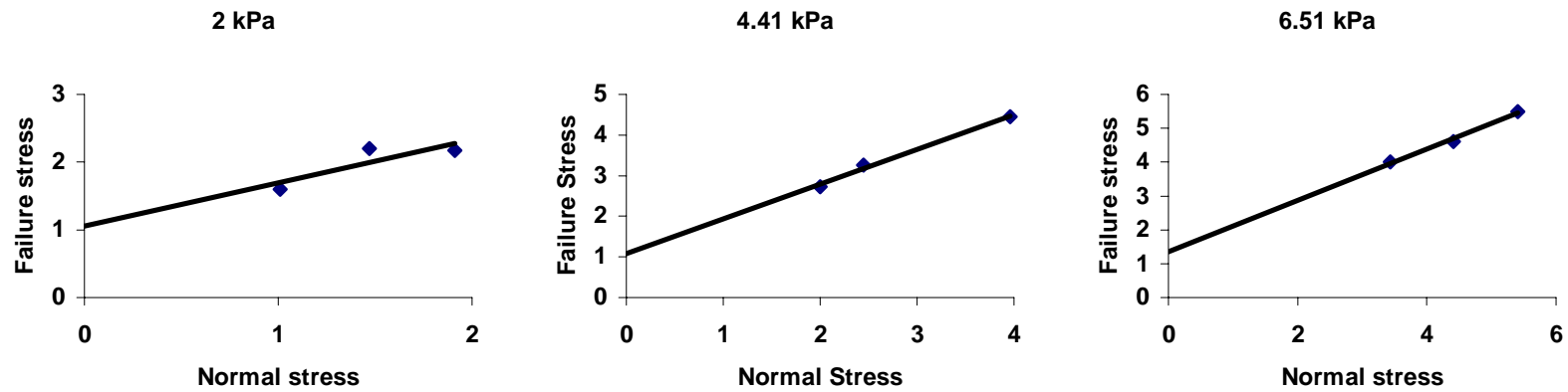


Figure: Obtained yield locus for placebo granulates at different preshear stresses

Appendix D8: Various flow indicators obtained from shear cell experiments.

Table: Flow indicators obtained from shear cell at 2 kPa, 4.41 kPa, and 6.51 kPa preshear stress.

	Aspartame			ML001			Lactose			Flour			HPMC			Placebo		
Flow Indicator	2 kPa	4.41 kPa	6.51 kPa	2 kPa	4.41 kPa	6.51 kPa	2 kPa	4.41 kPa	6.51 kPa	2 kPa	4.41 kPa	6.51 kPa	2 kPa	4.41 kPa	6.51 kPa	2 kPa	4.41 kPa	6.51 kPa
<i>C</i> (kPa)	1.42	1.67	2.23	1.29	1.47	1.68	1.21	1.39	1.64	1.11	1.19	1.63	1.08	1.16	1.43	1.05	1.08	1.35
<i>UYS</i> (kPa)	1.22	2.12	3.5	1.03	2	3.7	1.68	1.76	3.53	1.26	3.14	3.56	1.68	2.24	2.94	1.54	1.78	2.14
<i>MCS</i> (kPa)	2.88	5.76	8.1	2.85	5.75	9.3	3.32	5.78	9.06	2.74	6.84	9.84	3.31	7.1	9.14	3.41	6.78	9
δ ($^{\circ}$)	11	14	12	12	13	18	14	12	16	12	20	16	18	24	22	19	24	23

